



High Temperature Electrochemical Energy Storage: Advances, Challenges, and Frontiers

Journal:	<i>Chemical Society Reviews</i>
Manuscript ID	CS-SYN-01-2016-000012.R2
Article Type:	Review Article
Date Submitted by the Author:	03-Aug-2016
Complete List of Authors:	Lin, Xinrong; Boston University, Salari, Maryam; Boston University, Dept of Biomedical Engineering + Chemistry Arava, Leela Mohana Reddy; Wayne State University, Mechanical Engineering And Material Science M. Ajayan, Pulickel; Rice University, Department of Mechanical Engineering and Material Science Grinstaff, Mark; Boston University, Dept of Biomedical Engineering + Chemistry

TOC Graphic and text

This review summarizes the major developments, limitations, and opportunities in the field of high temperature electrical energy storage (EES) devices, with an emphasis on Li-ion batteries and supercapacitors.



Lin photo

81x82mm (72 x 72 DPI)



Salari photo

727x862mm (72 x 72 DPI)



Leela photo

393x496mm (72 x 72 DPI)



Ajayan photo

77x124mm (72 x 72 DPI)



Grinstaff photo

571x635mm (72 x 72 DPI)

High Temperature Electrical Energy Storage: Advances, Challenges, and Frontiers

Xinrong Lin,¹ Maryam Salari,¹ Leela Mohana Reddy Arava,² Pulickel M. Ajayan,³
and Mark W. Grinstaff^{1*}

¹Departments of Biomedical Engineering and Chemistry, Boston University, Boston, MA 02115.

²Department of Mechanical Engineering, Wayne State University, Detroit, MI 48202.

³Department of Materials Science and NanoEngineering, Rice University, Houston, TX 77005

1. **Introduction and Scope**
2. **High Temperature Electrical Energy Storage Market Opportunities**
 - 2.1 Oil and gas industry
 - 2.2 Military and aerospace
 - 2.3 Automotive and electric vehicles
3. **Existing High Temperature Energy Storage Technologies**
 - 3.1 Non-rechargeable systems
 - 3.2 Rechargeable systems
4. **Challenges Associated with High Temperature Electrical Energy Storage Systems**
 - 4.1 Limitations of traditional materials
 - 4.2 Stepwise thermal changes at elevated to high temperatures
5. **Development of New Materials for Thermally Stable Electrical Energy Storage Devices**
 - 5.1 High temperature electrolytes
 - 5.1.1 Reformulated carbonate solvents
 - 5.1.2 Ionic liquids
 - 5.1.3 Solid polymers
 - 5.1.4 Ceramics
 - 5.2 New thermally stable Li salts
6. **Critical Evaluation and Limitations of Current Systems**
7. **Concluding Remarks, Perspectives, and Future Directions**

High Temperature Electrical Energy Storage: Advances, Challenges, and Frontiers

Abstract: With the ongoing global effort to reduce greenhouse gas emission and dependence on oil, electrical energy storage (EES) devices such as Li-ion batteries and supercapacitors have become ubiquitous. Today, EES devices are entering the broader energy use arena and playing key roles in energy storage, transfer, and delivery within, for example, electric vehicles, large-scale grid storage, and sensors located in harsh environmental conditions, where performance at temperatures greater than 25 °C are required. The safety and high temperature durability are as critical or more so than other essential characteristics (e.g., capacity, energy and power density) for safe power output and long lifespan. Consequently, significant efforts are underway to design, fabricate, and evaluate EES devices along with characterization of device performance limitations such as thermal runaway and aging. Energy storage under extreme conditions is limited by the material properties of electrolytes, electrodes, and their synergetic

interactions, and thus significant opportunities exist for chemical advancements and technological improvements. In this review, we present a comprehensive analysis of different applications associated with high temperature use (40 - 200 °C), recent advances in the development of reformulated or novel materials (including ionic liquids, solid polymer electrolytes, ceramics, and Si, LiFePO₄, and LiMn₂O₄ electrodes) with high thermal stability, and their demonstrative use in EES devices. Finally, we present a critical overview of the limitations of current high temperature systems and evaluate the future outlook of high temperature batteries, with well-controlled safety, high energy/power density, and wide temperature operations.

1. Introduction and Scope

Electricity or electrical energy is the primary form of energy used in modern society. The need for electrical energy has been growing exponentially for portable consumer electronics as well as for transportation, grid-level applications, and load leveling.¹ For example, electricity accounted for 40% of all United States energy consumption in 2002,² and the demand for electricity is predicted to double by 2050. About 25% of electricity is produced via renewable resources and the remaining 75% is generated by burning fossil fuels (16,300 terawatt hours, TWh, $\times 10^{12}$ watt hours, as of 2013).³ This is compounded by the fact that most major industries (e.g., transportation, agriculture, public services and residential) still rely heavily on oil (39.9%), natural gas (15.1%) and coal (11.5%). Use of these non-renewable resources generates 32,190 Mt of carbon dioxide (CO₂) per year. Electrical energy is the preferred form of energy to gradually replace these fuels, as it can be generated from sustainable and clean resources such as solar, wind, and geothermal energy. Due to the intermittent and uncontrollable nature of these renewable resources, energy must be harvested and stored. While non-renewable fuels will continue to supply the majority of energy for the next several decades, electrical energy storage (EES) devices are penetrating new major markets and will eventually dominate future energy storage and supply.⁴

By definition, EES refers to the process of converting electrical energy from a power network into a form that can be stored for converting back to electrical energy when needed.⁵ This process enables electricity to be produced at times of either low demand or from intermittent energy sources and to be used at times of peak demand or when no other generation means is available. EESs are used in numerous applications including portable devices, transport vehicles, and stationary energy resources and, primary EES devices include pump hydro storage (PHS), compressed air energy storage (CAES), flywheel (FW), batteries, supercapacitors, and fuel cells.⁶ Batteries and supercapacitors will be the focus of this review.

Batteries and supercapacitors share a number of common material components, cell configuration, and electrochemistry.^{4, 7-11} Specifically, batteries and supercapacitors are comprised of electron-conducting electrodes, ion-conducting electrolyte, and separators that are ion-conducting but electron-insulating to prevent electrode shorting. Batteries are efficient energy storage devices with relatively high energy density (150 Wh · kg⁻¹) and high coulombic efficiency (> 90%). Supercapacitors, on the other hand, possess substantially higher power density (25 - 100 kW · kg⁻¹) because of fast charge transfer during charging and discharging. Therefore, they can be charged/discharged quickly for tens of thousands of cycles, and are useful in assisting the start-up of engines and regenerative braking systems, which require a short burst of power. For further comparison, fuel cells⁸ deliver about twice the combustion efficiency (~50%) of gasoline but the energy delivered is dependent on fuel supply. Fuel cells experienced a height of popularity in the 1990s, yet the high cost of producing hydrogen and the related infrastructure constrain their widespread commercial use.^{12, 13} Ongoing efforts are focused on improving power density, lifetime, and reliability.

Widely used at ambient conditions, EES devices are also subjected to extreme conditions – defined by the air temperature and the immediate surroundings. For example, batteries in our cell phones may suddenly shut down in harsh winter outdoors or catch fire in hot climates as the environmental temperature is beyond the working range of the battery. While the former leads to instability of energy supply and device malfunctioning, the latter raises significant safety issues with a resultant catastrophic thermal runaway of the system. Widely publicized accidents such as exploding laptops, glowing cellphones, plane crashes, and oil spills exemplify these safety issues.^{14, 15} Therefore, there is substantial research interest and market demand for EES devices that operate at low, high, and low-to-high temperatures for applications in oil drilling, mining, military, aerospace electronics, and electric vehicles. Since traditional EES material devices fail to meet this demand, thermal management and cooling systems are installed, adding increased weight, volume, and energy consumption to the integrated power system with often a subsequent reduction in reliability and efficiency. Moreover, these thermal management and cooling systems are not feasible in some compact or miniaturized devices.

There are many challenges to developing thermally stable EES devices. The major ones are chemical and materials centric, and include the thermal stability of cathodes, anodes, separators, and especially electrolytes, as well as the reactions within and between these essential components.^{8, 16-18} Discovery and development of stable materials working over a wider or higher temperature range (e.g., 40 - 300 °C) remain limiting factors because the elevated temperature or swings in temperature result in changes in structure and electrolyte properties, as well as undesirable electrolyte-electrode interfacial reactions. Accelerated material aging at higher temperatures can also lead to deterioration of the electrodes, separators, electrolytes, and salt. Thus, given the current knowledge base and market demand for new technologies in the consumer and industrial sector, there is an unprecedented research opportunity in the material and chemical fields. This review focuses on batteries and supercapacitors for use at temperatures from 40 to 300 °C. We start with a discussion of existing high temperature energy storage technologies and a brief market analysis, and follow with a discussion of the challenges with high temperature EES devices including material limitations, as well as thermal degradation mechanisms. We then present recent developments in the preparation of thermally stable electrolytes via cases studies using novel or reformulated materials. This includes general principles, successes, and failures, followed by a critical evaluation of the limitations of current high temperature systems. The review concludes with remarks on the field, the design requirements for an optimal battery with safety, high energy/power density, and wide temperature operation, and future directions.

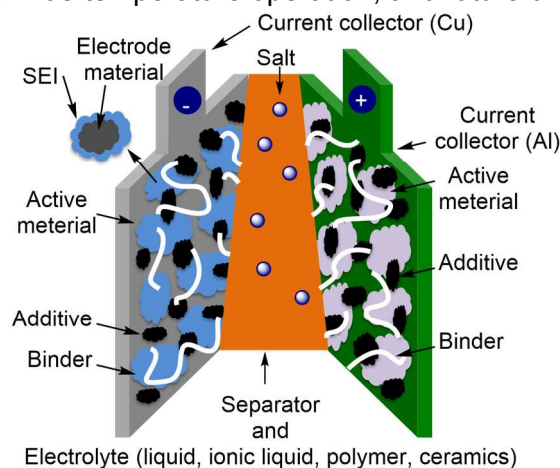


Figure 1. The structure and compositions of a lithium-based battery.¹⁹ Adapted from ref 19. Copyright 2009 Royal Society of Chemistry.

2. High Temperature Electrical Energy Storage Market Opportunities

Temperature has been long recognized as an important criterion that influences material stability, device life-span, safety, and performance; it also dictates the operation environment and corresponding applications. EES devices, first invented and commercialized to power small gadgets, are now an integral part of the broader energy storage arena and are intended to play key roles in future energy transfer and delivery in electric vehicles, large-scale grid storage, and demanding or restrictive specialty environmental applications. Traditionally, engineers relied on active or passive cooling systems when designing electronics that must function outside of normal temperature ranges. Although cooling systems effectively extend temperature limits of the electronics built with existing technologies, safety issue caused by thermal runaway cannot be fundamentally eliminated but only mitigated.²⁰⁻²³ Moreover, thermal management becomes more critical and difficult for a larger battery pack because the surface area/volume ratio of batteries decreases with increasing battery size, resulting in a lower heat transfer rate per unit of heat generation. In some applications where cooling may not be possible, or when it may be more appealing to operate at elevated temperatures in order to improve overall system performance, materials with low thermal stability are simply not appropriate choices for device components. Batteries possessing standard materials may indeed work at elevated temperatures, nevertheless, they are not safe. Size is an overarching issue when dealing with cooling systems. The extra weight and volume associated with the energy storage system greatly reduces the practical gravimetric and volumetric energy density that both the research and industry communities have strived to gain. The addition of a cooling system also increases the overall cost of the electronics. For example, the price of batteries in the Tesla S automobile is estimated to be 20% of the car cost in 2015. Nevertheless, despite the lack of materials and devices rated to power in elevated to high temperatures (as well as harsh environmental conditions), many industries are in need of electronics that operate reliably under these conditions. In 2020, the global high temperature energy storage (HTS) market is predicted to be \$2.5 billion.

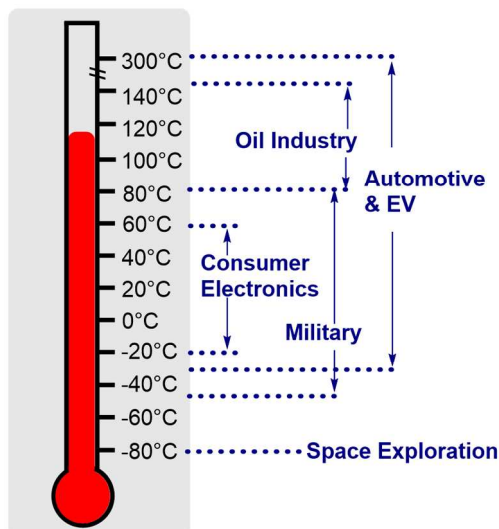


Figure 2. Temperature dependent applications of energy storage devices.

2.1 Oil and gas industry

The oldest market-pull for new and improved battery performance at elevated and high temperatures comes from the oil and gas industry, which is one of the largest user of high temperature electronics. Typically 30 to 50 feet away from the drill tip, electronics and sensors are integrated in measurement-while-drilling (MWD) and logging-while-drilling (LWD) equipment.²⁴ They record geological data and need to be powered by batteries to avoid the

inconvenience of using extension cords in high-angle, extended-reach, or horizontal conditions in many of today's wellbores. The total worldwide market for oil drilling batteries in 2011 was about \$100 million; it is expanding fast due to increasing popularity of unconventional fuels such as shale gas, and the emergence of new drilling technologies including horizontal and deep well drilling. The wellbore temperature is usually a complex function of wellbore geometry and depth, flow rate, fluid composition, and formation properties, etc.²⁵ In an over-simplified conversion, the typical geothermal gradient is about 17 °C per 100 ft of depth increase in the hydrocarbon-producing areas. This increase can be ten-fold greater in thin-crust areas such as volcanic and geothermal areas.²⁶ Reservoir temperatures typically ranged from 60 to 120 °C with the average temperature at around 85 °C.²⁷ Therefore, batteries used to power the MWD tools mainly employed lithium thionyl chloride (LiSOCl₂). Nowadays, with the declining number of easily accessible reservoirs, along with improved technologies for deeper drilling, the demand for specialty batteries is increasing. In the US alone, about 30% of the natural gas supply comes from reservoirs below 15,000 ft, where the reservoirs possess maximum temperatures of over 200 °C, and are considered as hostile high pressure/high temperature (HP/HT) environments. In these cases, active cooling is not practical, hence battery-operated equipment is not used. Instead, temperature and pressure data collection relies on mechanical registers that use a stylus to scratch marks on a metallic cylinder that turns at a constant slow rate. In response to this need, Industry partner FastCAP Systems recently reported an ultracapacitor that is fully operational at 200 °C, extending the upper limit of high-temperature energy storage and electronics.^{28, 29} The next generation of miniaturized sensors (i.e., freely mobile micro- or nano-sensors) require new battery technologies, as these independent sensors will be deployed in reservoirs, move towards desired locations, and collect real-time data on important metrics such as temperature, sulfur content, water/oil ratio, pressure, etc.

2.2. Military and aerospace

Energy storage devices are used in a wide range of specialized applications in the military and aerospace industries. Their market is significantly greater (10 to 100 times) than the oil drilling industry.³⁰ (Sandia National Laboratories, 2005) Military batteries encompass a number of different chemistries including lithium sulfur dioxide (LiSO₂), lithium manganese dioxide (LiMnO₂), silver-zinc, and lead-acid. Advances in military technology have led to an ever-increasing power requirement on the battlefield, and in turn, triggering a significant demand for reliable military batteries. A variety of high-tech military products, such as unattended ground sensors, sonobuoys, GPS, night vision, and radio systems depend on battery systems for their prompt and freely mobile functioning.^{31, 32} For military applications (military equipment is used in extreme environmental conditions, carried by soldiers on their backs for extended periods of time, and stockpiled during peace time for future wartime use) batteries must operate over a wide range of temperature conditions, be lightweight, and exhibit minimal energy loss when not in use. Furthermore, when used in miniature explosive devices, thermal batteries need insulation layers in order to continuously keep the temperature between 400 to 700 °C and to protect adjacent components from overheating

The aerospace industry utilizes high temperature electronics. One of the emerging applications driving battery performance is the motivation to migrate the traditional hydraulically driven actuators and associated systems on aircrafts to all electric counterparts in order to enhance reliability and reduce weight. Power electronics for motor controls and electric brakes require high temperature capacitors and control sensors since actuators raise the ambient temperature up to 350 °C. Replacement of the centralized engine controls with distributed control systems that are installed close to the engine on commercial aircrafts is underway, and could reduce the amount of interconnections by a factor of 10, saving hundreds of pounds of aircraft weight. Batteries or supercapacitors powering the electronics, near the engine, must endure temperatures ranging from -55 to 250 °C. Space exploration also requires power for

satellites, astronaut suits (extravehicular activities), planetary and lunar rovers, and surface systems during night-time or peak power operations.^{33,34} While most space applications require low temperature operation (-80 to 0 °C), battery operation at high temperatures is needed for planetary surface activities (e.g., Venus surface temperature can be as high as 480 °C). As with the military needs for batteries, similar demands in battery performance at elevated and high temperatures are required for the aviation and aerospace industries.

2.3 Automotive and electric vehicles

Another large market opportunity for high temperature electronics and corresponding energy storage and supply is in the automotive and vehicle traction industry. Compared to EESs in the highly specialized and relatively low volume markets in the above-mentioned industries, the competitive and high-volume electric vehicles market, which is projected to be worth \$25 billion by 2020, is very receptive to new battery technologies. High temperature electronics are used in the engine as well as the transmission and brake systems for conventional cars. The operating temperature is a function of location, power dissipation, and the thermal design.³⁵ For example, the temperature around the engine and transmission is 150 - 200 °C; the exhaust sensing element is usually under 300 °C but can reach up to 800 °C. In the hybrid electric vehicles (HEVs) or electric vehicles (EVs), not only are the mechanical and hydraulic systems for motor control and power conversion replaced with electronics, but also the major power source is switched from the fossil fuels to EES devices.^{35,36} In this regard, EES devices need to withstand temperatures of least at 60 °C, which is beyond existing technologies. Thus, extensive thermal management systems are used to control and offset the temperature. Such systems usually consist of long wires, interconnectors, and cooling plumbing, which significantly increase the weight, cost, and lowers the energy density of the EVs.³⁷ In addition, electronically controlled systems also require more sensors, most of which must work at high temperatures. While a modern Li-ion battery delivers about 150 Wh · kg⁻¹ of energy, the net calorific value (NCV) of fossil fuel is over 12,000 Wh · kg⁻¹. Even if at a low 30% efficiency of an internal combustion engine, the energy from a battery is only a fraction compared to fossil fuels. Despite these issues, consumer demand for more electronics in vehicles is increasing and expanding the market for EES devices. Finally, such EES systems will enable increased capability along with a reduced negative environmental impact.

Battery operation at elevated and high temperatures will meet current market demands as well as facilitate the advancement of new electronics for use in the oil and gas, military, aviation, aerospace, and the automotive and electric vehicle sectors. High temperature battery operation is also of interest for mainstream consumer products, and include: the battery inside a laptop, a starter battery under the car hood, or stationary batteries under the hot sun, to name a few. As technology and new product concepts are continuously emerging and evolving, the economic benefits of high temperature electronics in various energy storage systems is likely orders of magnitude greater than the markets described today.

3. Existing High Temperature Energy Storage Technologies

As of August 2013, the database of Department of Energy reported a cumulative energy storage of 24.6 GW ($\times 10^9$ watts) in the US alone, with the global value significantly larger and rising yearly with the commercial transformations undergoing in China and India.¹ In the US, pumped hydro electrical energy accounts for 95% of the operational capability as a result of its large unit sizes and longer history as the technology of choice for energy storage. The remaining 5% is divided between thermal storage, compressed air, and batteries. As opposed to thermal energy storage, which takes advantage of the heat capacity of medias (e.g., water or ice-slush tanks) and stored from nature or excessive heat from industrial processes, electrochemical energy storage is the most controllable and convenient way to convert energy

between electricity and chemical energy. These newer technologies enable facile transport and energy on-the-go use. Current commercial elevated-to-high temperature systems are primarily based on electrochemical devices, batteries, in particular.

Despite the desirability for lower or higher temperature operation, currently there is no “one-for-all” EES device suitable for applications over all temperature ranges. Temperature impacts the structure and properties of materials comprising the devices and the cell chemistry involved. Current EES devices are designed to operate at selected temperature ranges. For the convenience of discussion in this Review, these temperature ranges are categorized into low temperature ($< 0\text{ }^{\circ}\text{C}$), room temperature ($0 - 40\text{ }^{\circ}\text{C}$), elevated temperature ($40 - 80\text{ }^{\circ}\text{C}$), high temperature ($80 - 300\text{ }^{\circ}\text{C}$), and extremely high temperature ($> 300\text{ }^{\circ}\text{C}$). The borders between different temperature sections are not strictly set and adjacent regions may overlap with regard to discussions on the tested temperature and closely related applications. For the more challenging temperature ranges (low, elevated, high, and extremely high), EES operation is limited in performance time, rechargeability, and power.

3.1 Non-rechargeable systems

Non-rechargeable batteries or primary batteries are used because of their long shelf-life, readiness of operation, and simple construction. In situations where consistent power is required without charging, primary batteries are adequate as they do not exhibit voltage delays even after long storage periods. Some batteries possess a state-of-charge indicator that monitors the operational lifetime of the battery.

Li-SOCl₂ Battery. The lithium-thionyl chloride (LiSOCl₂) battery is one of the most robust lithium metal-based batteries. LiSOCl₂ batteries operate over a wide temperature range (up to $150\text{ }^{\circ}\text{C}$ and as low as $-55\text{ }^{\circ}\text{C}$) as well as in environments experiencing strong vibrations, and, consequently, are the most common type of batteries used in the oil and gas industry.^{24, 38} Liquid thionyl chloride (SOCl₂) serves as both the cathode and electrolyte in the battery configuration. Alternatively, SOCl₂ is the “catholyte” and when coupled with lithium metal as the anode provides a nominal voltage of 3.5 V per cell. Lithium aluminum chlorate (LiAlCl₄) is also dissolved in SOCl₂ to increase the ionic conductivity and a layer of nonwoven fiberglass, as a separator, is placed between the electrodes to prevent short-circuit. With a specific energy of over $500\text{ Wh}\cdot\text{kg}^{-1}$, LiSOCl₂ batteries offer about twice the capacity of the current Li-ion battery. One of the main advantages of the LiSOCl₂ battery is it produces limited emissions, even under abusive conditions, compared to other liquid-based battery technologies which generate gas byproducts at elevated temperatures. However, similar to alkaline batteries, LiSOCl₂ batteries exhibit high internal resistance and can only be used for moderate loads. A significant drawback of these batteries is that liquid SOCl₂ is toxic and reactive in contact with water and, thus, is a HAZMAT item. An additional concern is that the battery exhibits a delay in producing a good terminal voltage when put into service. Furthermore, the LiSOCl₂ battery is a non-rechargeable battery and possesses limitations of convenience, cost, and safety.

Lithium Sulfur Dioxide (Li-SO₂) Battery. Lithium Sulfur Dioxide (Li-SO₂) batteries are widely used in military and aerospace applications. In this battery, SO₂ is bonded onto carbon as the cathode and a mixture of lithium bromide, liquid SO₂, and a small amount of acetonitrile (ACN) are the electrolyte.³⁹ The Li-SO₂ battery exhibits high power density and stable performance from -55 to $60\text{ }^{\circ}\text{C}$. The ability to deliver high current especially at low temperatures, is a defining performance feature. However, the Li-SO₂ battery requires two atmospheres of pressure to retain the electrolyte in a liquid state and must be vented to prevent pressure build up. In addition, the service life and energy density is less than half of the Li-SOCl₂ battery.

Other Lithium-Metal based Batteries. Lithium manganese dioxide (Li-MnO₂) batteries are the most common consumer grade lithium-metal based batteries.⁴⁰ With many advantages including high energy density ($280\text{ Wh}\cdot\text{kg}^{-1}$), high power pulse, long life, and low cost, these devices constitutes 80% of the lithium battery market. It employs the Li/MnO₂ configuration with

lithium perchlorate (LiClO_4) dissolved in propylene carbonate (PC) and dimethoxyethane as the electrolyte. The nominal voltage is around 3 V and the working temperature range is between -30 °C and 60 °C. Battery performance is compromised at temperatures above 60 °C, including a high self-discharge rate.

The lithium copper oxide (Li-CuO) battery, with LiClO_4 dissolved in dioxolane or in mixtures of polyethylene oxide (PEO) and molten dimethyl sulfone (DMSO_2) as the electrolyte, operates from around -30 up to 150 °C, but is of limiting usefulness because it displays a high difference between the open-circuit and nominal voltage.^{38, 41-43} The CuO half-cell is known for its stability across a broad temperature range and can cycle over the potential range of 1.5 - 3.0 V (vs. Li/Li^+). Fast capacity loss and limited cycling are obtained at room temperature, however, new reaction pathways associated with the electrodes or electrolytes arise at higher temperatures. For example, early studies reported that the discharge curve of CuO exhibited two distinct voltage plateaus at 1.2 and 1.9 V (vs. Li/Li^+) at 70 °C, while affording only one discharge plateau at 1.5 V (vs. Li/Li^+) at 20 °C.^{38, 42} Li-CuO battery has been replaced by lithium-iron sulfide (Li-FeS_2), which utilize molten salts (e.g., LiCl-KCl binary eutectic halides) as the electrolyte with an increased working temperature range from 400 to 500 °C. A similar design was adopted for lithium chloride batteries (Li-Cl_2) where molten lithium chloride is used as the electrolyte along with a liquid lithium and chloride gas filled in carbon as the electrodes. This type of battery delivers high energy ($2,180 \text{ Wh} \cdot \text{kg}^{-1}$) but the operational temperature must be maintained at 650 °C or higher.⁴⁴

3.2 Rechargeable systems

Rechargeable batteries or secondary batteries possess higher energy density, higher capacity, and longer lifecycle, and are used for a wide range of applications. These batteries are also cost effective as they can be recharged using an external power source. Secondary batteries are subjected to normal self-discharge, and thus, they do incur maintenance costs. Proper maintenance procedures need to be followed depending on their application, environmental operational conditions, and their chemical composition. All of the rechargeable batteries discussed below share these merits and limitations.

Na-S and ZEBRA Batteries. Sodium-sulfur (Na-S) batteries are extensively used in industry and represent the largest category in the high temperature battery market since their initial development by the Ford Motor Company in the late 1960s.⁴⁵⁻⁴⁷ Sodium as a non-toxic, abundant, and low cost alkali metal with low reduction potential (-2.71 V) attracted significant research efforts with the goal to reduce global dependence on lithium.⁴⁸ The active materials in Na-S battery are molten sodium (m.p. 98 °C) as the negative electrode and molten sulfur (m.p. 115 °C) as the positive electrode. The two liquid electrodes are separated by a solid ceramic, sodium- β -alumina ($\text{NaAl}_{11}\text{O}_{17}$), which is electronically insulating and allows sodium ions to pass through. Na-S batteries exhibit high energy density ($150 \text{ Wh} \cdot \text{kg}^{-1}$), high coulombic efficiency (~90%), high specific power, and long lifecycle. In fact, it was successfully tested on the space shuttle mission STS-87 in 1997.⁴⁹ However, because of the high operating temperatures of 400 to 700 °C, and the highly corrosive nature of the sodium polysulfides in use, these cells are primarily suitable for large-scale non-mobile applications, such as grid energy storage.

Dendritic sodium forms in Na-S batteries and, thus, is a safety concern. To address this dendrite-sodium issue in Na-S battery, the Zeolite Battery Research Africa (ZEBRA) battery was invented in 1985, which utilizes a combined molten sodium tetrachloroaluminate (NaAlCl_4) / sodium- β -alumina and molten sodium electrolyte and molten nickel/nickel chloride (Ni/NiCl) as the negative and positive electrodes, respectively.^{46, 50} The operating temperature is in a range of 270 to 350 °C, where the resistance of β -alumina is marginal and NaAlCl_4 is melted (melting point 157 °C). Moreover, the battery has a shelf life of 10-20 years at room temperature.

Liquid-metal Battery. In contrast to other thermal batteries, where a solid-state electrolyte or separator is between the liquid cathode and anode at operational temperature, in

liquid-metal batteries all the essential components, namely the cathode, the anode and the electrolyte are in their liquid forms during operation, and are self-segregated via different densities.⁵¹⁻⁵³ There are several performance benefits of these batteries. For example, the fast charge transfer kinetics between all-liquid phases of electrodes and electrolytes leads to low ohmic losses and high rate capability. Also, the use of inexpensive, earth abundant electrodes and simple cell fabrication suggests that the energy cost can potentially be as low as \$100 kW/h, expanding market opportunities into wider applications such as grid-scale energy storage. However, despite these benefits, liquid metal batteries also possess several disadvantages. Corrosion of the cell construction materials including container, insulator, current collector, is a primary concern due to high working temperature and high reactivity of the electrodes. In addition, the operation temperature is typically between 500 to 1000 °C to maintain the liquid status of the electrodes, which consumes 2% - 5% of the energy it generates to maintain the extremely high temperature and requires advanced thermal management and insulation layer to protect nearby components from ultra-high heat related damage. Moreover, the three-liquid layer configuration renders the battery sensitive to vibration or motion, limiting liquid metal batteries for stationary EES applications.

Fuel Cells. Although not the focus of this review, several types of fuel cells operate at elevated or high temperatures.¹³ Proton Exchange Membrane (PEM) fuel cells use a polymeric film as an ion exchange membrane electrolyte, which possesses high proton mobility for high power density.⁵⁴ The typical working temperature is between 20 and 100 °C. Presently, high cost limits wide-spread adoption. Phosphoric Acid Fuel Cells (PAFCs) employ liquid phosphoric acid in an inorganic matrix as the electrolyte, and must operate at 150 to 220 °C due to the poor acid ionic conductivity at low temperatures. The low power density output restricts their use for only multi-kilowatt stationary applications. Alkaline fuel cells, which are used in the space shuttle, employ aqueous potassium hydroxide as the ionic conducting electrolyte. The operating range of the cell is between 20 and 100 °C. A fundamental limitation of these cells, is the sensitivity of the basic electrolyte to carbon dioxide, leading to the formation of potassium carbonate and precipitates. In addition, these systems use only pure oxygen, which lends them impractical for most applications.

Two other special classes of fuel cells work at extremely high temperatures (> 500 °C), namely Molten Carbonate Fuel Cell (MCFC) and Solid Oxide Fuel Cells (SOFC).⁵⁵ Similar to thermal batteries, molten carbonate fuel cells utilize an electrolyte composed of a molten carbonate salt mixture suspended in a porous ceramic matrix of β -alumina.⁵⁶ Typically working at temperatures greater than 650 °C, fuels convert hydrogen at the anode under the high temperatures, reducing cost and improving efficiency. An external reformer to convert fuels to hydrogen is not needed. In contrast, solid oxide fuel cells possess a solid oxide electrolyte.⁵⁷ Depending on the ceramics comprising the cell stack, SOFCs function at temperatures ranging from 500 to 1000 °C. These types of fuel cells usually exhibit high efficiency, long-term stability, relatively low cost, and can be used with a variety of fuels. In addition, as compared with batteries, fuel cells operate with unlimited cycles in theory, as long as fuel and oxidizer are supplied. However, the extremely high operating temperature results in longer start-up time and may bring about mechanical and chemical compatibility issues.

Table 1. Performance specifications of existing high temperature energy storage technologies

Battery chemistry	Type	Voltage (V)	Specific Energy (Wh/kg)	Operation Temperature (°C)
Li-SOCl ₂	non-rechargeable	3.5	500	-55 ~ 150
Li-SO ₂	non-rechargeable	2.9	250	-55 ~ 70
Li-MnO ₂	non-rechargeable	3.0	280	-30 ~ 60
Li-CuO	non-rechargeable	1.5	300	-30 ~ 150
Li-FeS ₂	non-rechargeable	1.5	300	400 ~ 500
Li-Cl ₂	non-rechargeable	3.5	2180	> 650
Na-S	rechargeable	1.7	150	400 ~ 700
Na/NiCl ₂ (ZEBRA)	rechargeable	2.6	90	270 ~ 350
Liquid-metal	rechargeable		787	500 ~ 1000
Solid oxide fuel cell	rechargeable	4.1	410	> 500

Despite their advantages and disadvantages, EES technologies exist and are being used for numerous applications. It is apparent that EES operation at temperatures between 25 and 60 °C is straightforward, and there are several devices for working at temperature greater than 300 °C. However, there is a void of EES options for operation between 60 and 300 °C, where a variety of important applications would fall into (vide infra). Thus, there is an opportunity for new chemistry and materials along with EES designs to fill this gap and to resolve this long-standing challenge.

4. Challenges Associated with High Temperature Electrical Energy Storage Systems

High temperature EES systems are important for a number of uses in both specialized fields and the broader markets, however, the storage and delivery of energy are challenging for five primary reasons.

1) The majority of the materials investigated for EES are those that exist and function nominally at room temperature. As expected, current EES devices incorporate material components that perform in a limited temperature range.

2) Some EES devices still experience heat loss in various circumstances despite having sophisticated internal and external protection mechanisms in place. It is possible that a failed cell could rupture, and the flame could spread across the cell pack, leading to failure of the whole pack. Materials with low flammability could effectively localize the damage to the individual cell in the event of one cell failing. Unfortunately, the materials used in EES devices, especially the electrolyte materials, are flammable and have low boiling points. These electrolyte materials are a critical safety concern.

3) The different materials comprising the EES devices function independently, as well as interact with each other to enable performance. The resulting electrochemical reactions and transfer phenomena are thermally controlled, as described by the Arrhenius equation.⁵⁸ At high temperatures, not only are the desired reaction kinetics and charge carrier mobility faster, but also the side reactions, interface deterioration, internal resistance increase, heat accumulation and self-discharge are accelerated, adversely affecting the life-span and performance of the devices. In other words, high temperature alters the compatibility of the cell components that are kinetically compatible and stable at room temperature, leading to more dynamic interaction(s), as a consequence of increased reactivity.

4) The performance and life cycle are highly dependent on the kinetic stability resulting from the synergetic interactions between the cell components. The replacement of a single

component with a thermally resistant material might reduce or minimize the added stability gained by the solid-electrolyte interphase (SEI) effect, for example, and would not necessarily lead to the thermal enhancement of the device overall.

5) The higher chemical reactivity of materials at elevated temperatures also causes increased corrosion of the non-active materials of the battery such as the current collectors, packaging container, circuits, insulators, and sealing, etc. These materials are important to the integrity of the energy storage cell performance. The degradation of such materials at high temperatures is destructive to the long-term performance and service life of the EES devices.

The above-mentioned challenges are diverse and multifaceted. Existing energy storage devices do not address all of these issues. In fact, tackling any one of them requires a thorough understanding of the failure and aging mechanisms at high temperatures as well as advances in new materials discovery or optimization – thus significant opportunities exist for basic and applied research. A variety of new or existing techniques, both post-term and in-situ, are being employed to investigate thermally-induced device performance reduction and to characterize the degradation products formed in the electrolyte or at the surface of the electrode. While many of the reactions or degradation mechanisms are still not clear, due to the complex nature of the co-existence of various species, as well as different materials utilized in different cell types with different chemistry, considerable efforts are devoted to gain a deeper understanding.⁵⁹ The reader is referred to excellent reviews by Bandhauer et al.⁶⁰ and by Choi et al.¹⁰ for additional information. Here, we will focus our discussion on the limitation of the electrolyte solvent, salt, electrode, and separator at high and elevated temperatures.

4.1 Limitations of traditional materials

Electrolyte solvent. While electrode materials determine the energy density of EES devices, electrolytes profoundly affect the rate capability and cell kinetics.^{61, 62} The electrolyte consists of a solvent that is a high dielectric medium and a salt. The operation of the electrodes in a cell requires suitable electrolyte with the following desired characteristics: 1) wide electrochemical window, within which the electrolyte is kinetically stable with the electrode couples; 2) high ionic conductivity to facilitate ion(s) transport between the electrodes and low electronic conductivity to inhibit self-discharge; 3) chemical and thermal stability in order for the electrolyte to be compatible with other cell components such as separators, electrodes, etc.; 4) non-flammability and low vapor pressure to avoid cell pressure build-up and fire in case of battery failure; 5) low toxicity; and 6) low cost.

Aqueous electrolytes are inexpensive and have high ionic conductivities, and were widely used before the emergence of non-aqueous solutions. However, the low decomposition voltage of aqueous electrolytes (1.5 V vs. Li/Li⁺) limits the operation voltage, thus motivating researchers to pursue new electrolytes with performance at higher voltages. In 1994 Tarascon and Guyomard discovered an optimized formulation using a blend of dimethyl carbonate (DMC) and ethylene carbonate (EC) which provides low viscosity and high dielectric constant.⁶³ This combination of solvents affords up to 5.0 V of electrochemical stability towards spinel cathodes and prolonged lifetime due to the formation of a stable SEI on the graphite anode. This materials discovery was quickly adopted by the battery community and industry, and this electrolyte is used in billions of lithium-ion batteries manufactured today. The linear carbonate can be replaced with diethyl carbonate (DEC), ethylmethyl carbonate (EMC), and propylmethyl carbonate (PMC), but these solvents exhibit either low boiling points or low flash points (Table 2), which limit their use for high temperature applications.⁶⁴⁻⁷⁰ Supercapacitors employ acetonitrile or an organic carbonate solvent with quaternary ammonium salts as the electrolytes, and, therefore, possess similar elevated and high temperature operational limitations as batteries. For example, the boiling point of acetonitrile is only 82 °C, near or above this temperature the solvent begins to evaporate and increase the internal cell pressure. In

addition, the flash points of the linear carbonate solvents are generally below 30 °C, resulting in a cell highly susceptible to ignition during a short-circuit.⁷¹

Besides the commonly used carbonate solvents shown in Table 2, γ -butyrolactone (GBL) based solvents with increased thermal stability are also being used and exhibit greater tolerance to operation at high temperatures. The melting point, boiling point, and flash point of gamma-butyrolactone are -44, 204 and 101 °C, respectively.⁷² An exothermic reaction was found from differential scanning calorimetry (DSC) profile above around 200 °C.^{73, 74}

The properties of commonly seen electrolyte solvents are summarized in Table 2. Despite the excellent performance of carbonate solvents in energy storage devices operating at ambient temperature, their instability at elevated to high temperatures limits their use in more temperature demanding applications. Another limitation of the carbonate-based electrolyte solvents is their narrow operation voltage window. They undergo continuous oxidative decomposition during cycling and form non-passivating SEI on the electrodes at operation beyond 4.3 V. The overall safety concern when using these flammable solvents is further exacerbated when operation is performed beyond their stable voltage limits and at high temperatures. To address these limitations, ionic liquids are being explored to replace the carbonate solvents as safe and stable electrolyte solvents. The detailed discussion on ionic liquids is forthcoming in Section 5.

Table 2. Common electrolyte solvents in energy storage devices.⁶¹ Adapted from ref. 61. Copyright 2004 American Chemical Society.

Name	Structure	M _w	T _m (°C)	T _b (°C)	η (cP, °C)	ϵ (25°C)	Dipole Moment (Debye)	T _f (°C)	d (g/mL, 25°C)
Ethylene Carbonate (EC)		88	36.4	248	1.90 (40°C)	89.78	4.61	160	1.321
Propylene Carbonate (PC)		102	-48.8	242	2.53	64.92	4.81	132	1.200
Dimethyl Carbonate (DMC)		90	4.6	91	0.59 (20°C)	3.107	0.76	18	1.063
Diethyl Carbonate (DEC)		118	-74.3	126	0.75	2.805	0.96	31	0.969
Ethylmethyl carbonate (EMC)		104	-53	110	0.65	2.958	0.89	27	1.006
γ -Butyrolactone (GBL)		86	-43.5	204	1.73	39	4.23	97	1.199

Salt. The conventional salt being used with the carbonate solvents, lithium hexafluorophosphate (LiPF₆), also limits battery usage at high temperatures.^{66, 75-77} LiPF₆ is by far the most widely used salt in commercial batteries because LiPF₆ possesses a high conductivity of 10 mS · cm⁻¹ in a 1.0 M solution of EC and DMC at room temperature, and it is able to form an SEI at the surface of graphite, kinetically stabilizing the anode and prolonging the life cycle.⁷⁸ However, it thermally decomposes starting at 50 °C and the degradation increases dramatically from 70 °C to 130 °C. Furthermore, LiPF₆ is reported to undergo an autocatalytic decomposition into lithium fluoride (LiF) and PF₅, with further hydrolysis to afford toxic hydrogen fluoride (HF).⁷⁹ This process occurs in the presence of trace amounts of moisture and/or above 60 °C.⁷⁹ Although hydrolysis cannot proceed completely without a

sufficient amount of water (<25 ppm), trace quantities of water can start hydrolysis, only with a slight increase in temperature, for instance from 25 to 35 °C.⁷¹ In addition to hydrolysis, LiPF₆ undergoes polymerization and alkoxylation reactions in the presence of carbonate solvents, giving decomposition products including dialkylethers (R₂O), phosphorus oxyfluoride (OPF₃), fluorophosphates (OPF₂OR, OPF(OR)₂), fluorophosphoric acid (OPF₂OH, OPF(OH)₂) and phosphorus polyethylene glycol (Figure 3).^{71, 75} These processes result in dissolution of the electrode materials and subsequent capacity loss.

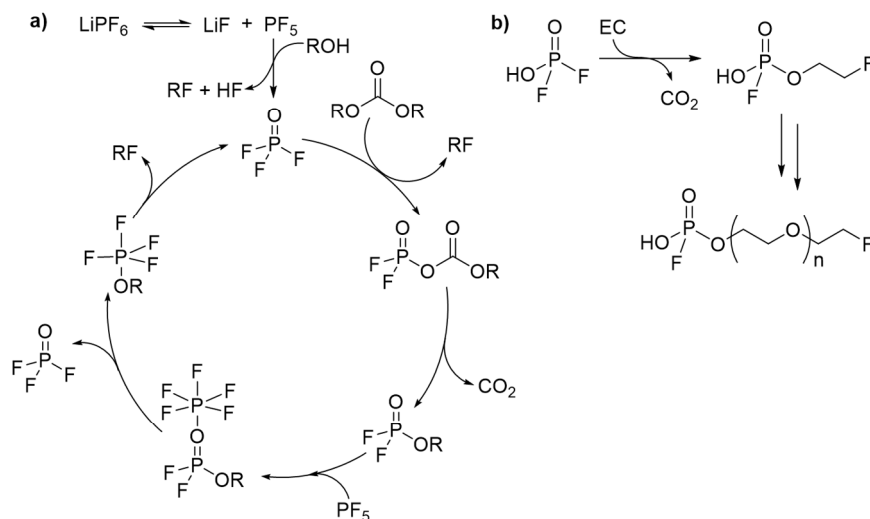
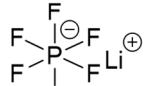
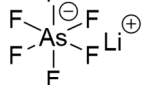
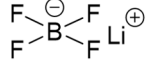
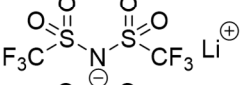
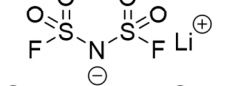
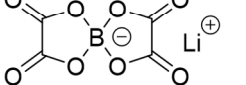


Figure 3. Decomposition mechanism of LiPF₆.^{75, 80} Adapted from ref. 74 and 79. Copyright 2005 The Electrochemical Society and 2015 Elsevier.

In contrast, lithium bisoxalatoborate (LiBOB) exhibits a lower conductivity of 4.5 mS · cm⁻¹ in a similar combination of solvents (Table 3). However, it is thermally stable up to 300 °C.⁸¹ It is also capable of forming a stable passivation layer on aluminum, which is used as the current collector, and on graphite anodes, inhibiting exfoliation of the intercalant material by the solvent. This improves the overall battery cycling stability. Lithium bistrifluoromethane sulfonimide (LiTFSI) is a new promising salt for high temperature operation.⁸²⁻⁸⁴ It possess a conductivity comparable to that of LiPF₆, thermal stability up to 250 °C, and forms a stable passivation layer on graphite and lithium metal. All of these salts are sensitive to the presence of impurities such as water, which decreases cycling efficiency and increases capacity fade, and it can also react with lithium metal and release hydrogen gas. The properties of other common salts as possible electrolyte salts for Li-ion batteries are summarized in Table 3.⁸⁵ The selection of an appropriate lithium salt is key to the thermal stability, electrochemical stability, conductivity, and compatibility with other parts (current collector, separators, etc.) of the electrolyte.

Table 3. Common lithium-ion conducting salts used in EES.

Salt	Structure	M _w (g/mol)	T _d (°C)	Conductivity (mS/cm)
LiPF ₆		151.98	107	10.7 EC:DMC = 1:1
LiAsF ₆		195.85	475	11.1 EC:DMC = 1:1
LiBF ₄		94.02	320	4.9 EC:DMC = 3:7
LiTFSI		286.93	360 236(melts)	9.4 EC:DMC = 1:1
LiFSI		187.06	200 145(melts)	9.7 EC:EMC = 3:7
LiBOB		193.98	306	4.5 EC:EMC = 1:1

Electrodes. Electrodes are the focus of intensive research since the electrode couple determines the cell chemistry and the maximum amount of energy the device can store. The cathode materials are classified into layered, spinel, and olivine structures. LiCoO₂ is the most common layered cathode material. Its discovery by John Goodenough in 1979 revolutionized rechargeable batteries, and it is the cathode material of choice.⁸⁶ LiCoO₂ possesses an average potential of 3.6 V relative to Li/Li⁺ in carbon, and a specific capacity of 140 mAh · g⁻¹, affording an energy density of about 0.5 kWh · kg⁻¹. Although ubiquitous in batteries, LiCoO₂ cathodes are known to become unstable in their delithiated states, particularly at high temperatures. Oxygen is released from the LiCoO₂ above 200 °C and becomes hazardous in presence of volatile electrolyte solvents.^{76, 87-91}

a)

Framework	Compound	Specific capacity (mAh/g)	Average potential (V vs Li^0/Li^+)
Layered	LiCoO_2	272 (140)	4.2
	$\text{LiNi}_{1/3}\text{Mn}_{1/3}\text{Co}_{1/3}\text{O}_2$	272 (200)	4.0
Spinel	LiMn_2O_4	148 (120)	4.1
	$\text{LiMn}_{3/2}\text{Ni}_{1/2}\text{O}_4$	148 (120)	4.7
Olivine	LiFePO_4	170 (160)	3.45
	$\text{LiFe}_{1/2}\text{Mn}_{1/2}\text{PO}_4$	170 (160)	3.4/4.1

b)

Layered LiCoO_2 Spinel LiMn_2O_4 Olivine LiFePO_4

Figure 4. a) Electrochemical characteristics of three classes of insertion compounds; b) crystal structures of three lithium-insertion compounds.⁹² Adapted from ref. 91. Copyright 2014 MDPI AG.

Among the various cathode materials, LiFePO_4 and LiMn_2O_4 show promise for use at elevated and high temperatures.⁹³⁻⁹⁶ While no oxygen is released below 400 °C from LiMn_2O_4 , it becomes a poor lithium-ion intercalant switching from $\lambda\text{-MnO}_2$ to $\beta\text{-MnO}_2$ above 190 °C. LiFePO_4 exhibits a voltage of 3.3 V, a specific capacity of $150 \text{ mAh} \cdot \text{g}^{-1}$, and an energy density of $0.5 \text{ k Wh} \cdot \text{kg}^{-1}$, comparable to LiCoO_2 . The PO_4 structure is more stable than the MO_2 structure at high temperatures, reducing the likelihood of oxygen-evolution and, thus, improving safety. Upon charging, lithium ions leave LiFePO_4 , forming FePO_4 . LiFePO_4 possesses several advantages over other cathode materials, including high thermal stability up to 300 °C.⁹⁷ Also, the strong P-O covalent bonds in $(\text{PO}_4)^{3-}$ of LiFePO_4 significantly reduce the rate of O_2 release. Additionally, iron is cheap and earth-abundant. The major drawback of working with LiFePO_4 is the poor electronic conductivity ($10^{-9} \text{ S} \cdot \text{cm}^{-1}$). This was improved by Chiang et al. demonstrating an increase of almost 10^8 in conductivity for a LiFePO_4 material by polyvalent cation doping and incorporation of nanosized particles.⁹⁸ LiFePO_4 is less reactive at high temperatures than spinel and layered cathode materials as measured by DSC (Figure 5c, in the presence of $1.2 \text{ mol} \cdot \text{L}^{-1} \text{ LiPF}_6$ in EC-EMC (3:7) electrolyte). Figure 5b shows the DSC profiles of LiMn_2O_4 at various voltages. Dashed lines are from the LiCoO_2 sample at the indicated voltage for a comparison. LiMn_2O_4 exhibits improved thermal stability over LiCoO_2 . The occurrence of the exothermic peaks is dependent on the charged voltage and in general higher voltage leads to weaker thermal stability. The DSC profiles of LiMn_2O_4 charged to 4.2, 4.4, and 4.6 V are very similar because minimal lithium remains in the structure at these voltages, and, thus, the electrodes are almost identical. Although LiMn_2O_4 at 4.2, 4.4, and 4.6 V display an initial thermal instability near 220 °C, it does not release the majority of heat until a temperature of 280 °C. The thermal behavior of other cathode materials which exhibit inferior thermal

stability have also been studied and include, for example, LiNiO_2 , $\text{Li}_2\text{FeSiO}_4$, LiVPO_4F , $\text{LiNi}_{0.8}\text{Co}_{0.2}\text{O}_2$, $\text{Li}_{1.1}[\text{Ni}_{1/3}\text{Mn}_{1/3}\text{Co}_{1/3}]_{0.9}\text{O}_2$, LiCoPO_4 , LiMnPO_4 , and $\text{LiMn}_{1.5}\text{Ni}_{0.5}\text{O}_4$, etc., (Figure 5a).^{77, 93, 99-103}

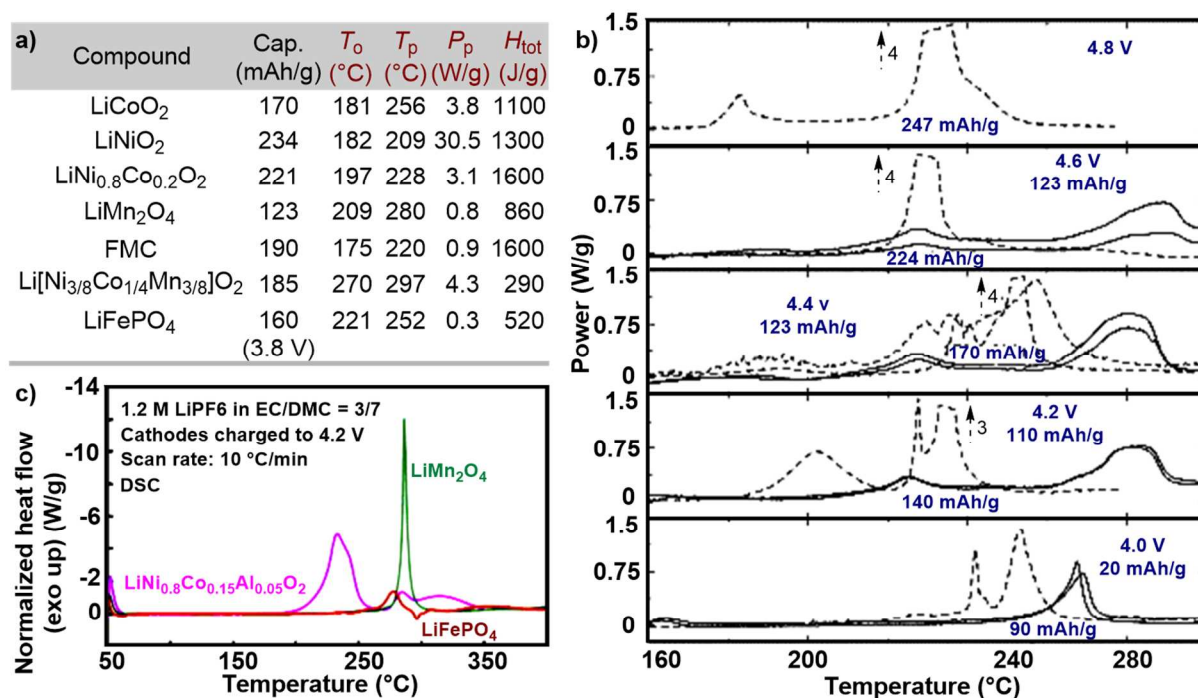


Figure 5. a) Analysis of DSC profiles (T_o : onset temperature; T_p : peak temperature; P_p : peak power; H_{tot} : total evolved heat);⁹³ b) DSC profiles of LiMn_2O_4 charged to indicated voltages (solid lines). Duplicate scans are from a nominally identical sample, while dashed lines are from the LiCoO_2 sample at the indicated voltage;⁹³ c) DSC spectra of over-charged layered, spinel and olivine cathodes with traces of 1.2 mol \cdot L $^{-1}$ LiPF_6 in EC-EMC (3:7) electrolyte at 10 $^{\circ}\text{C} \cdot \text{min}^{-1}$.¹⁰⁴ Adapted from refs. 92 and 103. Copyright 2002 and 2012 Elsevier.

While the cathode can produce appreciable amount of heat due to the release of oxygen at high temperatures (usually above 200 $^{\circ}\text{C}$, see discussion of thermal runaway below), the anode and its reaction with the electrolytes can occur at much lower temperatures. The melting temperature for lithium metal is 180 $^{\circ}\text{C}$, which is a thermal limit for the traditional Li-metal batteries, as well as advanced battery systems such Li-S battery or Li-air battery. For common Li-ion batteries, despite graphite's high thermal stability,¹⁰⁵ the carbon anodes may react with the electrolytes and the polymer binders decompose at elevated temperatures.¹⁰⁶⁻¹⁰⁸ The formation of the SEI is another important criterion associated with the thermal stability of the anode.^{62, 109-111} The formation of a SEI at the cathode will not be examined in this review, due to limited research reports. In a typical Li-ion battery, the SEI is formed during the initial charging process of a fresh lithium-ion cell using a graphite anode and an ethylene carbonate/ LiPF_6 -based electrolyte in the potential window 0.6 - 1.3 V versus Li/Li^+ .^{112, 113} It is commonly agreed that the conventional SEI formed on graphite is generally composed of organic components and some inorganic components, such as LiF , Li_2O , and Li_2CO_3 ; these inorganic components are insulators to both Li^+ ions and electrons.^{78, 114} The multilayered, mosaic-structured SEI on the graphite anode protects against the highly reactive electrolytes, typically undergoing decomposition at temperature 70 $^{\circ}\text{C}$ or greater. Continued decomposition and re-growth of the protective layer result in the consumption of both electrolyte and anode materials. These reactions accelerate the battery capacity loss and cause exothermic reactions that eventually

lead to thermal runaway. The composition of SEI depends on the anode and electrolyte materials used, thereby the thermal decomposition temperature also changes when new materials are employed. Considerable research is ongoing focused on understanding the SEI compositions with newly formulated anode/electrolyte combinations and on the development of a stable artificial solid electrolyte interphase to stabilize the lithiated graphite and improve both safety and cycling performance.

Separator. A separator is a porous membrane placed between electrodes of opposite polarity that is permeable to ionic flow but prevents electrical contact of the electrodes.¹¹⁵ Materials such as polymer membranes (e.g. polyethylene (PE), polypropylene (PP), poly(tetrafluoro-ethylene) (PTFE), poly(vinyl chloride) (PVC) and nonwoven fibers (e.g., cellulose, polyesters), are widely used as separators in batteries that operate at elevated high temperatures (<150 °C).^{115, 116} The separators need to be chemically and electrochemically inert to all other cell components including the electrodes and electrolytes. In addition, the pore size of the separator needs to enable ion flow. Commercial membranes possess a pore size in the range of 0.03 - 0.1 µm, and porosity of 30 - 50%. The most commonly used separators are comprised of PE, PP, or combinations thereof. However, as the operational temperature approaches the melting point of the polymers, 135 °C for PE and 165 °C for PP, the pores close and the battery stops performing. To overcome this limitation, ceramics such as SiO₂, Al₂O₃, CaCO₃ were coated or added as a filler to the polymer separator to increase the working temperature range. For example, SiO₂ and Al₂O₃ were coated onto a porous polyethylene terephthalate (PET) which increased the melting temperature to 220 °C.^{117, 118} Porous membrane separators have also been fabricated from ceramic particles.^{115, 116} Recently, Carvalho et al. prepared a separator using SiO₂ bonded with hydroxypropyl guar gum (HPG) and this membrane is stable up to a temperature of ~240 °C in N₂ and ~200 °C in O₂.¹¹⁹

Others (binder, sealing). In addition to the essential components described above, other seemingly trivial assembling components such as binder, cell casing, and the sealing material also play key roles in cell performance at elevated or high temperatures. PVDF is widely used as a binder for electrode materials because of its good electrochemical stability and strong adhesion to the electrodes and current collectors. However, at elevated temperatures, PVDF reacts with lithiated graphite (Li_xC₆) and metal lithium to form the more stable LiF and unsaturated >C=C-F- bonds.^{106, 107, 120, 121} In addition, PVDF can dissolve and swell in non-aqueous liquid electrolytes, especially at elevated temperatures, thus compromising the electrode integrity. As a result of PVDF swelling or dissolving, adhesion of the electrode materials to the current collector deteriorates causing an increase in the contact resistance between electrode materials and ultimately battery failure. Therefore, alternative binder that can overcome these drawbacks is needed.

In addition, high temperature tolerant adhesives are also needed to seal the joining materials on casing. Glass and metal adhesives are commonplace but they tend to be weak at elevated temperatures. Chemically bonded adhesives such as chalcogenide sealants (e.g., CaAl₂S₄) were developed to meet high temperature requirements and were proven successful in Li-FeS₂ batteries demonstrating 400 cycles with less than 10% capacity loss at 425 °C.¹²²

4.2 Stepwise thermal changes at elevated to high temperatures

The physicochemical and electrochemical properties of the above-mentioned materials are temperature dependent, and are susceptible to thermal damage. While understanding the thermal response of the individual cell components is crucial, thermal behavior of the whole cell should also be studied under various applied voltage and current rates to characterize the synergistic interactions between the cell components. These studies also reflect the thermal changes occurring in a real scenario.¹²³⁻¹³¹ Using extended volume accelerating rate calorimetry (EV-ARC), incremental capacity analysis (ICA), DSC and TGA to characterize battery aging, the heat released with increasing temperature and the onset temperature of the exothermic

chemical reactions can be determined. For example, Figure 6 shows the thermal processes ongoing within a 550 mAh prismatic Li-ion cells with a Sn-doped LiCoO_2 cathode and graphitic carbon anode in the presence of a 1 M LiPF_6 in EC:DMC:DEC electrolyte. PVDF was used as the binder.¹²⁹

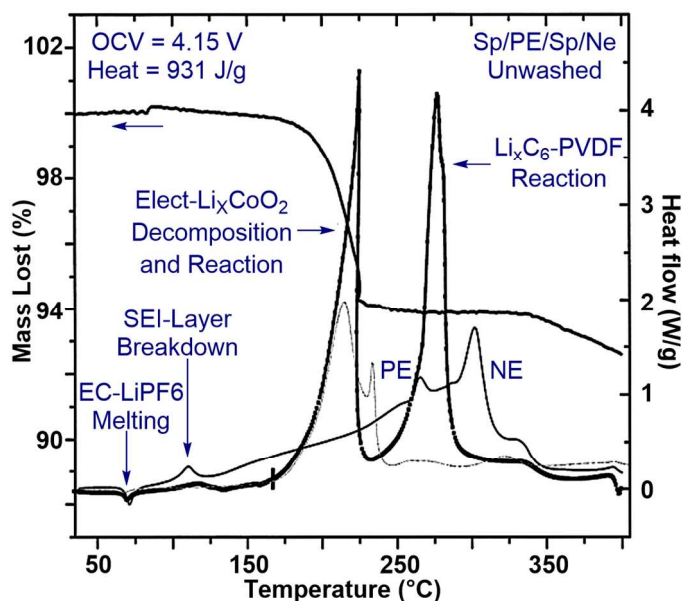


Figure 6. DSC and TGA scans of anode (negative) graphite and cathode (positive) LiCoO_2 after 100 % charging. (PE: positive electrode; NE: negative electrode).¹²⁹ Adapted from ref. 128. Copyright 1999 The Electrochemical Society.

The specific thermal response of cells composed of different electrode and electrolyte materials as well as the cell type and configuration will clearly vary. In addition the surface area of the anode, the amount of electrolyte, and state-of-charge (SOC) will also affect the decomposition temperature. Here we provide a general step-by-step process to guide our discussion and understanding of the thermal changes occurring within a conventional battery upon increasing the temperature.^{123, 129, 130}

I. In the first step, the capacity starts to fade at temperatures higher than 50 °C due to the increasing dissolution of active materials from the electrodes into the electrolyte solvent. This results in an increase of the electronic conductivity and, in turn, the rate of self-discharge.

II. In the second step, SEI decomposition begins with release of heat around 100 °C.

III. The negative and positive electrode material reacts exothermically with the solvent at temperatures above 150 °C, with the reaction peaking near 200 °C although this reaction may be complicated due to the presence of the salt, typically LiPF_6 . Fluorinated binders can also react with the lithiated carbon, but this usually does not occur because the reaction between the negative electrode and the electrolyte occurs first, depleting the available lithium. Heat generation from the cathode is usually greater than from the anodes at a fully charged state because of the oxygen evolution from the cathode lattice above 200 °C.

IV. In the next step, the separator begins to melt between 120 and 140 °C, and eventually, the melted separator will lead to a short circuit, generating additional heating.

V. In step five, electrolyte decomposition is evident (>200 °C).

VI. In step six between 140 and 240 °C, the cathode materials begin to react with the electrolyte and release heat.

VII. Finally, the aluminum current collector melts at 660 °C, along with decomposition of the binder and sealer.

These degradation processes occur over a wide temperature range as well as several degradation reactions can occur simultaneously, further complicating the analysis. Therefore, for high temperature applications, not only will self-discharge and capacity loss be evident, but also thermal runaway develops as substantial heat is generated within seconds from the latter steps at higher temperatures. The consequences are particularly significant in scale for large format batteries.

5. Development of New Materials for Thermally Stable Electrical Energy Storage Devices

The discovery of new thermally stable materials is at its infancy for battery applications despite market demand. These advanced materials may arise from exploratory basic research or result from clever combinations of existing materials to improve overall elevated and high temperature battery performance. Individual cell components are being developed for high temperature use, with electrolyte materials being one of the major ones for improvement. Current electrolytes prevent operation at elevated temperature ranges. The electrolyte performs a central role in energy storage devices as it directly contacts with every essential component in the cell, hence, the effect of temperature is paramount. Therefore, this review places an emphasis on the electrolytes and the recent advances in the development of thermally stable electrolytes and their demonstrative use in batteries and supercapacitors. Specifically, EES that demonstrated elevated to high temperature performance with three classes of electrolyte materials, namely ionic liquids, solid polymer electrolyte and ceramics are discussed. Several examples also describe blended electrolyte solutions to explore the combined advantages or enhanced properties at elevated temperatures. Materials that are potentially thermally stable but not employed in high temperature EES are not discussed or in limited detail. Aqueous electrolytes are also investigated in EES at elevated to high temperatures (40 - 80 °C). For example, Meng et al.¹³² reported the increase in specific capacitance from 128 F · g⁻¹ at 20 °C to 162 F · g⁻¹ at 60 °C (with current density of 1 A · g⁻¹) with a supercapacitor consisting of a 1.0 M KOH electrolyte and porous Fe₃O₄/carbon composite electrodes. These aqueous electrolyte systems are limited by the boiling point of water, and are not suitable for use at temperatures higher than 100 °C. Thus, they will not be a focus of this Review.

5.1 High temperature electrolytes

5.1.1 Reformulated carbonate solvents. Individual carbonate based electrolytes are known to be volatile and flammable (Table 2). However, this exothermic phenomenon can be suppressed by mixing multiple carbonate solvents together. The thermal stability of various carbonate solvent mixtures was recently re-investigated.¹³³ Among the selected solvents of EC, PC, DMC, DEC, DME and the combination of them, the EC:PC mixture displayed an onset temperature of exothermic process at nearly 250 °C, representing the highest thermal stability of a conventional carbonate solvent (Figure 7a).¹³³ Using this particular combination of carbonate electrolyte, a calcium-based battery successfully operated at 100 °C.¹³⁴ At relatively high temperatures (50 - 100 °C), the EC:PC mixture with dissolved Ca(BF₄)₂ enabled reversibly plating and stripping between -1 to 0 V (vs. Ca²⁺/Ca). The potential shifts depended on the temperature and salt concentration used, while interestingly no such reversible peaks are observed at room temperature or when using other calcium salts. A symmetric Ca/Ca cell demonstrated 30 repeated cycles with 0.45 M of Ca(BF₄)₂ in EC:PC at 100 °C without considerable decay (Figure 7b). The electrolyte is electrochemically stable at 100 °C between -0.5 to 3.5 V (vs. Ca²⁺/Ca), with a decrease in the current intensity during the initial CV cycles and then remaining constant afterwards. This finding is an indication of a gradual formation of an SEI (Figure 7c), the composition of which is mostly CaF₂ as determined by energy-dispersive X-ray analysis (EDX). Thus, high temperature in this case kinetically increased the rate of electroplating and stripping, while posing no noticeable impact on the electrolyte decomposition.

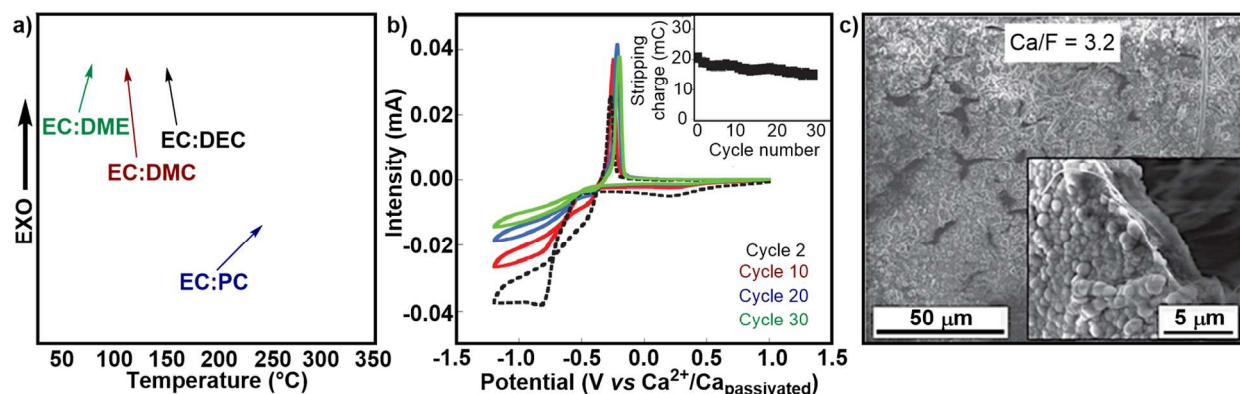


Figure 7. (a) DSC heating curves up to 350 °C of solvent mixtures;¹³³ (b) cyclic voltammograms (100 °C, 0.2 mV · s⁻¹) of a calcium deposit (grown by potentiostatic electrodeposition at -1.2 V versus Ca²⁺/Ca passivated, 5 h, 100 °C) in 0.45 M Ca(BF₄)₂ EC:PC electrolytes;¹³⁴ (c) SEM micrographs of deposits obtained in 0.3 M Ca(BF₄)₂ EC:PC at -1.5 V versus Ca²⁺/Ca passivated at 100 °C for 200 h.¹³⁴ Adapted from refs. 131 and 132. Copyright 2012 Royal Society of Chemistry and 2016 Macmillan Publishers.

5.1.2 Ionic liquids. Ionic liquids are salt-like materials bonded through ionic interactions, which have melting points below 100 °C. Despite being around since the early 1900s, this class of materials is undergoing a renaissance in interest due to their remarkable use as solvents and as functional materials.¹³⁵⁻¹⁴⁶ Ionic liquids are composed of one or more organic cationic centers, such as an imidazolium, pyridinium, pyrrolidinium, phosphonium, ammonium or sulfonium, and one or more inorganic or organic anions, such as alkyl sulfate, methanesulfonate, tosylate, hexafluorophosphate, tetrafluoroborate, halide or carboxylic acid. For example, the prototypical IL, 1-ethyl-3-methylimidazolium chloride, possesses a melting point of 77 °C, whereas NaCl has a melting point of 801 °C. The strong ionic interactions within ionic liquids result in negligible vapor pressure, non-flammable materials with high thermal, mechanical, electrochemical stability. Consequently, ionic liquids are being investigated for a wide range of use as “green” solvents, separation media, liquid crystals, thermal fluids, and electrolyte solvents.

The wide range of possible cation and anion combinations allows for a large variety of structures and compositionally dependent properties. Within this family of materials, several ionic liquids display melting temperature below room temperature, and hence are referred to as room temperature ionic liquids (RTIL).¹⁴⁷⁻¹⁵⁴ RTILs are promising electrolytes for batteries, supercapacitors, and fuel cells. Among them, imidazolium, piperidinium, and ammonium cations are extensively studied and combined with different cathodes and anodes. The majority of research efforts are devoted to room temperature studies, with or without additives.^{150, 155-159}

It is well known that one of the shortcomings of IL electrolyte solvents is their relatively low conductivities compared to carbonate based organic solvents. This low conductivity originates from their higher viscosities (ranging from several mPa · s to the order of Pa · s). In contrast to the 0.1 mS · cm⁻¹ of benchmark conductivity of a carbonate-based electrolyte, most ILs exhibit conductivities from 10⁻⁵ to 10⁻³ S · cm⁻¹ at room temperature. In addition, the high viscosity of the ILs leads to poor wetting with the electrodes. Therefore, significant efforts are underway to increase the conductivity of ILs, including means such as varying the chemical structure and doping with organic solvents. Several excellent reviews highlight the intensive research efforts being made on ILs in batteries, supercapacitors, and fuel cells, particularly at room temperatures and the reader is referred to these reviews.^{61, 62, 136, 148-150, 152, 154} The use of ILs also expands the anodic potential of electrolyte materials, thus enabling the utilization of high voltage cathodes. Improved conductivities could significantly address the low power density observed with ILs based systems at room temperature.

One strategy to decrease the viscosity (lowering the flow activation energy) of the IL is to increase the temperature. At higher temperature, the conductivity is also improved, enhancing the electrolyte performance. For example, an ether substituted ionic liquid N-methoxyethyl-N-methylpyrrolidinium bis(trifluoromethanesulfonyl)-imide (PYR_{1,201}-TFSI) possess a conductivity value of 1.9 mS · cm⁻¹ at room temperature, which increases to 6.7 mS · cm⁻¹ at 60 °C. This value is comparable to that of the carbonate based solvents (5 - 10 mS · cm⁻¹).¹⁶⁰ Cyclic and linear sulphites, specifically ethylene sulphite (ES) and dimethyl sulphite (DMS) when blended with PYR_{1,201}-TFSI, enable cycling in Li/MCMB and Li/LiFePO₄ based battery up to 60 °C (Figure 8).

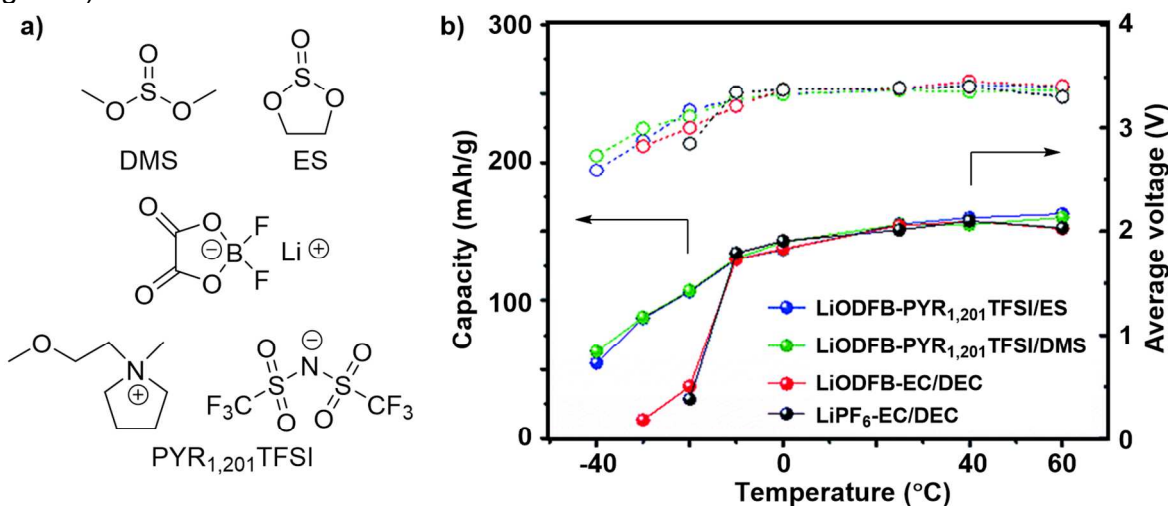


Figure 8. Molecular structures of the mixture components: dimethyl sulphite (DMS), ethylene sulphite (ES), N-methoxyethyl-N-methyl-pyrrolidinium bis(trifluoromethanesulfonyl)-imide (PYR_{1,201}-TFSI) and lithium difluoro(oxalate)borate (LiODFB); (b) Li/LiFePO₄ cells containing LiODFB-PYR_{1,201}-TFSI/ES, LiODFB-PYR_{1,201}-TFSI/DMS, LiODFB-EC/DEC or LiPF₆-EC/DEC electrolytes at various temperatures with a current density of 0.1C.¹⁶⁰ Adapted from ref. 158. Copyright 2015 Royal Society of Chemistry.

Shin et al.^{161, 162} also reported battery cycling with a blend of a *N*-methyl-*N*-propylpyrrolidinium bis(trifluoromethanesulfonyl)imide (PYR13-TFSI) ionic liquid and a polyethylene oxide salt P(EO)₂₀LiTFSI electrolyte in a Li/LiFePO₄ cell configuration at slightly elevated temperatures (40 - 60 °C). The free-standing film, prepared by hot-pressing the two salts with the polymer, exhibited low capacity loss (< 0.06% per cycle) over 500 cycles at 40 °C, with varied current rates from C/20 to 2C. Addition of 30 wt% IL to the neat polymer film increased the conductivity by an order of magnitude and the corresponding 150 wt% IL composition exhibited a conductivity of 10⁻³ S · cm⁻¹ at 40 °C. Operation at elevated temperature decreased the viscosity of the corresponding mixture and resulted in increased specific capacity by about 10 times from 20 °C to 60 °C.

Blending SiO₂ with a pyrrolidinium ionic liquid, specifically *N*-butyl-*N* methyl pyrrolidinium bis(trifluoromethanesulfonyl)imide (PP14-TFSI), afforded a quasi-solid-state Li⁺ conducting electrolyte as the SiO₂ serves as a solid matrix to immobilize the IL using a sol-gel route (Figure 9a).¹⁶³ The thermal decomposition of this electrolyte system occurred above 390 °C, which increased the degradation temperature by 30 °C compared to the neat ionic liquid. The addition of SiO₂ also enhanced the mechanical strength of the electrolyte and afforded a free-standing membrane as the electrolyte, without significant conductivity decrease and the use of extra separators. An assembled Li/LiFePO₄ half-cell underwent charge-discharge cycles at 40 °C and 55 °C, with a high coulombic efficiency approaching 100%. The capacity increased as the

operational temperature increased due to the conductivity change, as evidenced by the impedance decrease upon changing the temperature from 40 to 50 °C. The cells cycled without noticeable capacity loss over more than 30 times, yet a gradual increase in impedance occurred over the cycles, as determined via electrochemical impedance spectroscopy (EIS). Specifically, the impedance increased from 130 Ω to 200 Ω at 40 °C from the 3rd to 31st cycles, however, parallel cycling revealed that the impedance increased from 110 Ω to 300 Ω at 55 °C (Figure 9b). The authors concluded that thermal damage caused the impedance increase and might ultimately lead to faster capacity loss and shorter lifecycle, although high temperatures increased the conductivity of the electrolyte material and allowed the corresponding cell to generate a higher capacity.

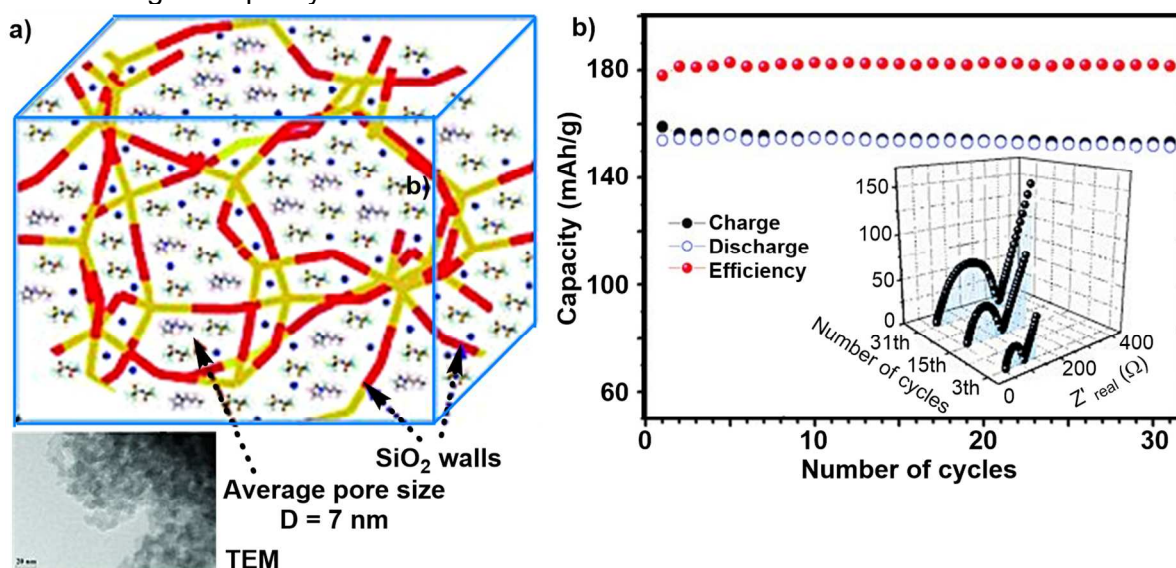
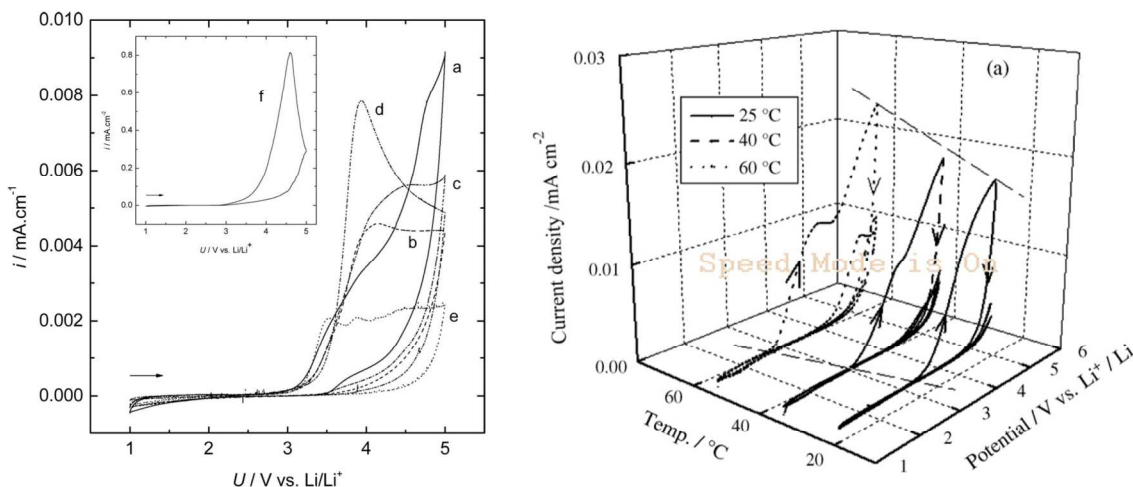


Figure 9. a) Schematic representation of the PP14-TFSI+SO₂ pore transporter and TEM image of mesoporous SiO₂ matrices; b) cycling performance of cells at 55 °C. Inset: Impedance spectra of cells discharged to 2.5 V after selected cycles at the two operating temperatures.¹⁶³ Adapted from ref. 161. Copyright 2011 Wiley-VCH.

LiTFSI is widely used in batteries as a novel thermally stable salt replacing LiPF₆. However, it is known that severe corrosion of the aluminum (Al) cathode current collectors occurs above 3.5 V vs. Li/Li⁺ when LiTFSI is used with carbonate based solvents.¹⁶⁴ Ionic liquids are reported to mitigate the aluminum corrosion. For example, Garcia et al.¹⁶⁵ found that Al corrosion is not as extensive when using ionic liquid electrolytes due to the poor dissolution of the as-formed Al-TFSI complex in the ionic liquids. Whether the same Al corrosion suppression effect in ILs stands at elevated temperatures is of importance to the development of high temperature electrolytes. Consequently, Nadherna et al. studied two ionic liquids, 1-butyl-2,3-dimethylimidazolium bis(trifluoromethanesulfonyl)imide (BMMI-TFSI) and 1-butyl-1-methylpyrrolidinium bis(trifluoromethanesulfonyl)imide (PYR14-TFSI) in the presence of LiTFSI at 60 °C (Figure 10a).¹⁶⁶ The electrolytes exhibited ionic conductivities of 3.3 mS · cm⁻¹ and 4.5 mS · cm⁻¹, respectively. Importantly, the IL electrolytes showed good stability (~ 3.0 V) towards the aluminum - still comparable to 1M LiPF₆ in EC:DEC at elevated temperature, as determined by cyclic voltammetry. In addition, no discernable differences in performance are noted between the two ILs, whether the electrolyte contained LiPF₆ or LiTFSI. This stability is even greater when the ILs are evaluated against an aluminum current collector covered with carbon black and binder (as a blank electrode without active compounds) and the anodic voltage extended to about 4.0 V. This observation agreed with the findings reported by Peng et al. in 2007, which

showed that increasing the temperature from 25 to 60 °C shifted the anodic oxidation potential of 1-butyl-3-methylimidazolium bis[(trifluoromethyl) sulfonyl] amide (BMI-TFSI) from 3.5 V to 2.9 V (first cycle, Figure 10b).¹⁶⁷

Figure 10. left) Cyclic voltammograms of the aluminum current collector in six different electrolytes. a: PYR14-TFSI with LiTFSI, b: PYR14-TFSI with LiPF₆, c: BMMI-TFSI with LiTFSI, d: BMMI-TFSI with LiPF₆, e: 1 M LiPF₆ in EC-DEC, and f: 1 M LiTFSI in EC-DEC at 0.5 mV s⁻¹



scan rate;¹⁶⁶ right) cyclic voltammograms for Al foil electrode in 1 M LiTFSI/BMI-TFSI at 25, 40 and 60 °C (sweep rate: 10.0 mV s⁻¹).¹⁶⁷ Adapted from refs. 164 and 165. Copyright 2009 The Electrochemical Society and 2007 Elsevier.

Ionic liquids generally exhibit high thermal stability between 300 and 450 °C, yet, their performance as electrolytes in batteries at temperatures higher than 80 °C has not been widely investigated. In 2009 by Mun et al.¹⁶⁸ reported seminal work on high temperature ionic liquid electrolyte based batteries. The authors compared the thermal and electrochemical stability of 1-ethyl-3-methylimidazolium bis(trifluoromethanesulfonyl)imide (EMI-TFSI), 1-propyl-1-methylpyrrolidinium bis(trifluoromethanesulfonyl)imide (PYR13-TFSI), and 1-propyl-1-methylpiperidinium bis(trifluoromethanesulfonyl)imide (PP13-TFSI) with carbonate-based organic solvent at 120 °C. Cyclic voltammetry (CV) results suggested that the broad lithiation and de-lithiation peak observed at 1.3 - 2.0 V (25 °C) evolved into three discrete pairs of redox peaks, as a result of increasing the temperature (Figure 11b). A shift in the reduction peak from 0.4 V (25 °C) to 1.1 V (120 °C) is also observed. Similar to observations at room temperature, the imidazolium-based RTIL undergo significant cathodic decomposition above 1.1 V resulting in the deposition of a resistive surface film on the electrode and eventual loss of cell performance. This effect is more pronounced at 120 °C, demonstrating the lower electrochemical stability of imidazoliums compared to pyrrolidiniums and piperidiniums. In sharp contrast, cathodic decomposition and concomitant film deposition are negligible with pyrrolidinium- and piperidinium-based RTILs even at this high temperature, supported by results from field emission scanning electron microscopy (FE-SEM) studies (figure 11e). X-ray photoelectron spectroscopy (XPS) investigations of the deposition layer revealed a significant N 1s peak indicating that the composition is a consequence of EMI-TFSI decomposition related to both the TFSI anion and EMI cation. The influence of this deposition layer is also noted by impedance measurements of the TiO₂-B/Li cells, where a remarkable increase of impedance is observed for the EC:DEC and imidazolium IL electrolytes, while that of PYR13-TFSI and PP13-TFSI showed marginal increase (Figure 11d). Subjecting the TiO₂-B/Li cells, each containing one of the three ionic liquids, to cycling at 120 °C from 1.2 to 2.5 V revealed the following

capacity dependencies. The capacity decreased after a short time period and even if left at 2.5 V in the charged state, the self-discharge yielded 3% to 33% of capacity loss (Figure 11c).

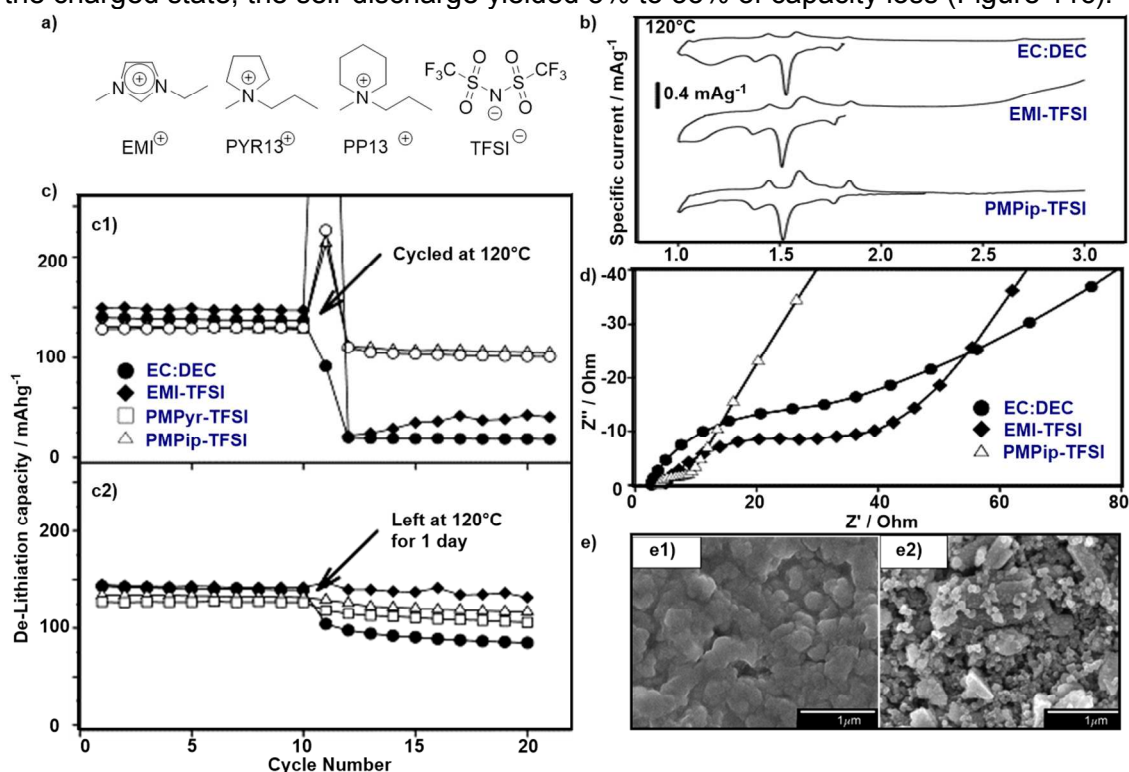


Figure 11. a) Structures of ionic liquids under investigation; b) cyclic voltammograms for $\text{TiO}_2\text{-B}$ electrode in three different electrolytes, Scan rate = $0.1 \text{ mV} \cdot \text{s}^{-1}$ and $T = 120 \text{ }^\circ\text{C}$; c) capacity loss at high-temperature ($120 \text{ }^\circ\text{C}$); d) impedance spectra for $\text{TiO}_2\text{-B/Li}$ cell after 5 cycles at $120 \text{ }^\circ\text{C}$. Measurements made at discharged state (1.2 V for $\text{TiO}_2\text{-B}$ electrode); e) FE-SEM images of $\text{TiO}_2\text{-B}$ composite electrode surface at initial state (e1), after 20 cycles at $120 \text{ }^\circ\text{C}$ in $1.0 \text{ M Li-PYR13-TFSI}$ (e2).¹⁶⁸ Adapted from ref. 166. Copyright 2009 Elsevier.

Lane et al.¹⁶⁹ investigated a morpholinium ionic liquid electrolyte, specifically *N*-methyl-*N*-butylmorpholinium bis(fluorosulfonyl)imide (C4mmor-FSI) (Figure 12a), in a Li/LiFePO_4 half-cell operated at $85 \text{ }^\circ\text{C}$ with a C rate of C/6.5. Morpholinium based ILs are more viscous than other commonly used ILs. The conductivity of the C4mmor-FSI electrolyte at $25 \text{ }^\circ\text{C}$ is $0.73 \text{ mS} \cdot \text{cm}^{-1}$, far less than that of a structurally similar piperidinium ionic liquid, PP14-FSI ($3.7 \text{ mS} \cdot \text{cm}^{-1}$). Thus, use at high temperature is expected to decrease the viscosity of this IL and facilitate ion transport. An in-depth mechanistic study revealed no obvious difference in electrochemical stability at $50 \text{ }^\circ\text{C}$ compared to $23 \text{ }^\circ\text{C}$, except that enhanced metal alloying and lithium plating and striping occurred from -4.0 to -2.0 V vs. Ag/Ag^+ at the high temperature. Operation at the higher temperature also eliminated dendrite formation, at the surface of lithium metal, in a lithium symmetrical setup and prolonged the lifecycle, especially at higher current densities. In a short-circuit test at $85 \text{ }^\circ\text{C}$, the cell continued to function for 15 hours, compared to 5 hours at $50 \text{ }^\circ\text{C}$ (Figure 12b).

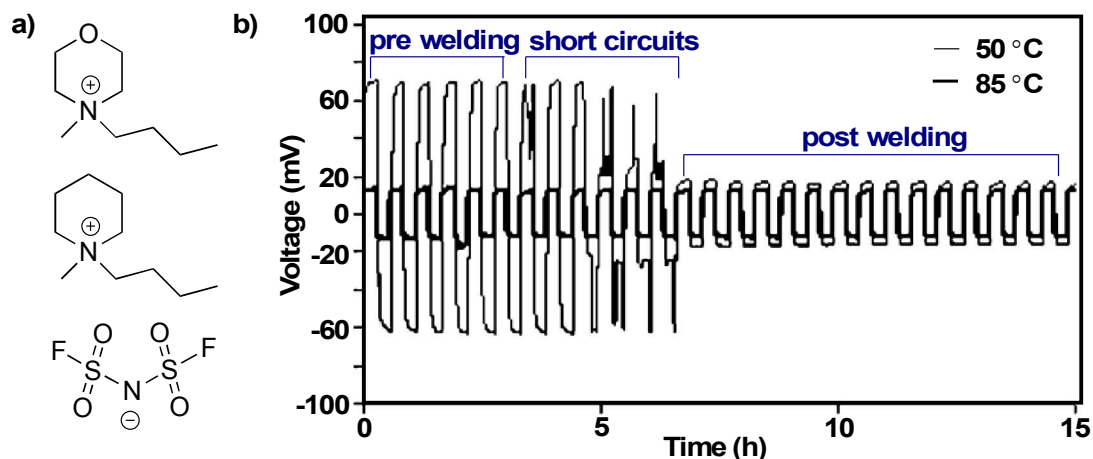


Figure 12. a) Structures of *N*-methyl-*N*-butylmorpholinium and *N*-methyl-*N*-propylpiperidinium, and bis(fluorosulfonyl)imide; b) c4mmor-FSI + 0.4 mol kg⁻¹ at 0.2 mA cm⁻², showing short circuit and possible welding behavior at 50 °C.¹⁶⁹ Adapted from ref. 167. Copyright 2010 American Chemical Society.

In contrast to the nitrogen based ionic liquids, phosphonium ionic liquids are less studied and exhibit both greater chemical and thermal stability than imidazolium and pyrrolidinium ionic liquids. Ab initio quantum chemical calculations (DFT-B3LYP) of the thermal stability of several ILs, with different cations incorporating similar alkyl chain length, paired with the tetrafluoroborate based ILs revealed that stability increased in the order of pyridinium, pyrrolidinium, ammonium, imidazolium and phosphonium, with calculated thermal activation energies ranging from 134 to 204 kJ · mol⁻¹.¹⁷⁰ Taking advantage of the enhanced thermal stability of phosphonium based ionic liquids, Lin et al.¹⁷¹ reported a prototype lithium metal battery using a phosphonium IL / LiTFSI electrolyte. The Li/LiCoO₂ battery cycled at 100 °C for a month with 50% of capacity loss at C/10. A series of long-chained alkyl phosphonium ionic liquid electrolytes are described where the tri-alkyl chain length is varied from two carbons to ten carbons, while maintaining a fourth decyl chain linked to the phosphonium center (Figure 13a). This design enhanced thermal stability and minimized potential crystallization or packing interactions via the alkyl chain asymmetry around the phosphonium. The selected IL mono-(C₆)₃PC10-TFSI electrolyte composition possessed a high decomposition temperature (355 °C), no phase transitions, and moderate conductivity (1.7 mS · cm⁻¹) and viscosity (0.3 Pa.s) at 100 °C. The results from a long-term thermogravimetric analysis (TGA) experiment at a constant temperature of 100 °C documented the high temperature stability of this phosphonium ionic liquid. The battery exhibited an initial high capacity of 135 mA h g⁻¹ which decreased to 70 mA h g⁻¹ after 70 cycles in a Li/LiCoO₂ cell (Figure 13b); this value still represents more than 50% of the initial capacity. Instant on-off battery operation is realized via the significant temperature dependence of the electrolyte material, demonstrating the robustness and potential for use at high temperature, while minimizing discharge during RT storage between uses (Figure 13c).

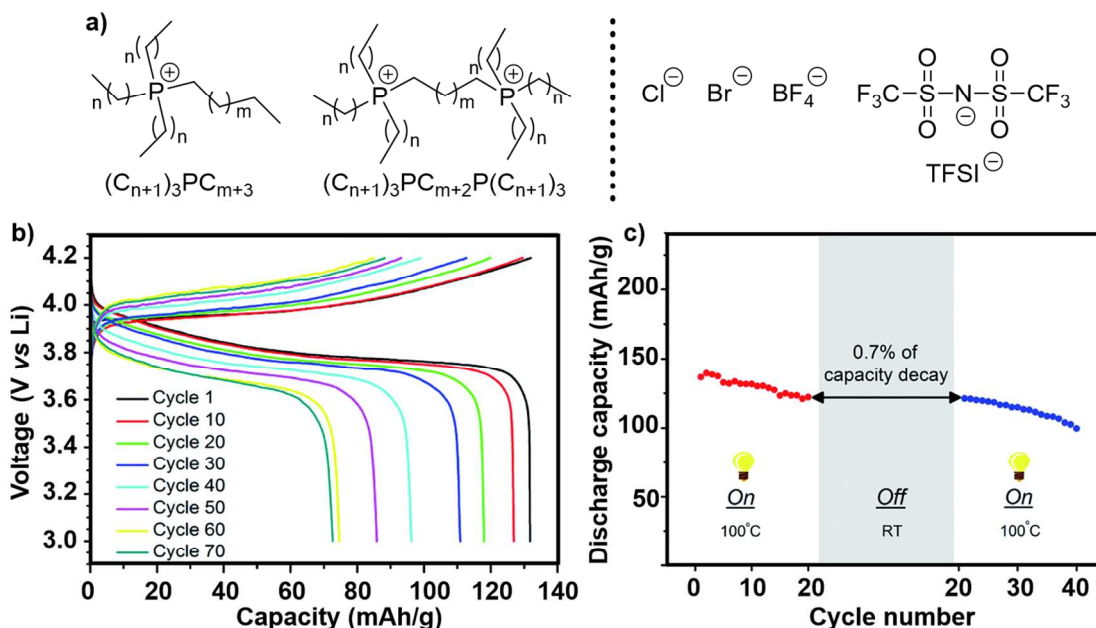


Figure 13. a) Chemical structures of a series of phosphonium ionic liquids; b) charge–discharge cycling for mono- $(C_6)_3PC_{10}$ -TFSI with 1.6 M LiTFSI, current rate at C/7; c) demonstration of battery working only at high temperature and retain capacity at room temperature.¹⁷¹ Adapted from ref. 169. Copyright 2015 Royal Society of Chemistry.

Kalaga et al.¹⁷² also reported stable battery cycling at 120 °C using a PP13-TFSI electrolyte blended with dry bentonite clay. The addition of clay afforded a slightly decreased thermal decomposition temperature of 355 °C, compared with that of the IL alone (370 °C), yet the use of clay eliminated the need for extra separators. The composite electrolyte displayed an electrochemical window of 3.0 V at 120 °C. The ionic conductivity is $\sim 3.0 \text{ mS} \cdot \text{cm}^{-1}$ at 120 °C with a lithium transport number of 0.08. When the Li/LTO half-cell cycled at C/3, the initial discharge capacity is approximately $75 \text{ mAh} \cdot \text{g}^{-1}$ and quickly decreased to $60 \text{ mAh} \cdot \text{g}^{-1}$ (Figure 14a). It remained constant thereafter likely due to the low lithium transport number. Changing the current rates (from C/16 to 1C) influenced the capacity, and higher rates, and in general, led to greater degrees of capacity loss (Figure 14b).

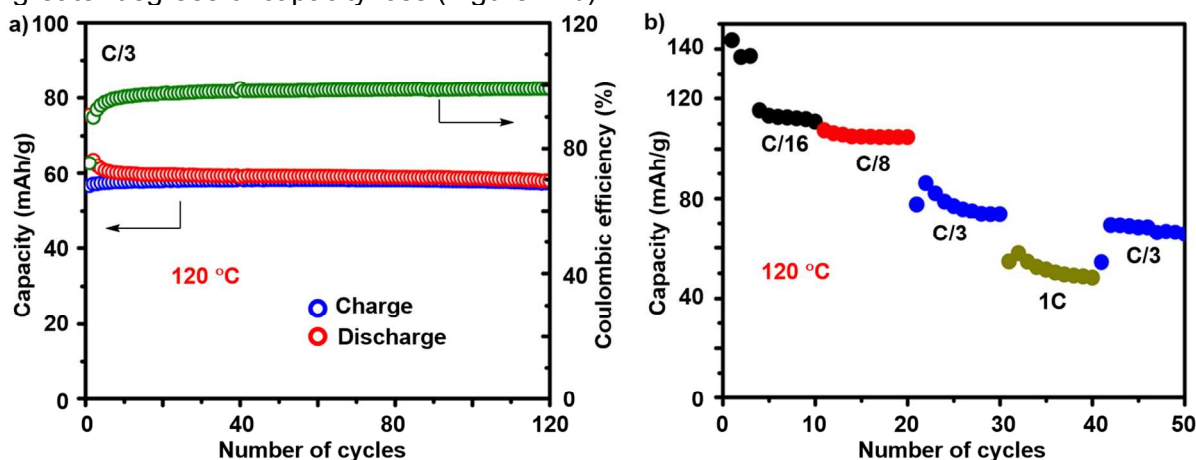


Figure 14. (a) Cyclic stability of LTO half cells cycled at 120 °C at C/3. (b) rate capability of LTO half cells at 120 °C cycled at different C-rates using clay/PP13-(1 M) LiTFSI composite electrolyte.¹⁷² Adapted from ref. 170. Copyright 2015 American Chemical Society.

In order to address the high reactivity of lithium metal, especially at elevated temperatures, silicon is being investigated as an alternative anode material. Markevich and Salitra et al.¹⁷³ reported stable cycling of a high loading Si electrode ($1.3 \text{ mg} \cdot \text{cm}^{-2}$ of loading, 7 mm thick) with PYR13-FSI containing LiFSI (0.5 M) at 60°C . Limiting the charge capacity to $600 \text{ mAh} \cdot \text{g}^{-1}$ ensured a failure-free cycling of more than 800 times. At elevated temperatures, the FSI-based IL electrolytes outperformed the 1 M LiPF_6 FEC/DMC electrolytes, which is known to be one of the most promising organic electrolyte solutions for Si anodes. Interestingly, a thinner surface passivating film formed on the Si electrodes in the LiTFSI/ PYR13-FSI electrolyte at 60°C as compared to the one formed in the 1 M LiPF_6 in FEC/DMC electrolyte solution (Figure 15a and 14b). This difference is attributed to the better performance of the Si anode in the IL electrolyte at elevated temperature. A three-dimensional (3D) nano Si coated porous electrode ($0.7 - 0.9 \text{ mg} \cdot \text{cm}^{-2}$ of loading, about 0.4 mm thick) was also fabricated by Ababtain et al.¹⁷⁴ When used with a PP13-TFSI /0.8 M LiTFSI electrolyte, the cell showed excellent cyclability at high temperatures from 60 to 100°C , as well as demonstrated minimum capacity loss (Figure 15c and 14d). The use of 3D nano-Si afforded high specific capacity of $0.41 \text{ mAh} \cdot \text{cm}^{-2}$ ($1912 \text{ mAh} \cdot \text{g}^{-1}$). The addition of 20% PC lowered the viscosity of PP13 and facilitated the operation of the battery at room temperature, while maintaining the safety and performance at 100°C .

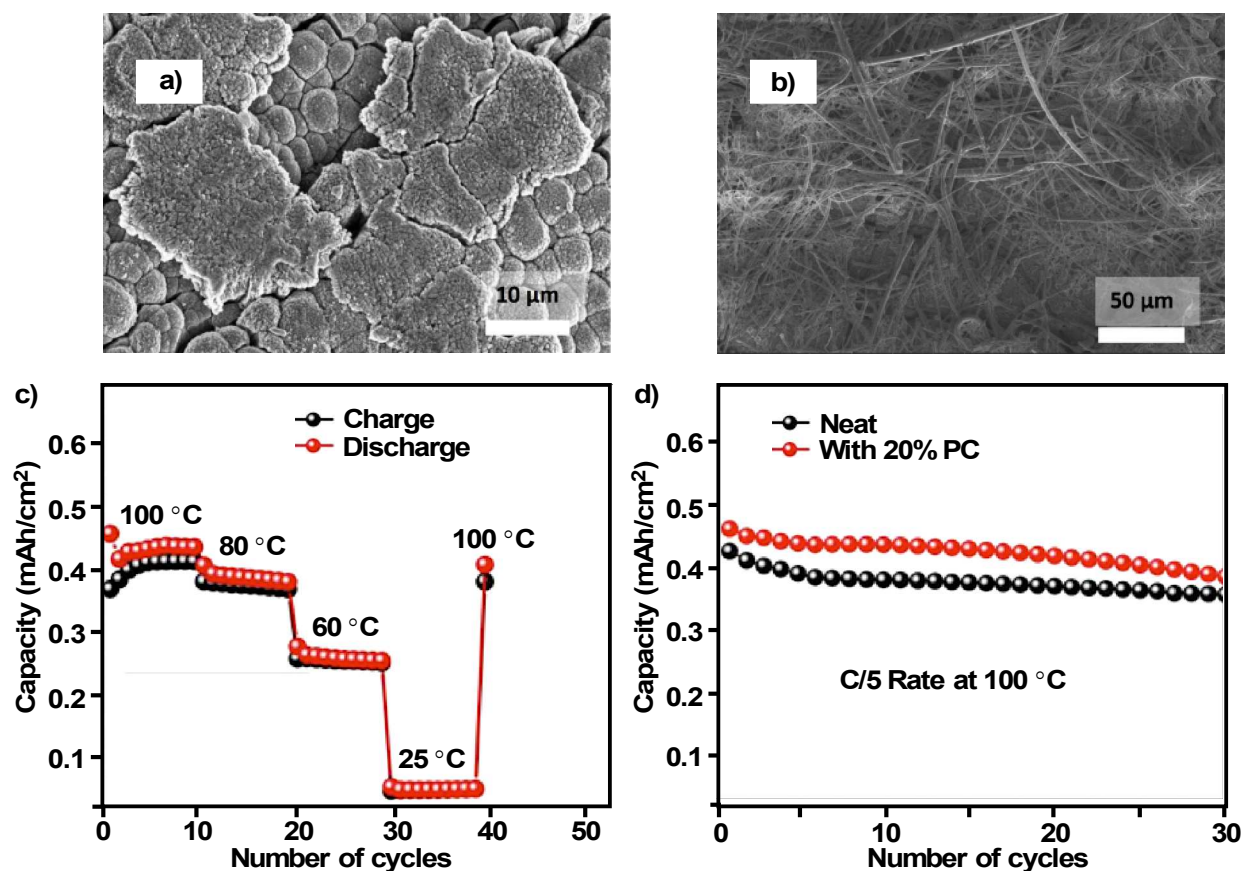


Figure 15. SEM images of the cycled at 60°C silicon electrodes a) after about 700 cycles in 1 M LiPF_6 in FEC/DMC 1:4 and;¹⁷⁵ b) after about 870 cycles in 0.5 M LiFSI in PYR13-FSI; c) temperature-dependent performance of 3D Si electrodes with PP13-TFSI; d) comparison of cycle life of 3D Si electrode at 100°C with PP13-TFSI and 20% PC+PP13-TFSI electrolyte mixtures.¹⁷⁶ Adapted from refs. 172 and 173. Copyright 2014 Royal Society of Chemistry and 2016 American Chemical Society.

Ionic liquid electrolytes are also finding applications in sodium-ion batteries. Sodium secondary batteries have attracted considerable attention as alternatives to lithium based batteries, as sodium is abundant, available, and of low cost. The motivation for investigating Na-ion batteries at elevated temperatures originated from the fact that at room temperature Na^+ transport is slow due to the large ionic radii of Na^+ (1.02 Å), which will increase at higher temperatures. Nevertheless, the above-mentioned much lower melting point of Na, limits the higher temperature range in its solid-state. Sodium iron pyrophosphate (NaFePO_4) is a commonly used sodium based cathode material, analogous to LiFePO_4 , and is synthesized via chemical delithiation of LiFePO_4 followed by electrochemical sodiation of FePO_4 .¹⁷⁷ Wongittharom et al.¹⁷⁸ studied the cycling behavior of NaFePO_4 in the presence of the PYR14-TFSI ionic liquid electrolyte with various sodium solutes, namely NaBF_4 , NaClO_4 , NaPF_4 , and $\text{NaN}(\text{CN})_4$ (Figure 16a). Of the investigated electrolytes, the PYR14-TFSI / NaBF_4 exhibited the highest conductivity and least capacity decay with 85% of the capacity maintained for 100 cycles at 50 °C. At 75 °C, the measured capacity increased to as high as 152 $\text{mAh} \cdot \text{g}^{-1}$ (at 0.05 C) nearing the theoretical value (154 $\text{mAh} \cdot \text{g}^{-1}$) (Figure 16b). This temperature effect is similar to that observed in lithium based batteries. Moreover, 60% of this capacity is retained when the charge–discharge rate is increased to 1 C. Recently, Chen et al.¹⁷⁹ reported a higher operational temperature for a Na-ion battery when using a sodium vanadyl(IV) orthophosphate (NaVOPO_4) cathode, and the PYR13-FSI electrolyte with NaFSI. Specifically, stable cycling of more than 300 times with near 100% of coulombic efficiency at 1C is observed at 90 °C. NaVOPO_4 possesses high operating potentials outside of the vanadium redox couple and a high theoretical capacity (145 $\text{mAh} \cdot \text{g}^{-1}$), which compensate for the lower overall energy density of Na-ion batteries compared with Li-ion batteries. XRD measurements revealed that the charge–discharge process involves a single-phase reaction. Analysis using galvanostatic intermittent titration technique (GITT) highlighted a three to five-fold increase of the apparent Na chemical diffusion coefficient in NaVOPO_4 upon increasing the temperature from 25 °C to 90 °C, which accounted for the superior electrochemical performance at 90 °C (Figure 16d). However, only capacities of 60 and 101 $\text{mAh} \cdot \text{g}^{-1}$ are observed after the first cycle, at 25 and 90 °C, respectively. A large irreversible capacity loss occurred, attributed to SEI layer formation, between the first and second cycle. After the latter, the capacity decay decreased only slightly due to the formation of this SEI layer.

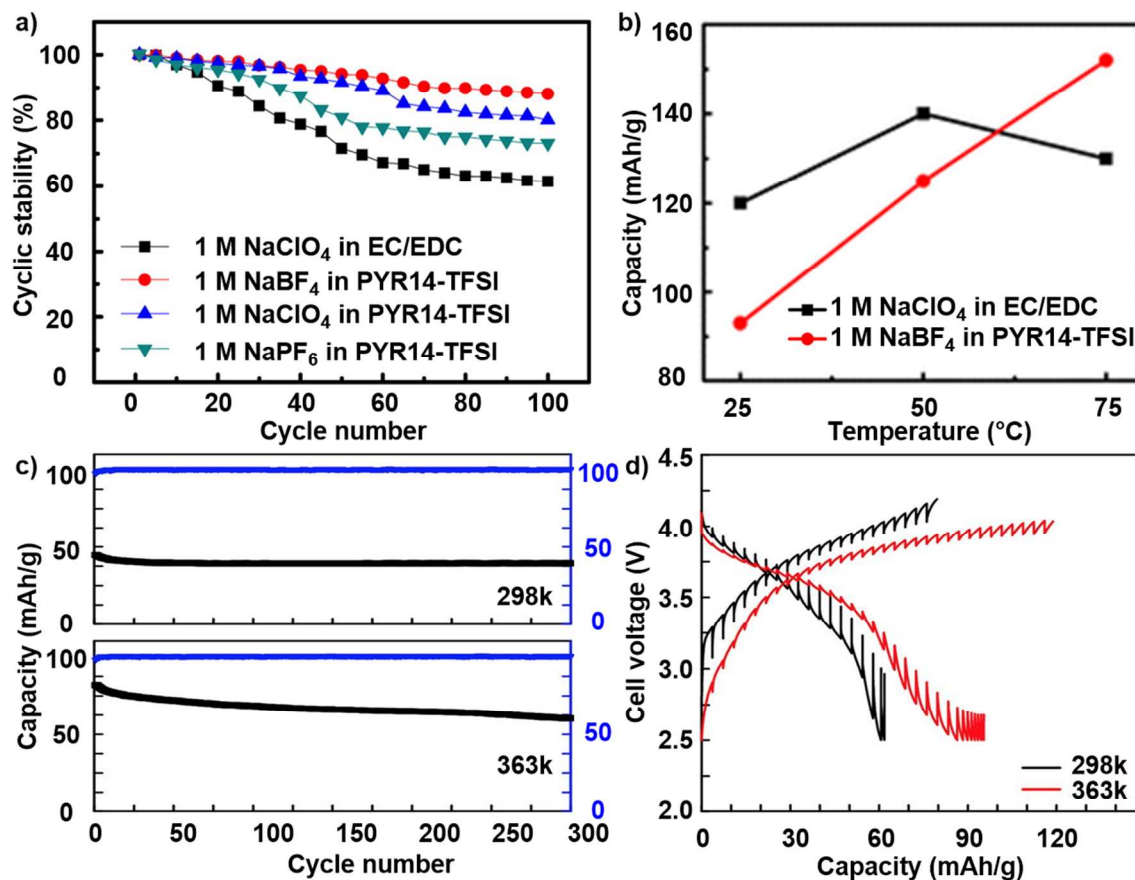


Figure 16. (a) Cyclic stability (measured at 0.3 C) of Na/NaFePO₄ cells with various kinds of electrolytes at 50 °C; (b) effects of temperature on discharge capacity at 0.05 C;¹⁷⁸ (c) cycling performance and coulombic efficiency of the NVP/AB-8h electrodes at 298 and 363 K. Cut-off voltage: 2.5 - 4.2 V. Current density: 1 C (145 mA · g⁻¹); (d) GITT evaluation of the NVP/AB-8h electrode at 298 K and 363 K. Conditions: 30 min charging/discharging segments at C/20 (7.25 mA · g⁻¹) followed by 12h relaxation.¹⁷⁹ Adapted from refs. 175 and 176. Copyright 2014 American Chemical Society and 2015 The Electrochemical Society.

Ionic liquids are used in other types of energy storage devices such as supercapacitors, which, in turn are widely used now in power electronics for back-up memories and peak power saving. For example, in electric cars supercapacitors are coupled with fuel cells or batteries to deliver high power during acceleration as well as to recover the energy during braking. Similar to batteries, the operation temperature of supercapacitors is limited by the stability of the electrolyte. The commonly used acetonitrile or carbonate based electrolytes are flammable and possess a high vapor pressure. Thus, additional thermal control devices such as cooling units are required. Sato et al.¹⁸⁰ described the first supercapacitor for high temperature applications. They used a *N, N*-diethyl-*N*-methyl-*N*-(2-methoxyethyl) ammonium tetrafluoroborate (DEME-BF₄) ionic liquid as the electrolyte. DEME-BF₄ exhibits a melting point of 10 °C and room temperature conductivity of 4.8 mS · cm⁻¹. Assembled with activated carbon electrodes, the supercapacitor delivered 500 cycles with only a 15% loss in capacity at 100 °C (V = 0 - 2.5 V, I = 15 mA). Three years later, Balducci et al.¹⁸¹ reported the construction of a supercapacitor using a microporous activated carbon as the electrodes and PYR14-TFSI ionic liquid as the electrolyte. The microporous activated carbon exhibited a specific capacitance of 60 F g⁻¹ measured from three-electrode cyclic voltammetry experiments at 20 mV · s⁻¹ scan rate, with a

maximum operating potential range of 4.5 V at 60 °C. The resulting supercapacitor cycled for 40,000 cycles without any change of capacity and cell resistance at current densities ranging from 10 to 100 mA · cm⁻², demonstrating stable elevated temperature cycling. Thus, this type of supercapacitor is suitable for high temperature applications (> 60 °C).

In 2011, Lin et al.¹⁸² reported the construction of an electrical double layer capacitor which not only extended the upper temperature limit to 100 °C, but also enabled device operation down to -50 °C, over a wide voltage window (up to 3.7 V) and at high charge/discharge rates of up to 20 V · s⁻¹. A 1:1 (molar ratio) eutectic mixture of PP13-FSI and PYR14-FSI gave a working electrolyte for this wide temperature range. In particular, the choice of blending two different IL cations with the same anion reduced ordered packing and crystallization affording no phase transitions from -50 to 100 °C. The voltage window is dependent on the temperature. At room temperature a broad voltage window of 3.7 V is observed, whereas at 100 °C the window decreased by almost 1.0 V, limiting high temperature operation up to 3.0 V (Figure 17a). Largeot et al.¹⁸³ reported the effect of pore-ion size on the capacitance of microporous carbon electrode combined with the PYR14-TFSI ionic liquid electrolyte at 100 °C. The authors noted that when the carbon pore size matched the ion size of the ionic liquid, ideal capacitive behavior and a maximum capacitance of 130 F · g⁻¹ are obtained (Figure 17b).

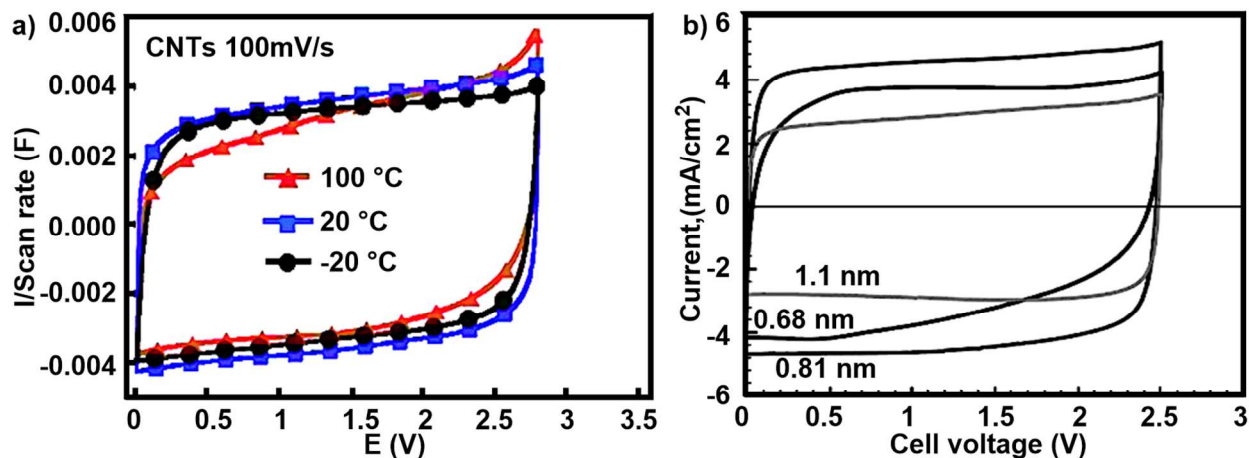


Figure 17. (a) CV at temperatures from 50 °C to 100 °C at 100 mV · s⁻¹ for CNTs; (b) cyclic voltammograms of carbide-derived carbon electrodes (TiC-CDCs) with various pore sizes tested in the PYR14-TFSI electrolyte at 100 °C; potential scan rate: 5 mV · s⁻¹.^{182, 183} Adapted from refs. 179 and 180. Copyright 2011 American Chemical Society and 2011 The Electrochemical Society.

If the maximum operational temperature is 100 °C, ammonium salts paired with high boiling point carbonate electrolytes may address this requirement. Masarapu et al.¹⁸⁴ compared the capacitive properties and long-term cycling performance of a supercapacitor assembled with single-walled carbon nanotube (SWNT) and a mixture of tetraethylammoniumtetrafluoroborate-propylene carbonate (TEA-BF₄/PC) at 25 and 100 °C, respectively. The cells showed excellent stability over more than 200,000 cycles with 80% efficiency (Figure 18a). Operation at high temperature afforded no noticeable cell damage but instead increased the specific capacitance, which is attributed to the enhanced adsorption of the electrolyte ions onto the surface of the electrode. To extend the temperature beyond 100 °C, Borges et al.¹⁸⁵ employed a composite electrolyte/separator structures composed of Bentonite clay and 1-butyl-2,3-dimethylimidazolium bis(trifluoromethylsulfonyl)imide (BMMI-TFSI) ionic liquid. This electrolyte is stable to temperatures as high of 300 °C. Conductivity is slightly compromised by introduction

of clay, reaching $1 \text{ mS} \cdot \text{cm}^{-1}$ above $50 \text{ }^\circ\text{C}$. Increasing the temperature increased the conductivity and afforded a maximum conductivity of about $5 \text{ mS} \cdot \text{cm}^{-1}$ at $180 \text{ }^\circ\text{C}$. The continuous increase in temperature led to a decrease in conductivity of about $2.5 \text{ mS} \cdot \text{cm}^{-1}$ at $200 \text{ }^\circ\text{C}$. The assembled device possessed a specific capacitance of $40 \text{ F} \cdot \text{g}^{-1}$ operated from 0 to 2.5 V with almost 20% of capacity loss after 10,000 cycles (Figure 18c). An abrupt decrease of capacity in the initial cycles is observed and attributed to the SEI formation. To prepare a free-standing electrolyte film (Figure 18d), the thermoplastic poly (urethane) (TPU) is added to the electrolyte mixture at 10% wt. The capacitance reduced ($20 - 35 \text{ F} \cdot \text{g}^{-1}$) at $200 \text{ }^\circ\text{C}$ within the 0 - 2.5 V window due to the decreased conductivity of the electrolyte membrane with added TPU.

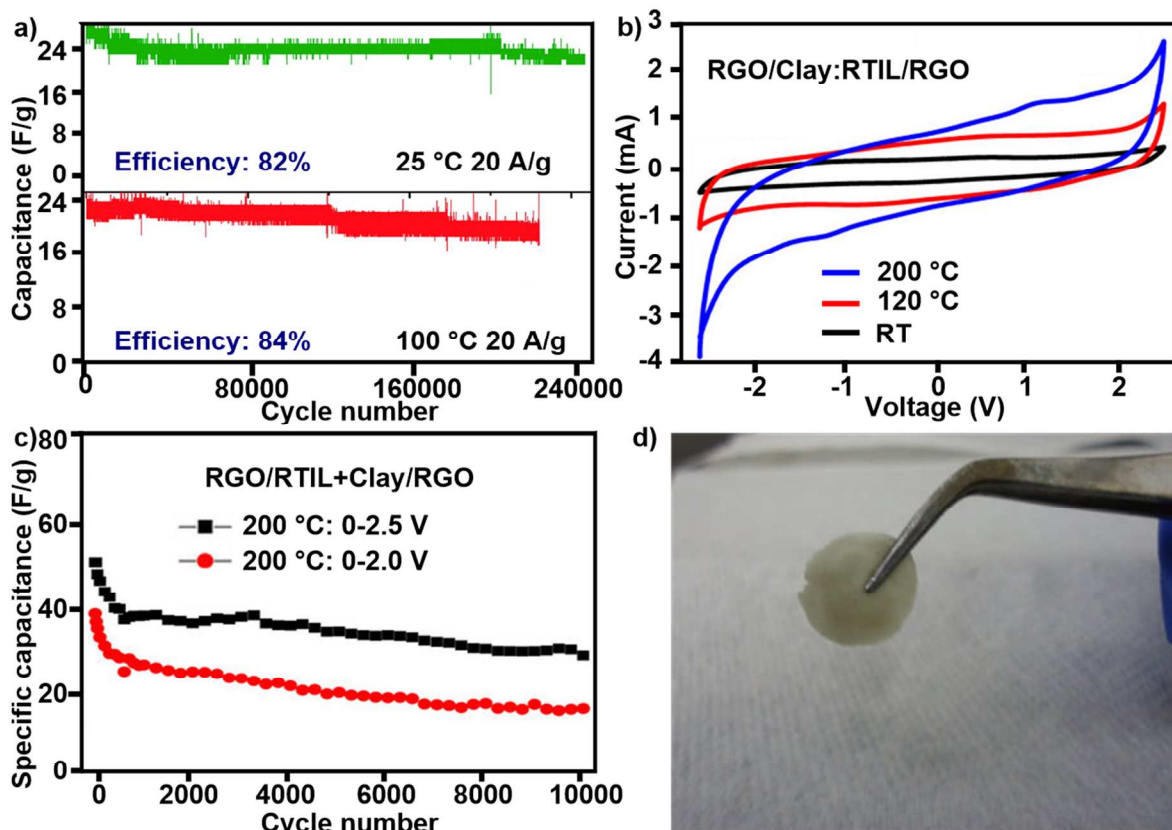


Figure 18. a) Displaying the ultralong cycling stability of the cell by running 246 700 and 224 000 cycles of charge-discharge with a current density of 20 A/g at 25 and $100 \text{ }^\circ\text{C}$;¹⁸⁴ b) Cyclic voltammograms for supercapacitor based on clay:RTIL electrolyte at 60 mV/s. The capacitor exhibits a box-like shape using a potential window of 5 V at different temperatures: RT, $120 \text{ }^\circ\text{C}$ and $200 \text{ }^\circ\text{C}$; c) Cycling stability of the capacitor RGO|Clay:RTIL|/RGO at $200 \text{ }^\circ\text{C}$ with different voltage windows 2 V and 2.5 V; d) Free standing membrane based on TPU:Clay:RTIL working as electrolyte/separator for supercapacitor until $200 \text{ }^\circ\text{C}$.¹⁸⁵ Adapted from refs. 181 and 182. Copyright 2009 American Chemical Society and 2013 Macmillan Publishers.

5.1.3 Solid polymers. Since Wright et al. first demonstrated ion conduction in poly(ethylene oxide)-salt complexes (PEO) in 1973,¹⁸⁶ the potential use of these polymers as the ion conducting electrolyte in energy storage devices has attracted significant attention.^{151, 187-190} This interest is motivated by a number of unique advantages such as non-flammability, lightweight, and processability. Thus, PEO-based electrolytes may provide a solution to the safety and leak problems associated with liquid electrolytes. Compared to ceramic or ionic liquid systems, polymers are flexible and easier to be shaped consistently according to the design

requirement and fabricated using roll-to-roll printing on large scale. These advantages support the development of polymers as an ideal electrolyte candidate for operation at room temperature or high temperature. An additional merit to using polymer electrolytes, as opposed to liquid electrolytes, is that separators are not required, which reduces the weight and cost of producing a cell as well as eliminates the thermal instability and compatibility issues associated with using liquid electrolytes and separators. State-of-the-art polymer electrolytes can be categorized into two types: 1) solvent-free solid polymer electrolytes where the salt is dissolved in a high-molecular-weight polymer. Lithium ion conduction is assisted by the segmental motion of the polymer chains, and these systems generally possess low conductivity ($10^{-5} \text{ S} \cdot \text{cm}^{-1}$) at room temperature. 2) Gel or plasticized polymer systems where liquid electrolyte is doped in a non-conducting solid polymer which provides both mechanical support and lithium-ion conduction. Gel systems can display comparable conductivity ($> 10 \text{ mS} \cdot \text{cm}^{-1}$) as liquid electrolytes, however, safety and thermal stability issues remain with loading of liquid electrolyte. Since polymer electrolytes also serve as separators, mechanical integrity is a critical requirement. Therefore, a balance is required between high conductivity, hence “liquid-like” electrical behavior, and mechanical integrity, hence “solid-like” mechanical behavior. The reader is referred to several excellent reviews on the development of polymer electrolytes.^{61, 62, 187, 188, 190, 191}

In 2011, Hu et al.^{192, 193} reported the charge and discharge cycling of a graft copolymer electrolyte (GCE)-based lithium-ion battery at temperatures up to 120 °C. The GCE consists of poly(oxyethylene) methacrylate-g-poly(dimethyl siloxane) (POEM-g-PDMS) (Figure 19b, inset), where the microphase separation between the hydrophilic block and the hydrophobic block yielded a flexible, ion-conducting domain to transport the ions, as well as a mechanically strong domain to support the matrix. The low T_g of POEM ($T_g = -60 \text{ °C}$) and PDMS ($T_g = -123 \text{ °C}$) conferred sufficient room-temperature ionic conductivity to the material. The authors demonstrated the potential of GCE-based Li-ion batteries for high-temperature applications by studying the temperature stability and cycling behavior of the GCE-based lithium-ion batteries in a Li/LiFePO₄ cell doped with LiTFSI. However, fast capacity loss ($> 60\%$) is observed within 30 cycles during charge-discharge cycling with a continuously decreasing coulombic efficiency (from $> 95\%$ to $< 70\%$) (Figure 19a). One possible explanation for this decrease in coulombic efficiency is the limited long-term thermal stability of the polymer. An isothermal TGA study at 140 °C of the graft polymer, under inert atmosphere, revealed a weight loss of less than 2% over 50 h, suggesting suitable stability. Yet, the graft copolymer showed discoloration after long exposure to elevated temperatures. FTIR analysis of the graft polymer before and after heating revealed degradation of the polymer. For instance, the decreases in intensity of the symmetric and asymmetric stretching modes of C-H in the methyl CH₃ (peaks between 2800 and 3000 cm^{-1}) and the stretching mode of the carbonyl (C=O) groups ($\sim 1730 \text{ cm}^{-1}$) are indicative of the decomposition of the methacrylate backbone (Figure 19b). Nevertheless, the GCE polymer electrolyte showed $> 30\%$ of capacity loss after 50 cycles at room temperature at the same current rate, despite an increasing coulombic efficiency reaching about 95% after cycling. The discrepancy in the cycling efficiency change behavior between high temperature and room temperature is unclear.

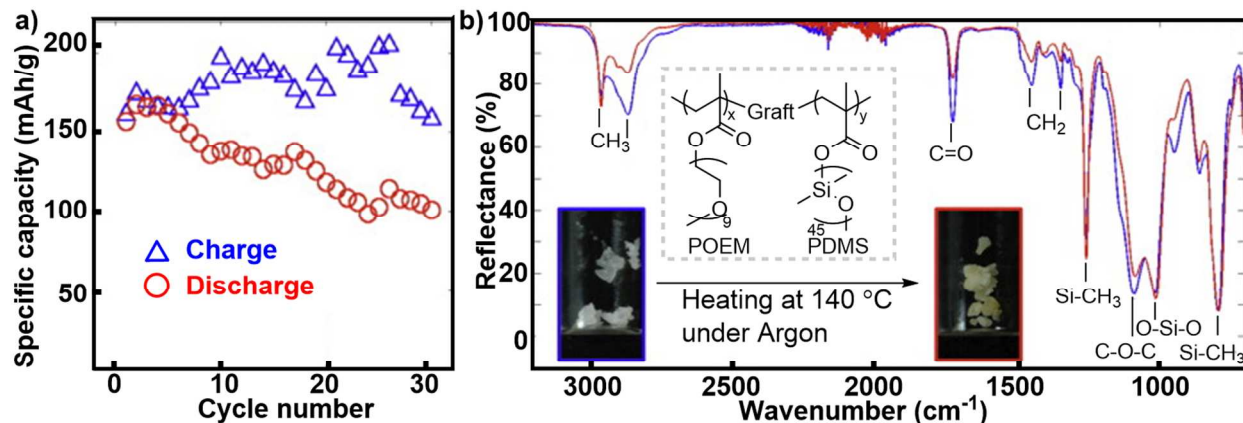


Figure 19. a) Charge and discharge curves of LiFePO₄/GCE/Li at 120 °C. The current density used was 10 mA · g⁻¹; b) FTIR spectra of unheated and heated (140 °C) graft copolymer. Chemical structure of the graft copolymer (inset). The graft copolymer shows discoloration after heating (inset).¹⁹² Adapted from ref. 189. Copyright 2011 Elsevier.

Compared with the reduced stability of the GCE polymers described above, an anionic block copolymer electrolyte (A-BCE), specifically a poly (ethylene glycol-co-lithium styrene trifluoromethanesulphonylimide) P(STFSiLi)-*b*-PEO-*b*-P(STFSiLi) (Figure 20a) showed promising performance at temperatures tested up to 80 °C as reported by Bouchet et al.¹⁹⁴ A short-term TGA study showed the thermal decomposition temperature of the copolymer to be 350 °C. A prototype cell based on the A-BCE polymer, a Li anode, and a LiFePO₄ cathode provided stable cycling at 60, 70, and 80 °C with varied current rates (from C/60 to 2C). The cell exhibited a large 5 V electrochemical window versus Li/Li⁺. No capacity fading was observed regardless of the tested temperature after 90 cycles. Of note is the fact that the polymer electrolyte generated extremely high current rates and subsequent power, which are greater than previous dry polymer systems. For example, even if operated at C/2, the system retained 85% of its capacity at 80 °C. This remarkable improvement in power density is realized through the “single-ion” effect polymer, as revealed by a Li⁺ transference number of greater than 0.85. Polyelectrolytes containing immobilized anions to increase the fraction of ionic conductivity via the cations (Li⁺) have been studied. In contrast to non-ionic polymers, these polymers prevent the build-up of a salt concentration gradient across the cell and the accumulation of anions on the anode, which are thought to cause lithium dendrite formation and power loss. Although the ionic conductivity of the A-BCE polymer is only 1.3 × 10⁻⁵ S · cm⁻¹ at 60 °C (Figure 20b), most of the conductivity is the result of the cations (Li⁺) and afforded higher power delivery and longer lifecycle. Theoretical calculations also support the conclusion that materials with high Li⁺ transport number exhibit better cycling performance compared to those with low Li⁺ transport number (typically 0.1 – 0.5 for IL or polymer based electrolytes) but higher conductivities.¹⁹⁵ Another advantageous feature of the polymer electrolyte is the enhanced mechanical strength compared to the gel-type electrolytes (10 MPa at 40 °C by stress-strain test). Due to the microphase separation effect, as observed in the GCE polymer as well, the A-BCE polymer, with 31 wt% P(STFSiLi) exhibited substantially stronger mechanical properties than the neutral triblock analogous copolymer, polystyrene-PEO-polystyrene (PS-PEO-PS, 25 wt% of PS), both with LiTFSI doping at [EO]/[Li] = 30 (Figure 20c). Yet, it was also noted that the mechanical properties quickly decreased by more than 10 times (0.55 MPa) at 60 °C, which may pose issues such as a short-circuit during high temperature operation.

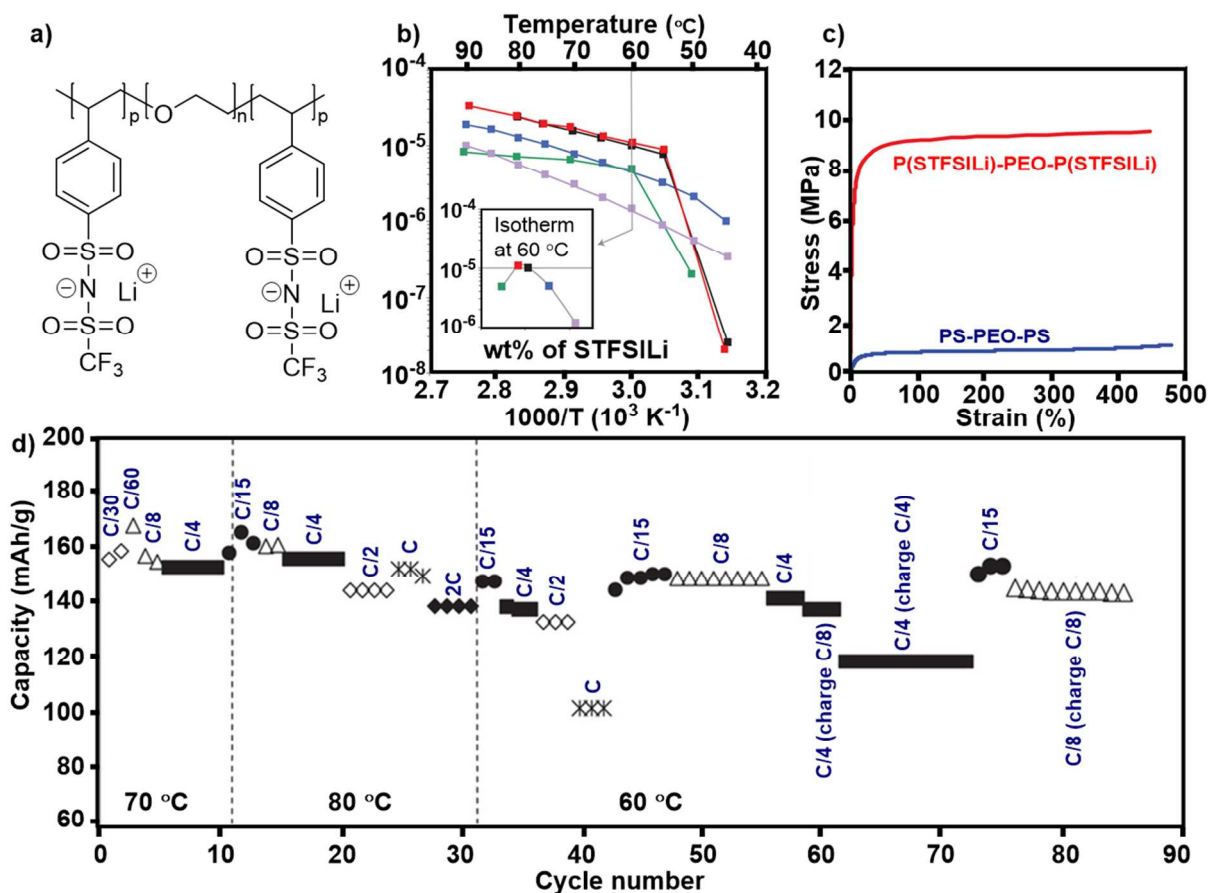


Figure 20. a) Chemical structure of the triblock copolymer P(STFSILi)-*b*-PEO-*b*-P(STFSILi); b) plots of conductivity as a function of inverse temperature for several P(STFSILi)-PEO-P(STFSILi) A-BCEs. Inset: isothermal conductivity at 60 °C according to the wt% of the P(STFSILi) block; c) comparative tensile tests at 40 °C for the neutral copolymer PS-PEO-PS with 25 wt% PS loaded with LiTFSI at [EO]/[Li] = 30 (blue curve) and the copolymer P(STFSILi)-PEO-P(STFSILi) with 31 wt% P(STFSILi) (red curve); d) cycle-life of the prototype with different temperatures and different C-rate.¹⁹⁴ Adapted from ref. 191. Copyright 2013 Macmillan Publishers.

The observation of high capacity cell performance with a low conducting electrolyte possessing a high Li⁺ transport number, which represents the portion of effective current carried by lithium ions in Li-ion batteries, is reported by Wong and Thelen et al.¹⁹⁶ They described a dry polymer electrolyte composed of a low molecular weight (Mw = 1000 - 4000) methyl carbonate-terminated perfluoropolyethers (PFPE-DMCs) that possessed a strikingly high Li transport number of 0.91 at 85 °C (Figure 21b). This value approaches unity at lower temperatures such as 40 °C. Regardless of a rather low conductivity of 2.5×10^{-5} S · cm⁻¹ measured for the polymer electrolyte at 30 °C, the Li/LiNi_{1/3}Co_{1/3}Mn_{1/3}O₂ (LiNMC) cell showed stable galvanostatic cycling at current rates varied from C/20 to C/8 at 30 °C, with a constant coulombic efficiency of > 98% after 20 cycles (Figure 21d). The authors speculated that the high lithium transport number arose from the: 1) increase in Li⁺ free movement caused by the delocalization of electrons due to the electron-withdrawing effect of fluorine moieties; and 2) concomitant decrease in mobility of the fluorinated anion (from LiTFSI) resulting from the strong interactions with the fluorinated PFPE polymer backbone. Although the cell was not evaluated at high temperatures, the absence of a flash point and burning when ignited along with the high

decomposition temperature ($> 200\text{ }^{\circ}\text{C}$) suggest that this polymer electrolyte is of potential use for high temperature energy storage.

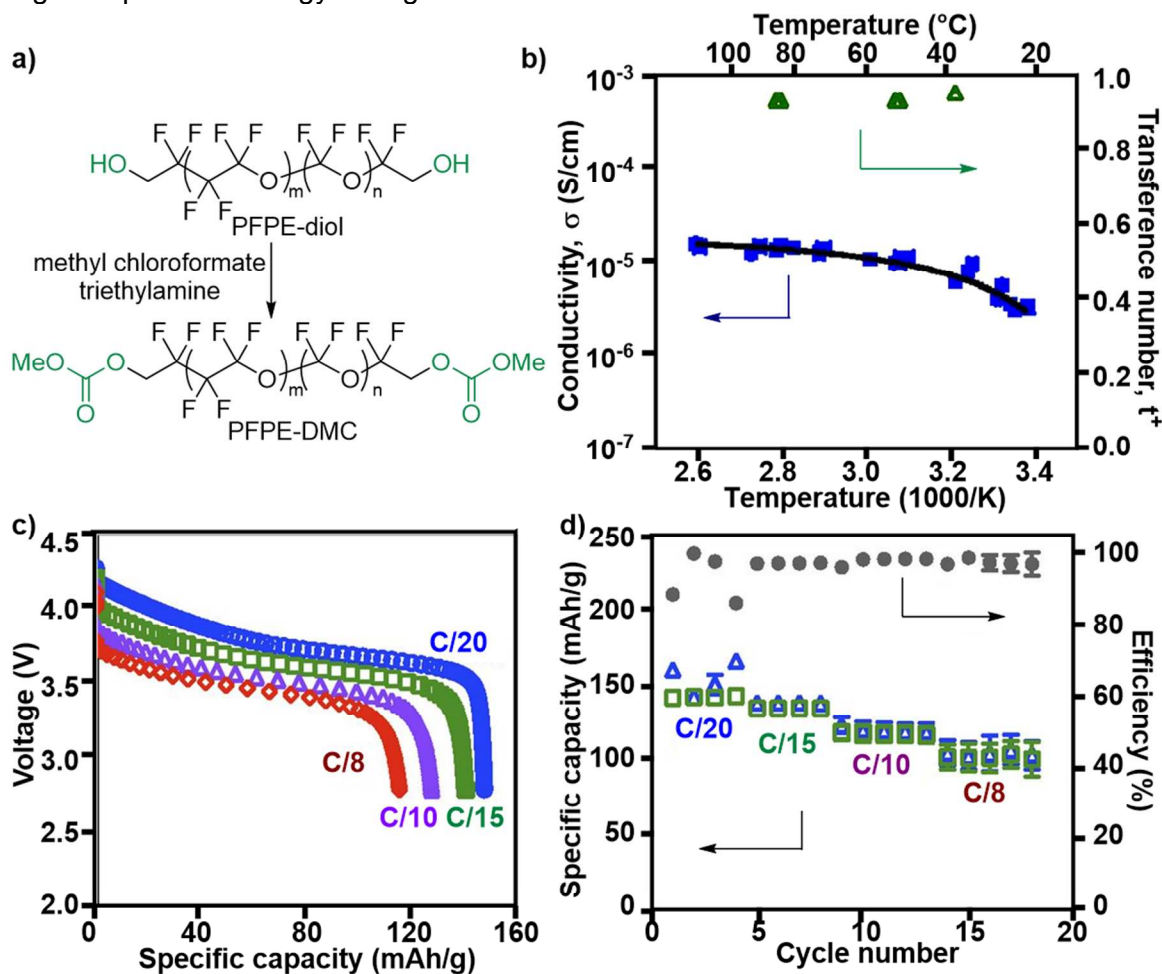


Figure 21. a) Chemical reaction scheme describing the synthesis of PFPE-DMC from PFPE-diol; b) transference number t^+ (green Δ) and temperature-dependent conductivity (blue \blacksquare) of PFPE1000-DMC; c) discharge profiles obtained at $30\text{ }^{\circ}\text{C}$ at different rates from C/20 to C/8 for a typical prototype Li/PFPE1000-DMC-LiTFSI/LiNMC; d) cycle performance of battery prototypes showing discharge (green \square) and charge (blue Δ) capacities, as well as overall efficiencies (gray \bullet).¹⁹⁶ Adapted from ref. 193. Copyright 2014 National Academy of Sciences.

Recently, Konieczynska et al.¹⁹⁷ explored a polycarbonate based on the biocompatible building block of glycerol as a high temperature electrolyte. The repeat unit of the polymer resembles the molecular structure of low molecular weight linear and cyclic carbonates, as well as possesses a higher oxygen to carbon ratio, than pure aliphatic polycarbonates for greater dissolution of lithium salt. Specifically, poly(butyl ether 1,2-glycerol carbonate), synthesized via the ring-opening copolymerization of the corresponding glycidyl ether with carbon dioxide using the [rac-SalcyColIIDNP] catalyst, does not possess a glass transition (T_g) and decomposes at temperatures $>200\text{ }^{\circ}\text{C}$ (Figure 22a). Low conductivity ($10^{-5}\text{ S}\cdot\text{cm}^{-1}$) is observed at $25\text{ }^{\circ}\text{C}$, but raising the temperatures to $100\text{ }^{\circ}\text{C}$ significantly increased the conductivity by approximately 2 orders of magnitude ($10^{-3}\text{ S}\cdot\text{cm}^{-1}$ at $120\text{ }^{\circ}\text{C}$) (Figure 22b). This result is consistent with increased polymer chain mobility and, thus, enhanced Li salt mobility and conductivity. Also, these values are comparable to those of well-optimized PEO-based electrolytes and higher than the existing polycarbonate-based systems. The storage modulus (G') of the polyglycerol

carbonate at 2% strain is approximately 10^4 Pa at 1 Hz and 25 °C, indicating insufficient mechanical properties for preparation of a free-standing membrane between the electrodes (Figure 22c).

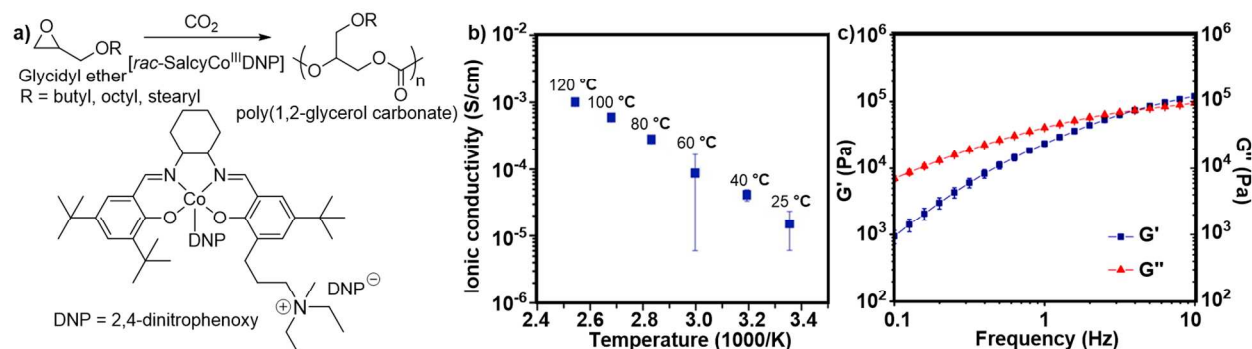


Figure 22. a) Reaction of glycidyl ether and CO_2 to yield poly(ether 1,2-glycerol carbonate) (DNP = 2,4-dinitrophenoxy); b) conductivity measurement of poly(butyl ether 1,2-glycerol carbonate) as a dependence of temperature by electrochemical impedance spectroscopy; c) frequency sweep at 2% strain of poly(butyl ether 1,2-glycerol carbonate) at 25 °C.¹⁹⁷ Adapted from ref. 194. Copyright 2015 American Chemical Society.

Khurana et al. reported on crosslinking polyethylene with poly(ethylene oxide) segments, using a ring-opening metathesis polymerization (ROMP), as one way to suppress crystallization of PEO chains (Figure 23a).¹⁹⁸ Copolymerization of cyclooctene (COE) with PEO using the Grubbs' 2nd generation catalyst gave a transparent film. The unsaturated double bonds were reduced via hydrogenation in the presence of an iridium catalyst to give the polymer electrolyte for lithium metal batteries. The conductivities of the polymers are on the order of 10^{-6} to $10^{-5} \text{ S} \cdot \text{cm}^{-1}$ at 25 °C with varied cross-linker length and different ratios of COE, similar to other improved PEO systems.^{199, 200} When a low molecular weight polyethylene glycol (PEG) (M_n 275 $\text{g} \cdot \text{mol}^{-1}$) is added to the cross-linked polymer (39 wt%), the ionic conductivity increased by about ten times to $2 \times 10^{-4} \text{ S} \cdot \text{cm}^{-1}$ at 25 °C (Figure 23b). A decrease of 65 °C for the glass transition temperature was also observed for this composition, indicating the suppression of PEO crystallization. At 100 °C, the ionic conductivity increased to the order of $10^{-2} \text{ S} \cdot \text{cm}^{-1}$. Galvanostatic lithium plate/strip electrochemical cycling measurements, in a symmetric Li/SPE/Li cell, quantified the effect of PE-PEO cross-linking on the dendrite formation time.^{201, 202} The measured short-circuit time, caused by dendrite formation, is dependent on the current density applied and the percentage of PEG added. Dendrite growth resistance is observed at 90 °C (short circuits at 430 hours) with the 39 wt% PEG at $0.26 \text{ mA} \cdot \text{cm}^{-2}$ (Figure 23c). As a comparison, Rosso et al. reported a short circuit time of 2 h at $0.25 \text{ mA} \cdot \text{cm}^{-2}$ and 90 °C for a PEO-LiTFSI polymer electrolyte.²⁰³

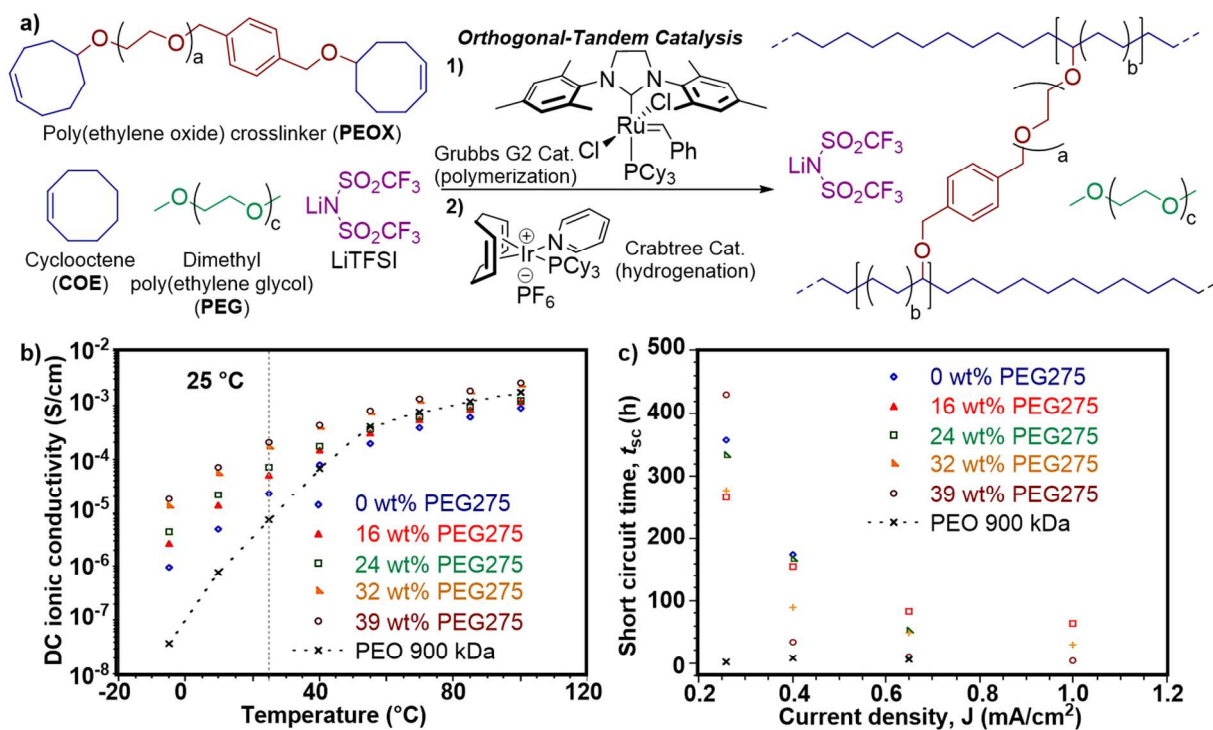


Figure 23. a) Polyethylene/poly(ethylene oxide) solid polymer electrolyte (SPE) synthesis; b) plot of DC ionic conductivity as a function of temperature for 70PEOX electrolytes having different weight percent of PEG275 plasticizer. All films had [COE]:[1] ratio of 15:1 and [EO]:[Li] composition of 18:1; c) galvanostatic polarization tests. Plot of short circuit time (t_{sc}) as a function of current density at 90 °C for various 70PEOX electrolytes having different weight percent (wt %) of the plasticizer (PEG275).¹⁹⁸ Adapted from ref. 195. Copyright 2014 American Chemical Society.

Solid polymer electrolytes are also investigated for high temperature tolerant supercapacitors, as these materials generally possess greater thermal stability. In contrast to ionic liquid electrolytes, solid polymer electrolytes have only limited contact with the electrode and can not access the porous structure. Thus, the electrical double layer (EDL) only forms at the surface of the electrode. A strategy to overcome this contact issue is to use a homogeneously distributed ionomer in the electrode and provide more sites for the electrolyte to form the EDL through the micro- or mesopores of the electrode material. Recently Kim et al.²⁰⁴ reported a high-temperature operating supercapacitor consisting of two reduced graphene oxide (RGO) electrodes and a poly-[2,20-m-phenylene-5,50-benzimidazole] (PBI) electrolyte doped with phosphoric acid (H_3PO_4) (Figure 24a). The polymer electrolyte exhibited a high conductivity of $\sim 100 \text{ mS} \cdot \text{cm}^{-1}$ immersed in a 85% of H_3PO_4 solution. The ion-hopping mechanism occurred at 100 °C and is facilitated by doping with H_3PO_4 . The substantially enhanced charge transfer led to a high capacitance of $170 \text{ F} \cdot \text{g}^{-1}$ at 160 °C (Figure 24b). Capacitive behavior is observed from 30 to 160 °C, with higher capacitance at higher temperatures. A high capacity of $150 \text{ F} \cdot \text{g}^{-1}$ along with $< 10\%$ of capacity loss is observed over 100,000 cycles at 120 °C. Coupling three RGO-PBI SCs devices in series powered a red light-emitting-diode (LED). An attractive feature of this system is the free-standing, mechanical strong, and bendable electrolyte film, which showed excellent mechanical durability after hundreds of bending cycles (at bend angles of 60 - 180°). Thus, the polymer film can be easily adapted to flexible and demanding cell configurations. A similar finding is reported by Hastak et al.,²⁰⁵ who mixed poly [2,5 benzimidazole] (ABPBI) with H_3PO_4 . They demonstrated supercapacitor operation at up to 200 °C using activated carbon

(AC) electrodes. Compared with the previous example, the conductivity of the ABPBI electrolyte at 100 °C is around $10 \text{ mS} \cdot \text{cm}^{-1}$ with 67% of H_3PO_4 doping (Figure 24c). The specific capacitance increased linearly with temperature and with the percentage of ABPBI polymer doping in the electrode, as the binder amount influenced the specific capacitance. The highest capacitance reached is around $200 \text{ F} \cdot \text{g}^{-1}$ at 120 °C, when 25% of ABPBI is used (Figure 24d).

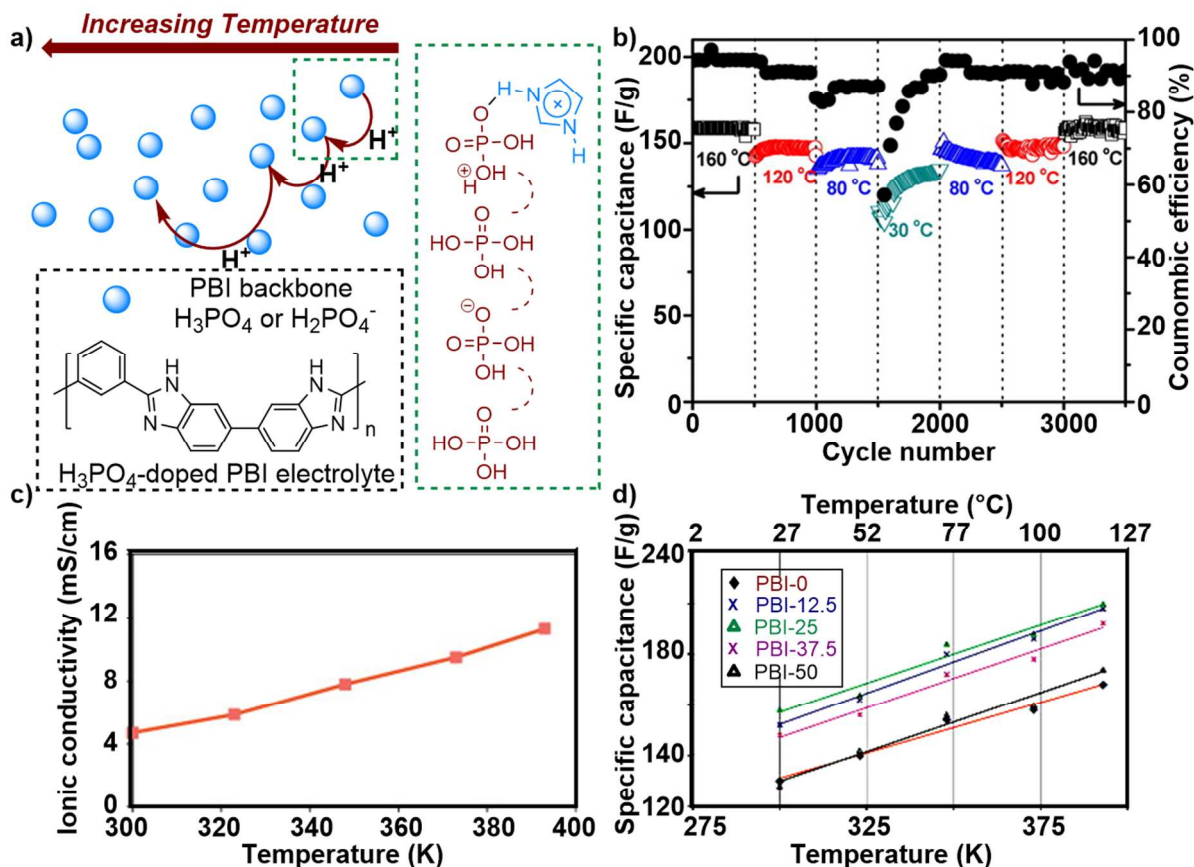


Figure 24. a) Schematic view of thermally activated, nanoscale-confined ionic transport at elevated temperatures; b) long-term stability (3500 GCD cycles at $1 \text{ A} \cdot \text{g}^{-1}$) of RGO-PBI SC under dynamic thermal stresses (temperature variations per 500 cycles);²⁰⁴ c) ionic conductivity of ABPBI doped with 67% of phosphoric acid at different temperatures; d) specific capacitance of supercapacitors at different temperatures.²⁰⁵ Adapted from refs 201 and 202. Copyright 2015 American Chemical Society and 2012 Elsevier.

5.1.4 Ceramics. Ceramic electrolytes offer potential advantages including thermal stability, a large electrochemical stability window, absence of fluid leakage, and a resistance to vibrations and shocks. Ionic transport occurs in solids due to atomic disorder in the crystal structures.^{189, 206-209} The conductivity is inversely related to the activation energy of the ions moving between the lattice, and the mobility is correlated to the ionic radius.²¹⁰ Multivalent ions exhibit lower conductivities because they carry larger charge and have higher activation energies. Most solid ion conductors use monovalent ions, such as lithium, potassium, and sodium. $\text{NaA}_2^{\text{IV}}(\text{PO}_4)_3$; $\text{A}^{\text{IV}} = \text{Ge}, \text{Ti}, \text{or Zr}$ and $\text{Na}_{1+x}\text{Zr}_2\text{Si}_x\text{P}_{3-x}\text{O}_{12}$, $0 < x < 3$ developed in the 1970s are well known and referred to as Na Super Ion Conductors (NASICON).^{46, 211-213} They exhibit high conductivities of 10^{-3} to $10^{-2} \text{ S} \cdot \text{cm}^{-1}$ at room temperature, which are comparable to liquid electrolytes, and are thermally stable up to 200 °C. For example, Lalère et al.²¹⁴ recently reported an all-solid sodium battery incorporating $\text{Na}_3\text{V}_2(\text{PO}_4)_3$ as the electrode and $\text{Na}_3\text{Zr}_2\text{Si}_2\text{PO}_{12}$ as the sodium ion

conducting electrolyte. The battery, assembled through spark plasma sintering at 900 °C, operated at 1.8 V and 200 °C to give a capacity of 1.04 mA h cm⁻² (C/10) with less than 10% of capacity reduction after 25 cycles.

On the other hand, inorganic solid Li ion conductors are of particular interest as solid-state electrolytes in Li-ion batteries, and the reader is referred to reviews by Adachi, Knuath, and Robertson.²⁰⁷⁻²⁰⁹ One of the most studied ceramic electrolyte is lithium phosphorus oxynitride (LiPON; Li_{2.88}PO_{3.73}N_{0.14}). LiPON exhibits a room temperature conductivity of 10⁻⁶ S · cm⁻¹. LiPON possesses a unity lithium cation transference number, an electrochemical window greater than 5 V versus Li/Li⁺, is stable at elevated temperatures, is compatible with lithium metal, and thin films can be prepared by sputtering. Li ion conductors based on the NASICON crystallographic structure are also prevalent with, for example, LiGe₂(PO₄)₃, LiTi₂(PO₄)₃, and LiTi_{0.5}Zr_{1.5}(PO₄)₃ exhibiting ionic conductivities ranging from 10⁻⁵ to 10⁻³ S · cm⁻¹ between 100 and 200 °C. The observed conductivity between 25 to 250 °C is governed by the grain boundaries present within the materials. Li ion conductivity is increased upon doping with Al, and Li_{1.3}Al_{0.3}Ti_{1.7}(PO₄)₃ exhibited a conductivity of 10⁻³ and 10⁻¹ at 25 and 200 °C, respectively. Replacing the large Ti⁴⁺ cations with smaller Al³⁺ cations reduces unit cell dimensions and increases ionic conductivity. The presence of the Ti cations and their susceptibility to reduction limits the use of these materials with Li metal electrodes. The perovskite (ABO₃)-type lithium lanthanum titanate ionic conductors (LLTO) exhibit conductivities that are dependent on the Li concentration and on the order of 10⁻³ S · cm⁻¹. Lithium transport occurs via a vacancy mechanism. Other solid conductors such as LiTi₂(PO₄)₃, thio-LISICON Li_{3.25}Ge_{0.25}P_{0.75}S₄, Li₅La₃Ta₂O₁₂, Li_{5.5}La₃Nb_{1.75}In_{0.25}O₁₂, and Li₃PO₄-Li₂S-SiS₂ have also been explored and possess conductivities on the order or less than 10⁻³ S · cm⁻¹.

One of the highest Li⁺ ionic conducting solids reported are Li₃N single-crystals. Li₃N exhibits a two-dimensional layered structure, similar to β-alumina (beta), where the Li⁺ transports between the layers.²¹⁵ A conductivity of 1.2 x 10⁻³ S · cm⁻¹ is measured for the crystal at room temperature. At temperatures above 100 °C, the conductivity of lithium nitride increases in magnitude to 10⁻³ to 10⁻¹ S · cm⁻¹ depending on the doping and stoichiometry, reaching as high as 8.8 S · m⁻¹ at 400 °C.²¹⁶ A low cathodic decomposition potential prevents it from being used with high-voltage cathodes and from wide-spread adoption. Similarly, the related Li₂S glasses also possess a conductivity of around 1 S · cm⁻¹ at room temperature.²¹⁷⁻²²⁰ The high conductivity is proposed to be a consequence of the smaller bonding energy between Li⁺-S and the larger tunnel size for Li⁺ migration in a glass compared to a crystal. Although these high Li⁺ conducting electrolytes show promise, decomposition in air remains a limitation.

As is shown in Figure 25, ceramics are generally more thermally stable than ionic liquids and solid polymer electrolytes, although they are brittle materials. While possessing excellent high temperature tolerance, up to 800 °C, they typically exhibit conductivities above 10⁻³ S · cm⁻¹ when the temperature is greater than 100 °C and are suitable electrolyte materials when the desired operation temperature falls into the range of 80 - 300 °C, where a number of ceramics may provide satisfactory conductivities (for example, the conductivity of LiPON is above 1 mS · cm⁻¹ above 100 °C). Their use is typically limited to as thin films (<1 μm thick) for batteries, where the electrolyte impedance is minimized. These solid electrolytes can be produced through thin-film techniques, such as RF magnetron sputtering, which is challenging to implement on the commercial scale. In addition, other processing conditions that utilize high-temperature sintering (> 1,300 °C) limit the practical implementation of ceramic based electrolytes.^{221, 222}

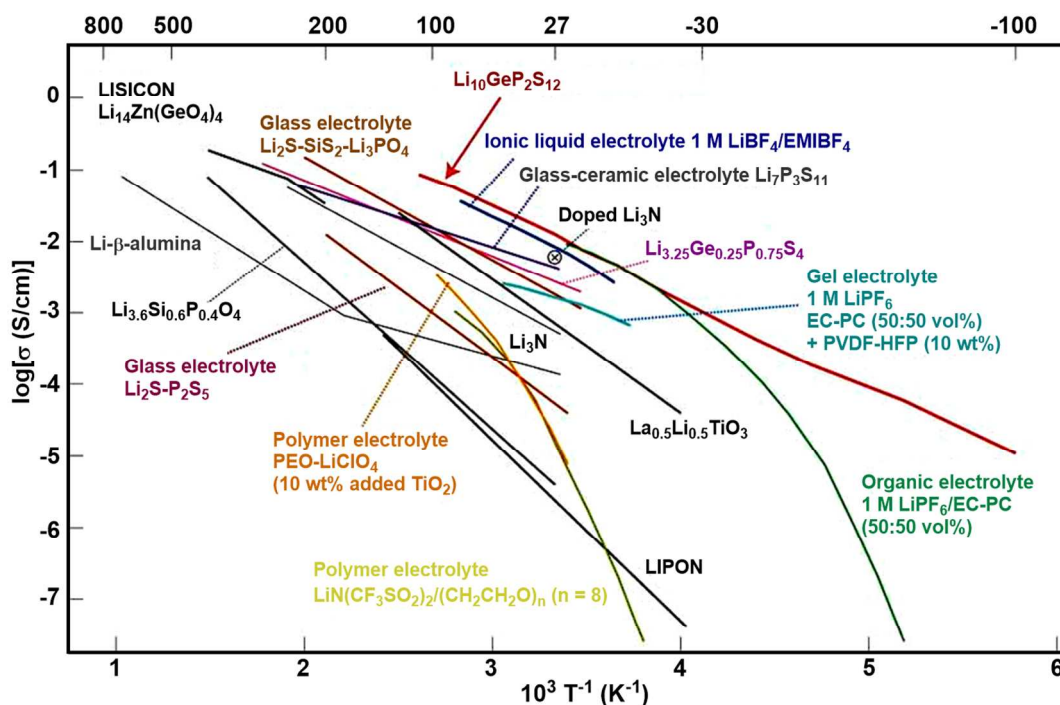


Figure 25. Ionic conductivity of ceramics, solid electrolytes, organic liquid electrolytes, polymer electrolytes, ionic liquids and gel electrolytes.²²³ Copyright 2011 Macmillan Publishers.

A significant advance in the field is reported by Kamaya et al.,²²³ who described a new solid-state electrolyte ($\text{Li}_{10}\text{GeP}_2\text{S}_{12}$) that exhibited an ionic conductivity of $10^{-2} \text{ S} \cdot \text{cm}^{-1}$ along with a wide electrochemical potential window from -0.5 to 5 V at 27 °C (Figure 26b). This lithium superionic conductor, is prepared using a thermal synthesis route. Synchrotron X-ray diffraction (XRD) and neutron diffraction studies revealed one-dimensional (1D) chains within the lattice formed by LiS_6 octahedra and $(\text{Ge}_{0.5}\text{P}_{0.5})\text{S}_4$ tetrahedra (Figure 26a). Specifically, a common corner shared by the PS_4 tetrahedra and LiS_6 octahedra defines the 1D chains. Li transport is proposed to occur via displacement from the 16h and 8f sites toward interstitial positions between two 16h sites and between the 16h and 8f sites. Subsequent evaluation of an all-solid-state battery comprising the $\text{Li}_{10}\text{GeP}_2\text{S}_{12}$ electrolyte, a LiCoO_2 cathode, and an In metal anode functioned for eight charge-discharge cycles at 27 °C. Upon cycling, the battery showed an initial 20% capacity loss, and then gradually stabilized at approximately $120 \text{ mAh} \cdot \text{g}^{-1}$, at a current density of $14 \text{ mA} \cdot \text{g}^{-1}$ (Figure 26c). The authors did not report the performance of the battery at elevated temperatures, but given the preparation of the electrolyte at 550 °C, and the conductivity versus temperature response measured, these experiments are of merit.

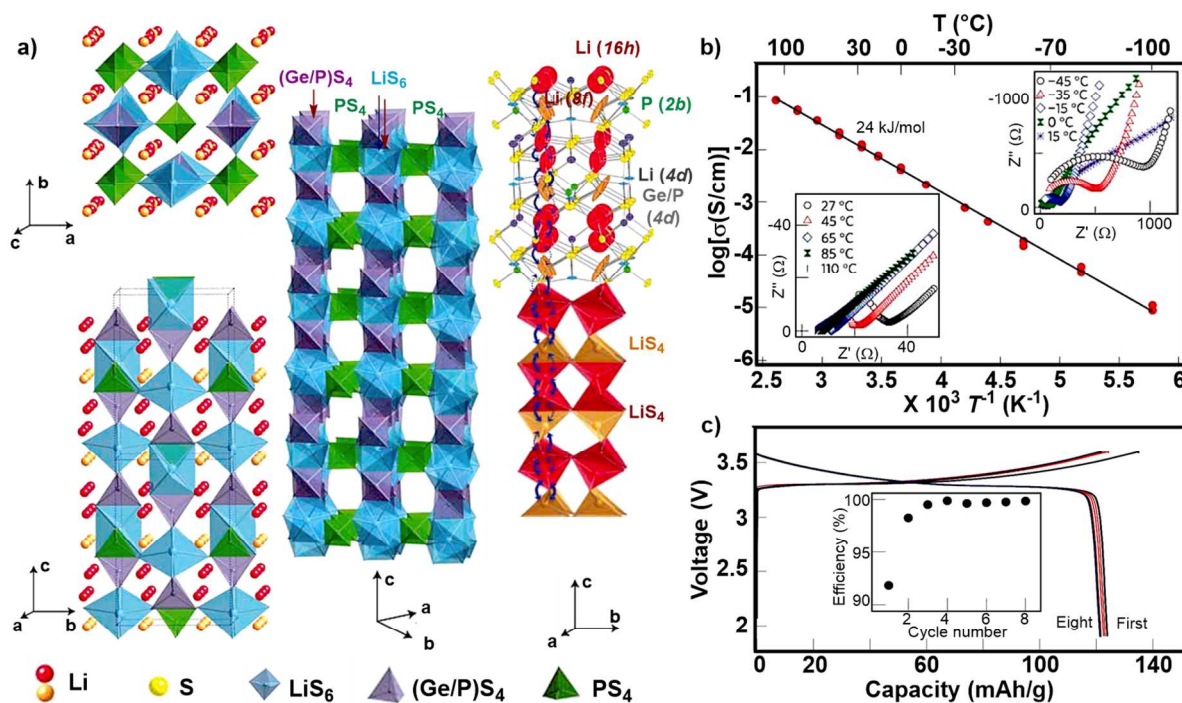


Figure 26. a) Crystal structure of $\text{Li}_{10}\text{GeP}_2\text{S}_{12}$; b) impedance plots of the conductivity data from low to high temperatures and Arrhenius conductivity plots of $\text{Li}_{10}\text{GeP}_2\text{S}_{12}$. The plotted conductivity represents the sum of the grain boundary and bulk conductivities; c) charge-discharge curves of an all-solid-state battery consisting of a LiCoO_2 cathode, a $\text{Li}_{10}\text{GeP}_2\text{S}_{12}$ electrolyte and an In metal anode. The current density is $14 \text{ mA} \cdot \text{g}^{-1}$.²²³ Adapted from ref 215. Copyright 2011 Macmillan Publishers.

Hibino et al.²²⁴ reported the performance of a solid-state supercapacitor composed of a $\text{Sn}_{0.95}\text{Al}_{0.05}\text{H}_{0.05}\text{P}_2\text{O}_7$ -polytetrafluoroethylene composite electrolyte sandwiched between two pre-treated acid carbon electrodes immersed in 105% H_3PO_4 . The $250 \mu\text{m}$ thick electrolyte membrane itself exhibited temperature independent ionic conductivity on the order of $0.01 \text{ S} \cdot \text{cm}^{-1}$ (Figure 27a), and CV experiments revealed stable performance between - 2 to 2 V. When operating the supercapacitor between 100 and 200 °C at low current densities (e.g., $3 \text{ A} \cdot \text{g}^{-1}$), high energy densities are achieved between 15 and $32 \text{ Wh} \cdot \text{kg}^{-1}$. Increasing the current density to as high as $13 \text{ A} \cdot \text{g}^{-1}$ still provided energy densities as high as $12 \text{ Wh} \cdot \text{kg}^{-1}$. At room temperature and at 100 °C, the energy density remained unchanged over 7000 cycles, with the supercapacitor operating at 100 °C providing approximately 50% more $\text{Wh} \cdot \text{kg}^{-1}$. Increasing the operational temperature to 150 °C afforded a 27% loss in capacity after 7000 cycles (Figure 27b). At the highest temperature reported (200 °C), the capacity retention and lifecycle of the device are significantly compromised within 1000 cycles. The poorer performance of the supercapacitor at higher temperatures is attributed to the dehydration and decomposition of the 105% H_3PO_4 as well as to the loss of adhesion from the sealing tape, used to secure the device, allowing air to leak into the supercapacitor.

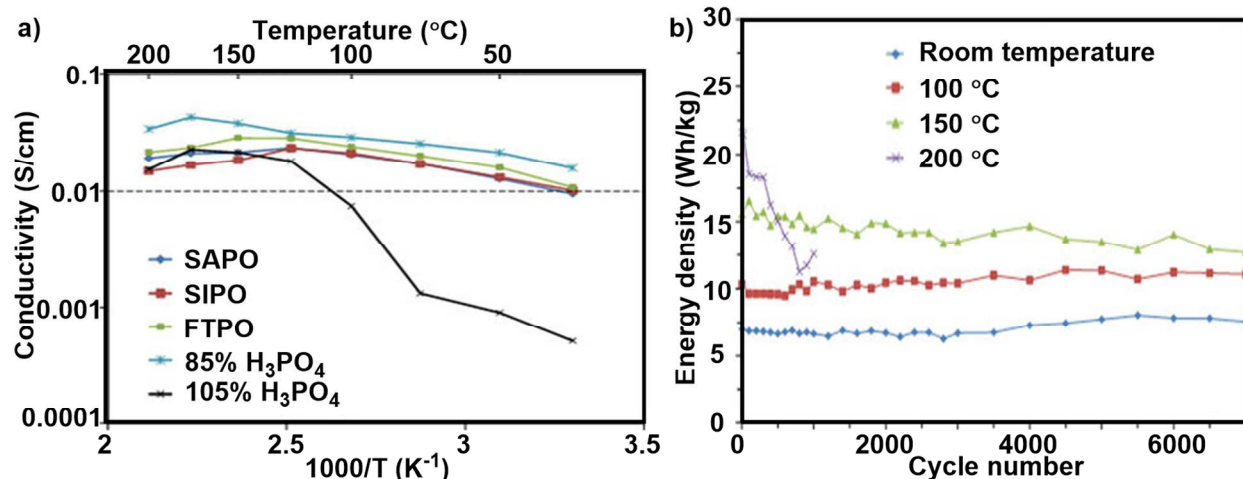


Figure 27. a) Temperature dependence of proton conductivity for the SIPO, SAPO, and FTPO-PTFE composite membranes, and 85% and 105% H₃PO₄; b) energy density as a function of cycle number measured at various temperatures with the current density set in the range of 4.5 - 6 A · g⁻¹.²²⁴ Adapted from ref 216. Copyright 2015 Macmillan Publishers.

5.2 New thermally stable Li salts

Xu et al.²²⁵ reported that lithium bis(oxalato)borate (LiBOB) can be used as a thermally stable Li salt, when dissolved in an electrolyte, between two electrodes and enable battery operation up to 70 °C. However, LiBOB possesses limited solubility in carbonate solvents or ionic liquids, and the SEI it forms is highly resistive leading to deterioration of cell capacity and rate capability. In response to these limitations, Zhang et al.^{226, 227} described the design and synthesis of lithium oxalyldifluoroborate (LiODFB) which resembles the structures of LiBOB and LiBF₄ (Figure 28). LiODFB, synthesized by reacting BF₃ etherate and Li₂C₂O₄ in a 1:1 molar ratio, possessed better solubility, a lower viscosity, and stabilized the SEI on the surface of a graphite anode. The conductivity of LiODFB is slightly higher than LiBOB at low temperatures (< 10 °C), however, as the temperature increased, the conductivity of LiODFB also increased but its value is lower than that of LiBOB and above LiBF₄. Although the decomposition temperature of LiODFB is approximately 100 °C lower than that for LiBF₄, the salt did not decompose until 250 °C at a heating rate of 10 °C · min⁻¹, enabling the potential of high temperature application. When this salt is dissolved in PC:EC:DCM and added to graphite/ LiNi_{0.8}Co_{0.15}Al_{0.05}O₂ cell, the cell performed for 200 cycles at 60 °C with less than 10% of capacity loss.

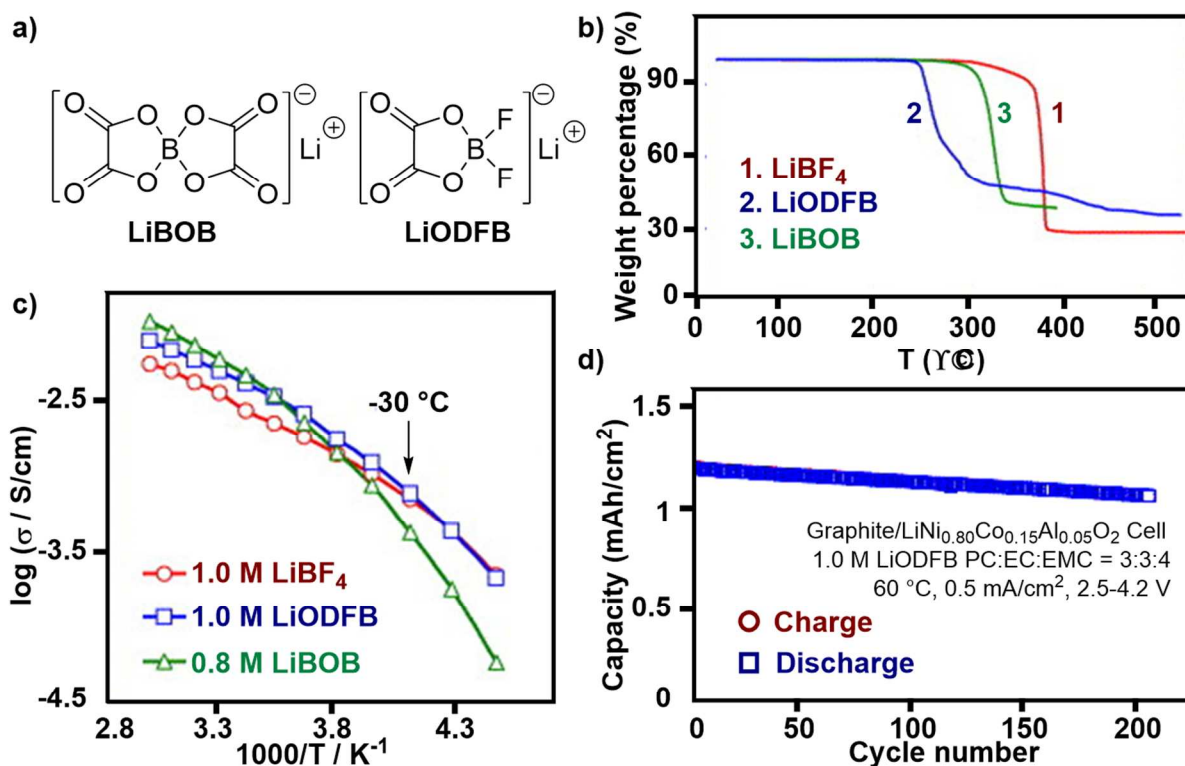


Figure 28. (a) Structure of LiBOB and LiODFB; (b) TGA traces of LiBF₄, LiODFB, and LiBOB, which were recorded during heating at a rate of 10 °C · min⁻¹ under a nitrogen flow; (c) Arrhenius plots of the ionic conductivity of LiBF₄, LiODFB, and LiBOB in a 1:1:3 (wt.) PC/EC/EMC solvent mixture; (d) high temperature (60 °C) cycling performance of the Li-ion cell with a 1.0 m LiODFB 3:3:4 (wt.) PC/EC/EMC electrolyte, which was recorded by charging and discharging at 0.5 mA between 2.5 V and 4.2 V with charging current tapered to 0.05 mA.²²⁶ Adapted from ref 218. Copyright 2006 Elsevier.

A lithium borate cluster salt Li₂B₁₂H₁₂-xF_x is recently described as a new electrolyte salt. It displays moderate conductivity from 2.5 mS · cm⁻¹ (25 °C) to 5 mS · cm⁻¹ (80 °C) with increasing temperature. An additional advantage of this lithium salt, is that it acts as a “redox shuttle” and provides overcharge protection in cells.²²⁸⁻²³² Chen et al.²³³ reported two variants of these salts, Li₂B₁₂F₉H₃ and Li₂B₁₂F₁₂, both of which showed redox reactions at 4.4 - 4.7 V (vs. Li/Li⁺) and prevented cathode de-lithiation above 4.4 V at 55 °C (Figure 29). Specifically, 0.4 M Li₂B₁₂F₉H₃ and 0.1 M LiBOB were dissolved in a 3:7 by weight ration of EC and ethyl methyl carbonate (EMC) followed by addition of 1.0 wt% of 2-(pentafluorophenyl)-tetrafluoro-1,3,2-benzodioxaborole (PFPTFBB), as a Lewis acid, to produce LiDFOB and LiTFOP in situ and enhance SEI stability. The graphite/ Li_{1.1}[Ni_{1/3}Mn_{1/3}Co_{1/3}]_{0.9}O₂ cell containing this electrolyte operated at 55 °C for 1200 cycles with only a 30% loss of capacity. The performance is superior to that of cells containing LiPF₆ or LiDFOB. In situ HEXRD experiments revealed that this lithium salt delayed the phase transformation of the spinel Li_{1.1}[Ni_{1/3}Mn_{1/3}Co_{1/3}]_{0.9}O₂ cathode and the reaction between the delithiated cathode and electrolyte by several tens of degrees. The better tolerance of Li₂B₁₂H₁₂ to the presence of water (up to 35,000 ppm) is also noted.

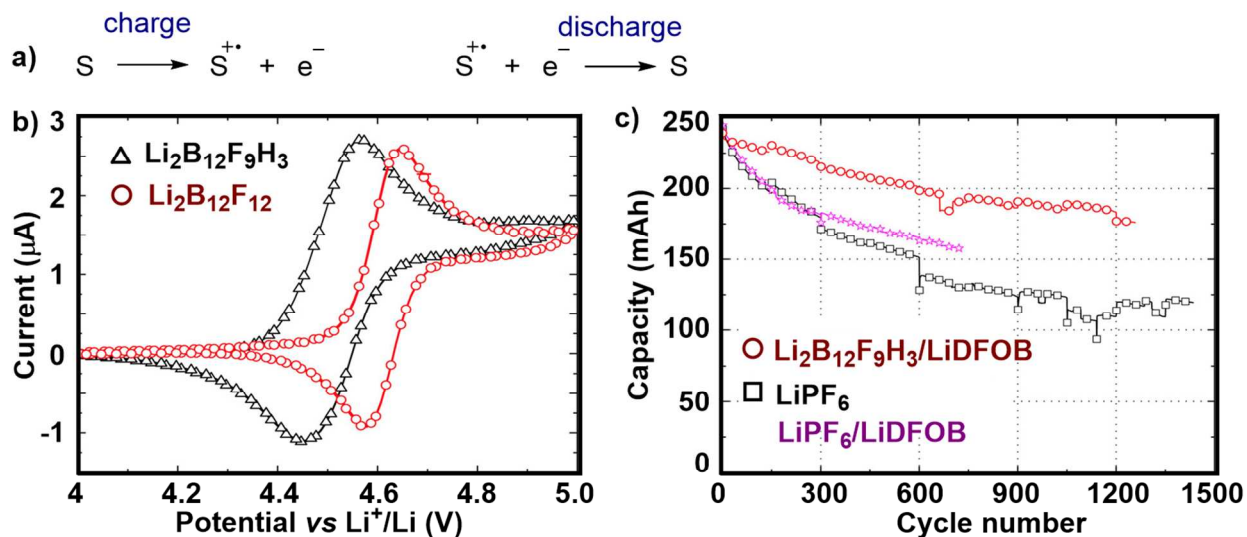


Figure 29. a) Reversible redox reaction of $\text{B}_{12}\text{F}_{12}^{2-}$ and $\text{B}_{12}\text{F}_9\text{H}_3^{2-}$ for overcharge protection of lithium-ion cells; b) cyclic voltammograms of 10 mM $\text{Li}_2\text{B}_{12}\text{F}_9\text{H}_3$ and $\text{Li}_2\text{B}_{12}\text{F}_{12}$ in 1.2 M LiPF_6 in EC/EMC using a Pt/Li/Li three-electrode cell at a scanning rate of $10 \text{ mV} \cdot \text{s}^{-1}$; c) discharge capacity as a function of cycle number for graphite/ $\text{Li}_{1.1}[\text{Ni}_{1/3}\text{Mn}_{1/3}\text{Co}_{1/3}]_{0.9}\text{O}_2$ lithium-ion cells cycled between 3.0 V and 4.1 V at a constant current of 0.5 mA (C/3) at 55°C .²³³ Adapted from ref 225. Copyright 2013 Macmillan Publishers.

There is also a special class of high temperature electrolyte utilizing molten salt. Munoz-Rojas et al.²³⁴ studied molten LiTFSI at 250°C as the electrolyte itself sandwiched between a Li anode and a LiFePO_4 cathode using a customized Swagelok cell. All plastic parts in Figure 30a were switched from plastic to metallic to enable high temperature operation up to 300°C . LiTFSI is an ideal molten salt for this application as it melts at approximately 230°C and does not decompose over the temperature range of interest. Glass fibers were utilized as separators in this cell. Direct contact between the liquid lithium metal and the cathode, at this high temperature, was avoided by placing a stainless steel grid (0.5 mm pore size) between the lithium anode and separators. This design prevents liquid lithium from penetrating through the separators by capillarity forces. A special high temperature silicone XTS 320 (INTEK Adhesives, UK) replaced the Al_2O_3 -based glue as the glue reacts with LiTFSI. All these modifications are important to enable high temperature operation ($>250^\circ\text{C}$). Eight charge-discharge cycles are obtained at 250°C with a capacity between 150 and $180 \text{ mAh} \cdot \text{g}^{-1}$. However, polarization is observed due to the low conductivity of LiTFSI at 250°C , and the use of a thick stainless steel grid. For example, a less significant polarization is observed when using the thinner grid of $25 \mu\text{m}$, compared to that of the $500 \mu\text{m}$ one.

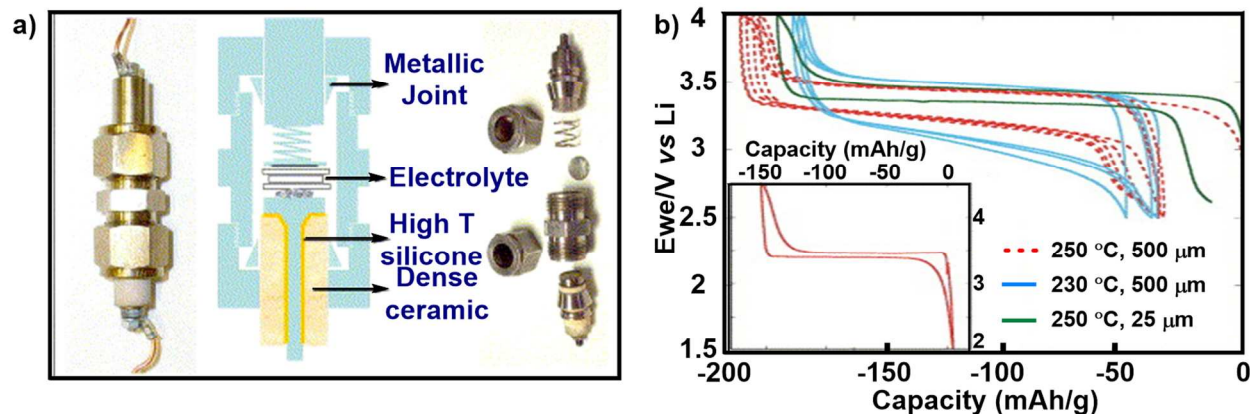


Figure 30. a) High temperature customized Swagelok cell; b) charge–discharge curves obtained at high temperature (230 and 250 °C) using molten LiTFSI as electrolyte and molten Li as negative electrode in a modified high temperature Swagelok-type modified cell using metallic grids of 500 and 25 μm . Inset: Charge–discharge curve for LiFePO_4 at room temperature using LiPF_6 in EC/DMC 1:1 as electrolyte.²³⁴ Adapted from ref 226. Copyright 2007 Elsevier.

6. Critical Evaluation and Limitations of Current Systems

In a number of respects, the existing EES systems are far from ideal, as demonstrated by the preceding summary. Therefore, additional EES research and development efforts are needed to further understand the fundamental thermodynamics and kinetic processes at temperatures above ambient temperature and to discover new materials or refine existing materials with optimized properties that integrate with the other components of the device.

- Ionic conductivity.** Despite the improved ionic conductivity observed with new electrolyte materials, which is further enhanced by virtue of operation at temperatures greater than room temperature, the conductivity is still less than $10 \text{ mS} \cdot \text{cm}^{-1}$ with an unsatisfactory rate capability term (i.e., high C-rates cannot be reached) compared to carbonate solvents. At temperatures greater than 100 °C, the conductivities of most ionic liquids are still on the order of $10^{-4} - 10^{-3} \text{ S} \cdot \text{cm}^{-1}$ in magnitude, while that of most polymers and ceramics are on the order of $10^{-5} - 10^{-3} \text{ S} \cdot \text{m}^{-1}$, with a few exceptions in which the polymers and ceramics showed exceptional conductivities. Structure-property relationships are needed for describing the dependence of conductivity on electrolyte composition, viscosity, and temperature to guide future studies.

From a polymer perspective, low T_g polymers are being designed, synthesized, and evaluated to increase the ionic conductivity. However, it has been proposed that polymers also need to possess a high shear modulus (at the magnitude of 10^9 Pa , Chazalviel theory)^{201, 235, 236} to reliably separate the electrodes and effectively suppress dendrite growth. However, Khurana et al. recently reported that a polymer of relatively low-modulus on the order of 10^5 Pa at 90 °C mitigates dendrite growth.¹⁹⁸ Unfortunately, most of the polymers that achieve high ionic conductivities (10^{-3}) by doping in a liquid plasticizer, lead to a reduction of mechanical strength. Some of the systems that show conductivity at high temperatures (e.g., polycarbonates) also possess low T_g , and the viscous character precludes the formation of a free-standing film, further limiting the processability required for industry scale manufacturing. Moreover, the lack of systematic conductivity and mechanical data on the polymers at high temperatures exacerbates the challenge to generate composition-structure-property relationships to aid in the identification or the design of new polymer-based electrolytes. Increasing the temperature softens the polymeric material, reduces the shear modulus, hence deteriorating the mechanical strength. The requirement for ionic conductivity and mechanical strength appear to be contradictory, and optimal materials may represent a compromise on both fronts. A few reports described an alternative strategy to the prevailing low T_g solution, and proposed that ion

transport is facilitated in an ordered environment of the crystalline phase, instead of solely relying on the segmental movement of the polymer chains in the amorphous phases.^{237, 238} Using this approach high ionic conductivity and high shear modulus may be obtained simultaneously, and additional research is required to validate this approach and understand the underlying ion transport mechanism(s).

- **Long-time thermal stability.** Ionic liquids, polymers, and ceramics are generally considered as thermally stable materials, but this is dependent on the working temperature. While ceramics are stable at temperatures between 200 to 300 °C, ionic liquids and solid polymers are generally not. At temperatures between 40 and 150 °C, all three electrolyte materials exhibit thermal stability, but the ionic conductivity can be significantly different between the classes of materials. The thermal decomposition temperatures of the materials are most commonly measured by TGA, where the temperature is ramped relatively quickly at a heating rate of 10 °C/min or even faster. Consequently, there may be insufficient time for the heat to dissipate throughout the material, thus, the measured decomposition temperature may not reflect the actual temperature at which the material starts to degrade and overestimates the thermal decomposition temperature.^{239, 240} The specific heating rate may also influence the thermodynamics and kinetics of thermal reactions being studied. In addition, TGA is an analytical technique that measures only the weight loss of the material. However, chemical transformations or phase transitions can occur before the weight loss is detected, which would alter the ion transport properties of the electrolyte. For example, Del Sesto et al. reported that the ionic liquid butylmethylimidazolium bis(trifluoromethanesulfonyl)amide (C4MIM-TFSI) started to decompose around 200 °C as observed by optical techniques, and this temperature is significantly lower than the previously reported decomposition temperature of around 400 °C.²⁴¹ This may explain why some electrolyte materials are reported to have superior thermal stability, yet show poor performance at temperatures below their decomposition temperatures.

Furthermore, long-term thermal stability at a constant desired high temperature is rarely determined, which is critical for selecting the materials for rechargeable energy storage devices that will perform for hundreds or thousands of charge-discharge cycles. Unfortunately, most of the TGA measurements or voltammetric cycling studies are conducted within a short time frame (within hours or tens of minutes for most cases), which provides minimal insight to predicting long-term stability, performance, and/or shelf-life. The study conducted by MacFarlane and co-workers exemplifies this point, where they showed the decomposition of 1 wt% of PYR14-TFSI electrolyte occurred after isothermal heating for 10 hours at 271 °C, while the same electrolyte decomposed at 435 °C when using a fast ramp heating process.²⁴²

Finally, the confirmation of material thermal stability is further complicated by the sensitivity of the instruments used. The bulk material, chemical bonds changes, and small amounts of impurities are being detected using standard techniques such as TGA and NMR. However, it is difficult to detect trace amount of species using these techniques. Del Sesto et al.²⁴¹ reported that when more sensitive spectroscopic detection methods are used, for example, fluorescence spectroscopy, decomposition of several commonly used pyrrolidinium and imidazolium ionic liquids occurred at hundreds of degrees below the TGA measured temperatures previously reported.²⁴⁰ Pyschik et al. also studied the long-term aging of the commonly used PYR14-TFSI and EMI-TFSI at 95 °C.²⁴³ After 16 months the decomposition species were detected by ion chromatography / mass spectrometer (IC-MS). The mass spectrum and proposed decomposition mechanism at 95 °C for PYR14-TFSI is shown in Figure 31. The side chain of the cation cleaves at high temperature and subsequently reacts with the cationic center to form the new decomposition species. Such decomposition or degradation processes will adversely affect the cell performance and lead to persistently fading capacity, increasing internal gas generation, and decreasing power density. This may also explain the long-standing observation that some ionic liquids slowly change color upon heating at temperatures below their decomposition temperature. Nevertheless, the decomposition routes of existing and new

materials are poorly understood, and additional detailed studies are needed to gain more insight into the corresponding device failure. These thermal stability studies need to be carefully performed via thoughtfully designed protocols with identification of the underlying chemical reactions and products using highly sensitive spectroscopic methods.

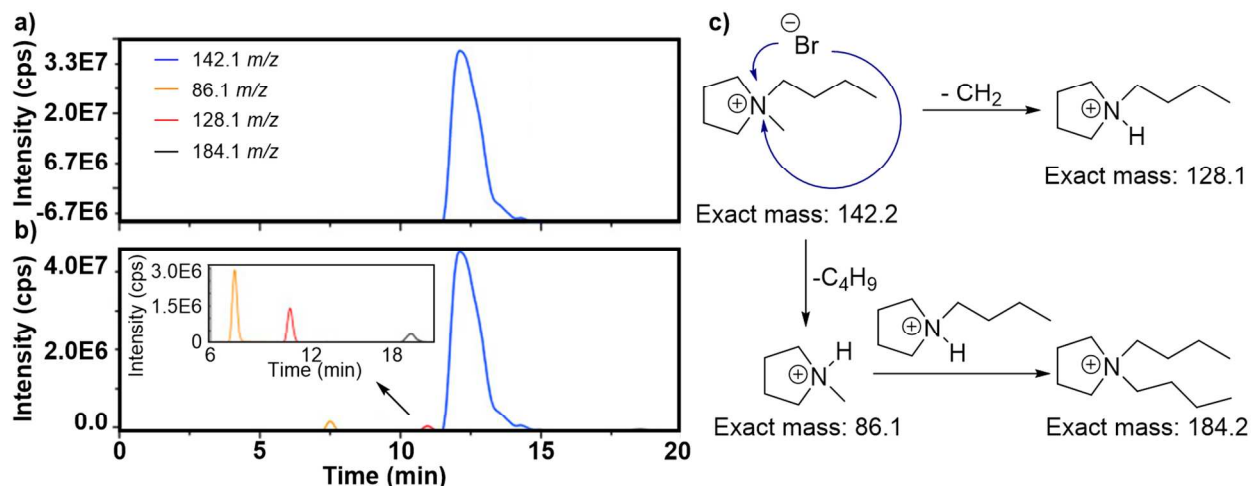


Figure 31. m/z -ratios of the decomposition products of PYR14⁺ (from the IL PYR14-TFSI) in the ESI-MS chromatogram a) after storage at room temperature for 16 months with/without electrolyte salts and; b) after storage at 95 °C for 16 months; c) proposed decomposition mechanism of the cation PYR14⁺.²⁴³ Adapted from ref 235. Copyright 2015 Elsevier.

- Compatibility between cell components and SEI stability.** In addition to addressing the thermal stability and performance of the individual cell components, it is also critical to assess the effect of temperature on the interfacial reactions and changes in material properties. Increasing the temperature, for many reactions, not only accelerates the kinetics of known reactions occurring at room temperature, but also promotes new chemical or electrochemical reactions. Electrolytes, in particular, are in contact with almost every cell component, thus compatibility is required across a range of temperatures from 25 to 300 °C. The above-mentioned examples showed decreased anodic potential in the electrochemical window as temperature increased. Therefore, operation at a specific temperature greater than ambient conditions pose stringent requirements on stability. Once the operational temperature is identified, every component needs to be evaluated in concert with each other, optimized, and validated for long-term studies.

It is well accepted that the formation of the passivating SEI stabilizes the interface between the electrolyte and electrode, especially the anode in conventional batteries, and affords extended cycling. However, this may not be the case for battery operation at high temperatures as the SEI (produced by the standard carbonate solvents and graphite) is found to degrade at higher temperatures, resulting in persistent consumption of electrolyte and electrode, as well as a build-up of internal resistance. Currently there are no reports of a stable SEI at elevated to high temperatures. In fact, due to the elusive nature of this thin and fragile interface, it is still unclear whether non-carbonate electrolytes can form an effective SEI, or SEI at all. Since the composition and properties of the SEI are highly dependent on electrolyte, salt, and electrode composition, comprehensive data are needed to construct composition-structure-property relationships to guide the rational choice of electrolyte and electrode to yield the desired, protective SEI at high temperatures.

- Energy density.** As mentioned above, energy density is determined by the electrode couples and the efficiency of Li conduction in the electrolyte and transference between the

electrodes and electrolyte. For the electrode materials, high temperature limits the choice of known cathodes to LiFePO_4 , which has a low theoretical capacity compared to other non-thermally stable cathode materials. The relatively low operational voltage of LiFePO_4 also limits the energy density of this material. Therefore, the search for new thermally stable cathode materials is a high priority. For the anode, graphite exhibits high thermal stability but the polymer binders used decompose at high temperature leading to degradation of the electrode. Lithium metal, which is still considered as the “holy grail” among anode materials with the lightest weight and lowest potential, unfortunately melts at $180\text{ }^\circ\text{C}$, thus restricting operational temperature to below this value. In addition, lithium metal is a key component in high temperature Li-air and Li-S batteries, which provide several times higher energy densities than other systems. For supercapacitors, where cyclability and power density are usually not the greatest concern, substantial effort are focused toward increasing the energy density using pseudocapacitive materials, such as metal oxides or conducting polymers. However, the use of pseudocapacitive materials can limit the cyclability of the device. Therefore, high surface area electroactive materials, with thermal stability, are of particular interest to enhance the energy density. Moreover, developing hybrid devices combining the features of batteries and supercapacitors that bridge the energy density and power density gap between these two primary energy storage devices, as desired for room temperature applications, may also represent future endeavors in developing high temperature thermal stable EES.

- **Long-term cyclability.** For room temperature applications, tens of thousands of cycles are required for commercial products. At temperatures greater than $80\text{ }^\circ\text{C}$, cycling beyond 100 times without capacity decay remains a significant challenge. Long-term cyclability is directly related to the quality of SEI and its stability at high or fluctuating temperatures. It also depends on the composition of the electrolyte, electrodes, separators, etc. that comprise the cell. The requirement for long-term cyclability will become particularly important for high temperature batteries as the application space transitions from the specialty industries to the automotive industry, for example, where tens of thousands of cycles are required. Thus, improvements in cyclability will likely rely on advances in the individual material components as well as engineering the interfacial stability between the electrolyte and the electrode materials.

7. Concluding Remarks, Perspectives, and Future Directions

The past decade witnessed an ever-increasing demand for high temperature EES with concurrent expanding research activities in discovering, developing, and understanding the thermal behavior of batteries and supercapacitors. At present, the range of applications for temperature-stable lithium-ion batteries is large and the market is likely underestimated. Potential applications include but are not limited to electrical vehicles (EVs), exploration vehicles for planetary surfaces, and measure-while-drilling (MWD) tools used by the oil industry. These established and forthcoming emerging applications, require components that are stable in elevated or high temperature environments. High temperature energy storage devices are advancing from single-use, hazards-containing systems that require mandatory cooling systems to ensure proper function, to rechargeable and safer systems that utilize inherently non-flammable electrolytes.

However, high temperature EES systems are still in an early stage of development and suffer from limited thermal, chemical, and electrochemical stability at increased temperatures, resulting in short working lifetimes. Among the various cell components, electrolyte and electrode materials are the greatest impediment to the progress towards high temperature operation. Nevertheless, improvements in the thermal stability of the separator, binder and other assembling parts are welcomed. Meanwhile, future successful development of high temperature durable and efficient energy storage devices requires not only the introduction of innovative materials such as ionic liquids, solid polymers, cathode and anode materials that individually suit the high temperature applications, but also the synergetic interaction between the

components needs to be understood and enhanced to afford an the optimized combination with improved cycling, rate capability, and capacity. In order to design high temperature energy storage devices at a faster pace, there is a need for further advances and for continued systematic studies to understand the reaction pathways and mechanisms involved with the material itself or its interfacial reactions with other cell components.

While we have focused on EES operation at elevated and high temperatures, future efforts should extend the working temperature range to include those at room temperature or below. Despite the wide-spread success of Li-ion batteries, safety continues to be a concern due to the flammable nature of the conventional electrolytes. The use of non-flammable electrolytes is a fundamental logical solution to this safety issue, as opposed to reformulating the flammable electrolyte by adding flame retardant or installing safety control devices.^{74, 244-247} In addition, the discovery of new materials or new properties as a function of shape or size are likely to create unique solutions to challenges in ionic conductivity and materials, as well as the interface stability at non-ambient temperature conditions. By leveraging new materials, approaches, and designs, we are positioned to advance battery technology for the benefit of systems that operate over a wider temperature range than previously feasible in a high performance, reliable, and safe manner. These concerted efforts from both academia and industry will address the energy density, rate capability, and cycling duration needs of modern society.

The purpose of this manuscript is to review the field of high temperature batteries and supercapacitors, to promote new research in materials and materials characterization, and to stimulate discussion. Our interest in high temperature EES devices arose from discussions, funding, and a collaboration with the Advanced Energy Consortium, and we are grateful to them for facilitating our work as a team composed of PIs, and their corresponding graduate students and postdoctoral fellows, with diverse backgrounds and expertise: Grinstaff (synthetic and physical organic chemistry, ionic liquids, polymers, biomaterials) Ajayan (engineering and nanoscience, supercapacitors, carbon electrodes, Li storage), and Reddy (mechanical engineering, material science, Li ion batteries, electrodes, device integration). This team approach to science is both scientifically rewarding and intellectually stimulating. We encourage all to investigate this exciting area of energy storage and use, and its potential commercial applications.

AUTHOR INFORMATION

Corresponding Author

Mark W. Grinstaff at mgrin@bu.edu

Notes

The authors declare no competing financial interest.

ACKNOWLEDGEMENTS

This article was supported in part by BU and by the Advanced Energy Consortium: <http://www.beg.utexas.edu/aec/>. Advanced Energy Consortium Member companies include Petrobras, Repsol, Shell, Statoil, and Total.

TOC Graphic and text



This review summarizes the major developments, limitations, and opportunities in the field of high temperature electrical energy storage (EES) devices, with an emphasis on Li-ion batteries and supercapacitors.

ABBREVIATION LIST

Acetonitrile (ACN)
Activated carbon (AC)
Aluminum (Al)
Anionic block copolymer electrolyte (A-BCE)
Bis(oxalato)borate (LiBOB)
1-butyl-3-methylimidazolium bis[(trifluoromethyl) sulfonyl] amide (BMI-TFSI)
1-butyl-2,3-dimethylimidazolium bis(trifluoromethanesulfonyl)imide (BMMI-TFSI)
Carbide-derived carbon (CDC)
Compressed air energy storage (CAES)
Cyclic Voltammetry (CV)
Cyclooctene (COE)
Density functional theory, B3LYP hybrid functional (DFT-B3LYP)
Dialkylethers (R_2O)
Diethyl carbonate (DEC)
Diethylene glycol dimethacrylate (DEGDMA)
Differential scanning calorimetry (DSC)
Dimethyl carbonate (DMC)
Dimethyl sulphite (DMS)
Electric vehicles (EVs)
Electrical energy storage (EES)

Electrical double layer (EDL)
Electrochemical impedance spectroscopy (EIS)
Energy-dispersive X-ray (EDX)
Ethylene carbonate (EC)
Ethylene sulphite (ES)
Ethylmethyl carbonate (EMC)
Extended volume accelerating rate calorimetry (EV-ARC)
1-ethyl-3-methylimidazolium bis(trifluoromethanesulfonyl)imide (EMI-TFSI)
Field emission scanning electron microscopy (FESEM)
Fluoroethylene carbonate (FEC)
Fluorophosphates (OPF_2OR , $\text{OPF}(\text{OR})_2$)
Fluorophosphoric acid (OPF_2OH , $\text{OPF}(\text{OH})_2$)
Fourier transform infrared spectroscopy (FTIR)
Galvanostatic intermittent titration technique (GITT)
Gamma-butyrolactone (GBL)
Gas chromatography mass spectrometry (GC-MS)
Gel polymer electrolyte (GPE)
Glass transition (T_g)
Graft copolymer electrolyte (GCE)
Gel polymeric electrolytes (GPEs)
High pressure/high temperature (HP/HT)
High resolution electrospray-ionization mass spectrometry (HR-ESI-MS)
High temperature energy storage (HTS)
Hybrid electric vehicles (HEVs)
Hydrogen fluoride (HF)
hydroxypropyl guar gum (HPG)
Incremental capacity analysis (ICA)
Ionic liquid (IL)
Ion chromatography / mass spectrometer (IC-MS)
Lithium bisoxalato-borate (LiBOB)
Lithium bistrifluoromethane sulfonimide (LiTFSI)
Lithium copper oxide (Li-CuO)
Lithium hexafluorophosphate (LiPF_6)
Lithium manganese dioxide (Li-MnO_2)
Lithium perchlorate (LiClO_4)
Lithium phosphorus oxynitride (LiPON)
Lithium-iron sulfide (Li-FeS)
Lithium iron phosphate (LiFePO_4)
Lithium nickel cobalt manganese oxide; $\text{LiNi}_{1/3}\text{Co}_{1/3}\text{Mn}_{1/3}\text{O}_2$ (LiNMC)
Lithium sulfur dioxide (Li-SO_2)
Lithium-thionyl chloride (Li-SOCl_2)
Lithium fluoride (LiF)
Lithium titanium oxide; $\text{Li}_4\text{Ti}_5\text{O}_{12}$ (LTO)
Lithiated graphite (Li_xC_6)
Logging-while-drilling (LWD)
Low temperature plasma ambient ionization high-resolution mass spectrometry (LTP-HR-MS)
Measurement-while-drilling (MWD)
Methyl carbonate-terminated perfluoropolyethers (PFPE-DMCs)
Molten dimethyl sulfone (DMSO_2)
Molten carbonate fuel cell (MCFC)
N-butyl-*N*-methyl pyrrolidinium bis(trifluoromethanesulfonyl)imide (PP14-TFSI)

N-methyl-*N*-propylpyrrolidinium bis(trifluoromethanesulfonyl)imide (PYR13-TFSI)
N-methyl-*N*-butylpyrrolidinium bis(trifluoromethylsulfonyl)imide (PYR14-TFSI)
N-methyl-*N*-butylmorpholinium bis(fluorosulfonyl)imide (C4mmor-FSI)
N-methyl-*N*-propylpiperdinium bis(fluorosulfonyl) imide (PP13-FSI)
Net calorific value (NCV)
Nuclear magnetic resonance (NMR)
N-methoxyethyl-*N*-methylpyrrolidinium bis(trifluoromethanesulfonyl)-imide (PYR_{1,201}-TFSI)
N, *N*-diethyl-*N*-methyl-*N*-(2-methoxyethyl) ammonium tetrafluoroborate (DEME-BF₄)
Nickel/nickel chloride (Ni/NiCl)
Oxalyldifluoroborate (LiODFB)
Propylene carbonate (PC)
Proton exchange membrane (PEM)
Phosphoric acid fuel cell (PAFC)
Polyacrylonitrile (PAN)
Poly [2,5 benzimidazole] (ABPBI)
Polyethylene (PE)
Polyethylene oxide (PEO)
polyethylene terephthalate (PET)
Polypropylene (PP)
Poly-[2,20-*m*-phenylene-5,50-bibenzimidazole] (PBI)
Polystyrene-Polyethylene glycol-polystyrene (PS-PEO-PS)
Polytetrafluoroethylene (PTFE)
Poly(tetrafluoroethylene) (PTFE)
Poly(vinylidene fluoride) (PVDF)
Poly(vinyl chloride) (PVC)
2-(pentafluorophenyl)-tetrafluoro-1,3,2-benzodioxaborole (PFPTFB)
Phosphorus oxyfluoride (OPF₃)
Polytriphenylamine (PTPAN)
Poly(oxyethylene) methacrylate-*g*-poly(dimethyl siloxane) (POEM-*g*-PDMS)
Poly(ethylene glycol-*co*-lithium styrene trifluoromethanesulphonylimide) (P(STFSiLi)-*b*-PEO-*b*-P(STFSiLi))
Phosphoric acid (H₃PO₄)
Phosphorus pentafluoride (PF₅)
Propylmethyl carbonate (PMC)
Pump hydro storage (PHS)
Radio frequency (RF)
Reduced graphene oxide (RGO)
Red light-emitting-diode (LED)
Ring-opening metathesis polymerization (ROMP)
Single-walled carbon nanotube (SWNT)
Solid polymer electrolyte (SPE)
Sodium tetrachloroaluminate (NaAlCl₄)
Sodium iron pyrophosphate (NaFePO₄)
Sodium vanadyl(IV) orthophosphate (NaVOPO₄)
Sodium-sulfur (Na-S)
Solid oxide fuel cell (SOFC)
Solid-electrolyte Interphase (SEI)
State-of-charge (SOC)
Thermogravimetric analysis (TGA)
Tetraethylammoniumtetrafluoroborate (TEA-BF₄)
Thermoplastic poly (urethane) (TPU)

X-ray diffraction (XRD)
X-ray photoelectron spectroscopy (XPS)
Zeolite battery research Africa project (ZEBRA)

REFERENCES

1. Department of Energy, Grid energy storage, <http://energy.gov/oe/downloads/grid-energy-storage-december-2013>, (accessed February 2016).
2. Z. Yang, J. Zhang, M. C. Kintner-Meyer, X. Lu, D. Choi, J. P. Lemmon and J. Liu, *Chem. Rev.*, 2011, **111**, 3577-3613.
3. The International Energy Agency, Key World Energy Statistics, https://www.iea.org/publications/freepublications/publication/KeyWorld_Statistics_2015.pdf, (accessed January 2016).
4. B. Dunn, H. Kamath and J.-M. Tarascon, *Science*, 2011, **334**, 928-935.
5. J. B. Goodenough, Basic research needs for Electrical Energy Storage, http://www.sc.doe.gov/bes/reports/files/EES_rpt.pdf, (accessed February 2016).
6. H. Chen, T. N. Cong, W. Yang, C. Tan, Y. Li and Y. Ding, *Prog. Nat. Sci.*, 2009, **19**, 291-312.
7. D. Linden and T. B. Reddy, *Handbook Of Batteries*, McGraw Hill, New York, 3rd edn., 2001.
8. B. Scrosati, *Chem. Rec.*, 2005, **5**, 286-297.
9. J. B. Goodenough and Y. Kim, *Chem. Mater.*, 2010, **22**, 587-603.
10. N.-S. Choi, Z. Chen, S. A. Freunberger, X. Ji, Y.-K. Sun, K. Amine, G. Yushin, L. F. Nazar, J. Cho and P. G. Bruce, *Angew. Chem. Int. Ed.*, 2012, **51**, 9994-10024.
11. J.-M. Tarascon and M. Armand, *Nature (London)*, 2001, **414**, 359-367.
12. M. Winter and R. J. Brodd, *Chem. Rev.*, 2004, **104**, 4245-4270.
13. L. Carrette, K. A. Friedrich and U. Stimming, *Fuel Cells*, 2001, **1**, 5-39.
14. M. Jacoby, *Chem. Eng. News*, 2013, **91**, 33-37.
15. Q. Wang, P. Ping, X. Zhao, G. Chu, J. Sun and C. Chen, *J. Power Sources*, 2012, **208**, 210-224.
16. S. M. Whittingham, *MRS Bull.*, 2008, **33**, 411-419.
17. M. Armand and J.-M. Tarascon, *Nature (London)*, 2008, **451**, 652-657.
18. A. S. Aricò, P. Bruce, B. Scrosati, J.-M. Tarascon and W. van Schalkwijk, *Nat. Mater.*, 2005, **4**, 366-377.
19. M. R. Palacin, *Chem Soc Rev*, 2009, **38**, 2565-2575.
20. D. Doughty and E. P. Roth, *The Electrochemical Society Interface* 2012, **Summer**, 37-44.
21. J. Watson and G. Castro, *Analog. Dialog*, 2012, **46**, 1-7.
22. B. Allard, C. Buttay, D. Tournier, R. e. Robutel and J.-F. Mogniotte, *Automotive Power Electronics*, 2011, **April**, 1-10.
23. P. G. Neudeck, R. S. Okojier and L.-Y. Chen, *Proc. IEEE.*, 2002, **90**, 1065-1076.
24. D. Hensley, M. Milewits and W. Zhang, *Oilfield Review*, 1998, **Autumn**, 1-16.
25. M. Kutasov and L. V. Eppelbaum, *Proceedings World Geothermal Congress*, 2015, **April**, 1-12.

26. http://petrowiki.org/Reservoir_pressure_and_temperature, (accessed January 2016).
27. F. R. Haeberle, *Oil and Gas Journal*, 2001, **2**, 30-38.
28. J. Cooley, R. Signorelli, M. Green, P. S. Kuttipillai, C. Deane and L. A. Wilhelmus, *Power system for high temperature applications with rechargeable energy storage*, US 20120268074, 2012.
29. N. M. Brambilla, F. Martini, J. J. Cooley and R. H. Signorelli, Kyle, *Advanced Electrolytes for High Temperature Energy Storage Device*, WO 2015102716 A2 20150709, 2015.
30. R. A. Normann, *First High-Temperature Electronics Products Survey 2005*, Sandia Report, 2006.
31. H. Oman, *IEEE Aerosp. Electron. Syst. Mag.*, 2002, **17**, 29 - 35.
32. G. Bruce and B. Audette, Military takes aim at high battery costs, www.rfdesign.com, (accessed January 2016).
33. R. A. Marsha, S. Vuksona, S. Surampudib, B. V. Ratnakumarb, M. C. Smartb, M. Manzoc and P. J. Dalton, *J. Power Sources*, 2001, **97-98**, 25-27.
34. C. Buttay, D. Planson, B. Allard, Dominique Bergogne, P. Bevilacqua, C. Joubert, M. Lazar, C. Martin, H. Morel, D. Tournier and C. Raynaud, *Mater. Sci. Eng., B* 2011, **176**, 283-288.
35. R. W. Johnson, J. L. Evans, P. Jacobsen, J. R. R. Thompson and M. Christopher, *IEEE Trans. Electron. Packag. Manuf.*, 2004, **27**, 164-176.
36. E. Karden, S. Ploumen, B. Fricke, T. Miller and K. Snyder, *J. Power Sources*, 2007, **168**, 2-11.
37. Z. Rao and S. Wang, *Renew. Sust. Energ. Rev.*, 2011, **15**, 4554-4571.
38. R. Bates and Y. Jumel, *Lithium Batteries*, Academic Press, London, 1983.
39. D. Linden and B. McDonald, *J. Power Sources*, 1980, **5**, 35-55.
40. C. Julien, A. Mauger, A. Vijn and K. Zaghbi, *Lithium Batteries- Science and Technology*, Springer, New York, 2016.
41. N. A. Hampson, S. A. G. R. Karunathilaka, R. Leek and T. J. Sinclair, *Surface Technology*, 1982, **15**, 101 - 112.
42. A. Tranchant, R. Messina and J. Perichon, *J. Electroanal. Chem. Interfacial Electrochem.*, 1987, **233**, 189-198.
43. P. NovAk and P. Podhajecky, *J. Power Sources*, 1991, **35**, 235-247
44. G.-A. Nazri and G. Pistoia, *Lithium Batteries - Science and Technology*, Springer, New York, 2003.
45. N. Weber and J. T. Kummer, *Annual Power Sources Conference*, 1967.
46. B. L. Ellis and L. F. Nazar, *Curr. Opin. Solid State Mater. Sci.* , 2012, **16**, 168-177.
47. J. T. Kummer and N. Weber, *Battery Having a Molten Alkali Metal Anode and a Molten Sulfur Cathode*, U.S. Patent 3,413,150, 1968.
48. J. M. Tarascon, *Nat. Chem.*, 2010, **2**, 510.
49. J. Garche, *Encyclopedia of Electrochemical Power Sources*, Elsevier, 2009.
50. J. L. Sudworth, *J. Power Sources*, 2001, **100**, 149-163.
51. H. Kim, D. A. Boysen, J. M. Newhouse, B. L. Spatocco, B. Chung, P. J. Burke, D. J. Bradwell, K. Jiang, A. A. Tomaszowska, K. Wang, W. Wei, L. A. Ortiz, S. A. Barriga, S. M. Poizeau and D. R. Sadoway, *Chem. Rev.*, 2013, **113**, 2075-2099.
52. R. D. Deshpande, J. Li, Y.-T. Cheng and M. W. Verbrugge, *J. Electrochem. Soc.*, 2011, **158**, A845-A849.
53. K. Wang, K. Jiang, B. Chung, T. Ouchi, P. J. Burke, D. A. Boysen, D. J. Bradwell, H. Kim, U. Muecke and D. R. Sadoway, *Nature*, 2014, **514**, 348-350.
54. K. V. Kordesch and G. R. Simader, *Fuel Cells: and Their Applications*, VCH, Germany, 2006.
55. E. D. Wachsman and K. T. Lee, *Science*, 2011, **334**, 935-939.
56. A. Kulkarni and S. Giddey, *J. Solid State Electrochem.* , 2012, **16**, 3123-3146.

57. N. Q. Minh, *J. Am. Ceram. Soc.*, 1993, **76**, 563–588.
58. J. Vetter, P. Novák, M. R. Wagner, C. Veit, K. C. Möller, J. O. Besenhard, M. Winter, M. Wohlfahrt-Mehrens, C. Vogler and A. Hammouche, *J. Power Sources*, 2005, **147**, 269–281.
59. D. P. Abraham, E. P. Roth, R. Kosteki, K. McCarthy, S. MacLaren and D. H. Doughty, *J. Power Sources*, 2006, **161**, 648–657.
60. T. M. Bandhauer, S. Garimella and T. F. Fuller, *J. Electrochem. Soc.*, 2011, **158**, R1–R25.
61. K. Xu, *Chem. Rev.*, 2004, **104**, 4303–4418.
62. K. Xu, *Chem. Rev.*, 2014, **114**, 11503–11618.
63. J. M. Tarascon and D. Guyomard, *Solid State Ionics*, 1994, **69**, 293–305.
64. N. Katayama, T. Kawamura, Y. Baba and J.-i. Yamaki, *J. Power Sources*, 2002, **109**, 321–326.
65. T. Kawamura, A. Kimura, M. Egashira, S. Okada and J.-i. Yamaki, *Journal of Power Sources*, 2002, **104**, 260–264.
66. T. Kawamura, S. Okada and J.-i. Yamaki, *J. Power Sources*, 2006, **156**, 547–554.
67. A. Hammami, N. Raymond and M. Armand, *Science*, 2003, **301**, 1063–1063.
68. P. Handel, G. Fauler, K. Kapper, M. Schmuck, C. Stangl, R. Fischer, F. Uhlig and S. Koller, *J. Power Sources*, 2014, **267**, 255–259.
69. D. D. MacNeil and J. R. Dahn, *J. Electrochem. Soc.*, 2003, **150**, A21–A28.
70. D. Yaakov, Y. Gofer, D. Aurbach and I. C. Halalay, *J. Electrochem. Soc.*, 2010, **157**, A1383–A1391.
71. S. Nowak and M. Winter, *J. Electrochem. Soc.*, 2015, **162**, A2500–A2508.
72. P. Ping, Q. Wang, J. Sun, X. Feng and C. Chen, *J. Power Sources*, 2011, **196**, 776–783.
73. Y. Shigematsu, S.-i. Kinoshita and M. Ue, *J. Electrochem. Soc.*, 2006, **153**, A2166–A2170.
74. Y. Shigematsu, M. Ue and J.-i. Yamaki, *J. Electrochem. Soc.*, 2009, **156**, A176–A180.
75. C. L. Champion, W. Li and B. L. Lucht, *J. Electrochem. Soc.*, 2005, **152**, A2327–A2334.
76. Q. Wang, J. Sun, X. Yao and C. Chen, *Thermochim. Acta* 2005, **437**, 12–16.
77. H. F. Xiang, H. Wang, C. H. Chen, X. W. Ge, S. Guo, J. H. Sun and W. Q. Hu, *J. Power Sources*, 2009, **191**, 575–581.
78. V. Eshkenazi, E. Peled, L. Burstein and D. Golodnitsky, *Solid State Ionics*, 2004, **170**, 83–91.
79. S. E. Sloop, J. K. Pugh, S. Wang, J. B. Kerr and K. Kinoshita, *Electrochem. Solid-State Lett.*, 2001, **4**, A42–A44.
80. M. Pyschik, V. Kraft, S. Passerini, M. Winter and S. Nowak, *Electrochim. Acta*, 2014, **130**, 426–430.
81. M.-H. Ryou, J.-N. Lee, D. J. Lee, W.-K. Kim, Y. K. Jeong, J. W. Choi, J.-K. Park and Y. M. Lee, *Electrochim. Acta* 2012, **83**, 259–263.
82. J. F. Jr. and D. D. DesMarteau, *Inorg. Chem.*, 1984, **23**, 3720–3723.
83. J. R. Dahn, U. v. Sacken, M. W. Juzkow and H. Al - Janaby, *J. Electrochem. Soc.*, 1991, **138**, 2207–2211.
84. L. A. Dominey, V. R. Koch and T. J. Blakley, *Electrochim. Acta*, 1992, **37**, 1551–1554.
85. V. Aravindan, J. Gnanaraj, S. Madhavi and H.-K. Liu, *Chem. Eur. J* 2011, **17**, 14326–14346.
86. K. Mizushima, P. C. Jones, P. J. Wiseman and J. B. Goodenough, *Mater. Res. Bull.*, 1980, **15**, 783–789.
87. Y. Baba, S. Okada and J.-i. Yamaki, *Solid State Ionics*, 2002, **148**, 311–316.
88. S.-Y. Lee, H. H. Yong, S. K. Kim, J. Y. Kim and S. Ahn, *J. Power Sources*, 2005, **146**, 732–735.
89. Q. Huang, M. Yan and Z. Jiang, *J. Power Sources*, 2006, **156**, 541–546.

90. H. Gabrisch, M. Kombolias and D. Mohanty, *Solid State Ionics*, 2010, **181**, 71-78.
91. P. Peng, Y. Sun and F. Jiang, *Heat and Mass Transfer*, 2014, **50**, 1405-1416.
92. C. M. Julien, A. Mauger, K. Zaghieb and H. Groult, *Inorganics*, 2014, **2**, 132-154.
93. D. D. MacNeil, Z. Lu, Z. Chen and J. R. Dahn, *J. Power Sources*, 2002, **108**, 8-14.
94. I. Belharouak, Y. K. Sun, W. Lu and K. Amine, *J. Electrochem. Soc.*, 2007, **154**, A1083-A1078.
95. H. Joachin, T. D. Kaun, K. Zaghieb and J. Prakash, *J. Electrochem. Soc.*, 2009, **156**, A401-A406.
96. K. Amine, J. Liu, S. Kang, I. Belharouak, Y. Hyung, D. Vissers and G. Henriksen, *J. Power Sources*, 2004, **129**, 14-19.
97. A. K. Padhi, K. S. Nanjundaswamy and J. B. Goodenough, *J. Electrochem. Soc.*, 1997, **144**, 1188-1194.
98. S.-Y. Chung, J. T. Bloking and Y.-M. Chiang, *Nat. Mater.*, 2002, **1**, 123-128.
99. I. Belharouak, W. Lu, J. Liu, D. Vissers and K. Amine, *J. Power Sources*, 2007, **174**, 905-909.
100. Y. Makimura, C. Okuda, T. Nonaka, Y. F. Nishimura, T. Sasaki and Y. Takeuchi, *ECS Electrochem. Lett.*, 2014, **3**, A66-A68.
101. Y. Piao, C.-k. Lin, Y. Qin, D. Zhou, Y. Ren, I. Bloom, Y. Wei, G. Chen and Z. Chen, *J. Power Sources*, 2015, **273**, 1250-1255.
102. R. Venkatachalapathy, C. W. Lee, W. Lu and J. Prakash, *Electrochem. Commun.*, 2000, **2**, 104-107.
103. R. Dominko, *J. Power Sources*, 2008, **184**, 462-468.
104. K. Zaghieb, J. Dubé, A. Dallaire, K. Galoustov, A. Guerfi, M. Ramanathan, A. Benmayza, J. Prakash, A. Mauger and C. M. Julien, *Journal of Power Sources*, 2012, **219**, 36-44.
105. H. Yang, H. Bang, K. Amine and J. Prakash, *J. Electrochem. Soc.*, 2005, **152**, A73-A79.
106. Y.-S. Park, E.-S. Oh and S.-M. Lee, *J. Power Sources*, 2014, **248**, 1191-1196.
107. H. Maleki, G. Deng, I. Kerzhner-Haller, A. Anani and J. N. Howard, *J. Electrochem. Soc.*, 2000, **147**, 4470-4475.
108. D. D. MacNeila, D. Larcherb and J. R. Dahn, *J. Electrochem. Soc.*, 1999, **146**, 3596-3602.
109. P. Verma, P. Maire and P. Novák, *Electrochim. Acta*, 2010, **55**, 6332-6341.
110. A. M. Andersson and K. Edström, *J. Electrochem. Soc.*, 2001, **148**, A1100-A1109.
111. T. Zheng, A. S. Gozdz and G. G. Amatucci¹, *J. Electrochem. Soc.*, 1999, **146**, 4014-4018.
112. P. Arora, R. E. White and M. Doyle, *J. Electrochem. Soc.*, 1998, **145**, 3647-3667.
113. S. Zhang, M. S. Ding, K. Xu, J. Allen and T. R. Jow, *Electrochem. Solid-State Lett.*, 2001, **4**, A206-A208.
114. P. B. Balbuena and Y. Wang, *Lithium-Ion Batteries: Solid-Electrolyte Interphase*, World Scientific Publishing Company, 2004.
115. P. Arora and Z. J. Zhang, *Chem. Rev.*, 2004, **104**, 4419-4462.
116. S. S. Zhang, *J. Power Sources*, 2007, **164**, 351-364.
117. S. Augustin, V. D. Hennige, G. Horpel and C. Hying, *Desalination*, 2002, **146**, 23.
118. C. J. Orendorff, *The electrochemical society interface*, 2012, **Summer**, 61-65.
119. D. V. Carvalho, N. Loeffler, G. T. Kim and S. Passerini, *Membranes*, 2015, **5**, 632-645.
120. S. S. Zhang and T. R. Jow, *J. Power Sources*, 2002, **109**, 422-426.
121. E. P. Roth, D. H. Doughty and J. Franklin, *J. Power Sources*, 2004, **134**, 222-234.
122. T. D. Kaun, M. C. Hash and D. R. Simon, *Sulfide Ceramics in Molten Salt Electrolyte Batteries*, Report American Ceramic meeting, 1995.
123. X. Feng, M. Fang, X. He, M. Ouyang, L. Lu, H. Wang and M. Zhang, *J. Power Sources*, 2014, **255**, 294-301.

124. L. Terborg, S. Weber, F. Blaske, S. Passerini, M. Winter, U. Karst and S. Nowak, *J. Power Sources*, 2013, **242**, 832-837.
125. X. Liu, S. I. Stolarov, M. Denlinger, A. Masias and K. Snyder, *J. Power Sources*, 2015, **280**, 516-525.
126. C. F. Lopez, J. A. Jeevarajan and P. P. Mukherjee, *J. Electrochem. Soc.*, 2015, **162**, A2163-A2173.
127. C. F. Lopez, J. A. Jeevarajan and P. P. Mukherjee, *J. Electrochem. Soc.*, 2015, **162**, A1905-A1915.
128. E. Mengeritsky, P. Dan, I. Weissman, A. Zaban and D. Aurbach, *J. Electrochem. Soc.*, 1996, **143**, 2110-2116.
129. H. Maleki, G. Deng, A. Anani and J. Howard, *J. Electrochem. Soc.*, 1999, **146**, 3224-3229.
130. R. Spotnitza and J. Franklin, *J. Power Sources*, 2003, **113**, 81-100.
131. E. V. Thomas, H. L. Case, D. H. Doughty, R. G. Jungst, G. Nagasubramanian and E. P. Roth, *J. Power Sources*, 2003, **124**, 254-260.
132. W. Meng, W. Chen, L. Zhao, Y. Huang, M. Zhu, Y. Huang, Y. Fu, F. Geng, J. Yu, X. Chen and C. Zhi, *Nano Energy*, 2014, **8**, 133-140.
133. A. Ponrouch, E. Marchante, M. Courty, J.-M. Tarascon and M. R. Palacín, *Energy Environ. Sci.*, 2012, **5**, 8572-8583.
134. A. Ponrouch, C. Frontera, F. Barde and M. R. Palacín, *Nat. Mater.*, 2016, **15**, 169-172.
135. T. P. Lodge, *Science*, 2008, **321**, 50-51.
136. G. Gebresilassie Eshetu, M. Armand, B. Scrosati and S. Passerini, *Angew. Chem. Int. Ed.*, 2014, **53**, 13342-13359.
137. P. Wasserscheid and T. Welton, *Ionic Liquids in Synthesis*, Wiley-VCH, Weinheim, Germany, 2003.
138. H. Ohno, *Ionic Liquids: The Front and Future of Material Developments*, (CMC, Tokyo, 2003.
139. T. Welton, *Chemical Reviews*, 1999, **11**, 2071-2084.
140. J. P. Hallett and T. Welton, *Chem. Rev.*, 2011, **111**, 3508-3576.
141. R. D. Rogers and K. R. Seddon, *Science*, 2003, **302**, 792-793.
142. P. Wasserscheid and W. Keim, *Angew. Chem. Int. Ed.*, 2000, **39**, 3772-3789.
143. K. R. Seddon, *J. Chem. Technol. Biotechnol.*, 1999, **68**, 351-356.
144. R. P. Swatloski, S. K. Spear, J. D. Holbrey and R. D. Rogers, *J. Am. Chem. Soc.*, 2002, **124**, 4974-4975.
145. B. Kirchner, *Ionic Liquids*, Springer, Berlin, 2009.
146. J. S. Wilkes and Z. M.J., *Chem. Commun.*, 1992, 965-967.
147. J. F. Wishart, *Energy Environ. Sci.*, 2009, **2**, 956-961.
148. D. R. MacFarlane, M. Forsyth, P. C. Howlett, M. Kar, S. Passerini, J. M. Pringle, H. Ohno, M. Watanabe, F. Yan, W. Zheng, S. Zhang and J. Zhang, *Nat. Rev. Mater.*, 2016, **1**, 15005.
149. M. V. Fedorov and A. A. Kornyshev, *Chem. Rev.*, 2014, **114**, 2978-3036.
150. M. Galiński, A. Lewandowski and I. Stępnia, *Electrochim. Acta*, 2006, **51**, 5567-5580.
151. E. Quartarone and P. Mustarelli, *Chem. Soc. Rev.*, 2011, **40**, 2525-2540.
152. A. Lewandowski and A. Świdorska-Mocek, *J. Power Sources*, 2009, **194**, 601-609.
153. H. Ohno, *Electrochemical Aspects of Ionic Liquids*, John Wiley & Sons, New Jersey, 2005.
154. M. Armand, F. Endres, D. R. MacFarlane, H. Ohno and B. Scrosati, *Nat. Mater.*, 2009, **8**, 621-629.
155. Y. Lu, K. Korf, Y. Kambe, Z. Tu and L. A. Archer, *Angew. Chem. Int. Ed.*, 2013, **53**, 488-492.

156. E. Paillard, Q. Zhou, W. A. Henderson, G. B. Appetecchi, M. Montanino and S. Passerini, *J. Electrochem. Soc.*, 2009, **156**, A891-A895.
157. H. Sakaebe and H. Matsumoto, *Electrochem. Commun.*, 2003, **5**, 594-598.
158. B. Garcia, S. Lavallée, G. Perron, C. Michot and M. Armand, *Electrochim. Acta*, 2004, **49**, 4583-4588.
159. H. Matsumoto, H. Sakaebe, K. Tatsumi, M. Kikuta, E. Ishiko and M. Kono, *J. Power Sources*, 2006, **160**, 1308-1313.
160. F. Wu, Q. Zhu, R. Chen, N. Chen, Y. Chen and L. Li, *Chem. Sci.*, 2015, **6**, 7274-7283.
161. J.-H. Shin, W. A. Henderson and S. Passerini, *Electrochem. Comm.*, 2003, **5**, 1016-1020.
162. J.-H. Shin, W. A. Henderson, S. Scaccia, P. P. Prosini and S. Passerini, *J. Power Sources*, 2006, **156**, 560-566.
163. F. Wu, G. Tan, R. Chen, L. Li, J. Xiang and Y. Zheng, *Adv. Mater.*, 2011, **23**, 5081-5085.
164. X. Wang, E. Yasukawa and S. Mori, *Electrochim. Acta*, 2000, **45**, 2677-2684.
165. B. Garcia and M. Armand, *J. Power Sources*, 2004, **132**, 206-208.
166. M. Nadherná, R. Dominko, D. Hanzel, J. Reiter and M. Gaberscek, *J. Electrochem. Soc.*, 2009, **156**, A619-A626.
167. C. Peng, L. Yang, Z. Zhang, K. Tachibana and Y. Yang, *J. Power Sources*, 2007, **173**, 510-517.
168. J. Mun, Y. S. Jung, T. Yim, H. Y. Lee, H.-J. Kim, Y. G. Kim and S. M. Oh, *J. Power Sources*, 2009, **194**, 1068-1074.
169. G. H. Lane, P. M. Bayley, B. R. Clare, A. S. Best, D. R. M. Forsyth and A. F. Hollenkamp, *J. Phys. Chem. C*, 2010, **114**, 21775-21785.
170. M. C. Kroon, W. Buijs, C. J. Peters and G.-J. Witkamp, *Thermochim. Acta*, 2007, **465**, 40-47.
171. X. Lin, R. Kaviani, Y. Lu, Q. Hu, Y. Shao-Horn and M. W. Grinstaff, *Chem. Sci.*, 2015, **6**, 6601-6606.
172. K. Kalaga, M. T. Rodrigues, H. Gullapalli, G. Babu, L. M. Arava and P. M. Ajayan, *ACS Appl. Mater. Inter.*, 2015, **7**, 25777-25783.
173. E. Markevich, V. Baranchugov, G. Salitra, D. Aurbach and M. A. Schmidt, *J. Electrochem. Soc.*, 2008, **155**, A132-A137.
174. K. Ababtain, G. Babu, X. Lin, M.-T. F. Rodrigues, H. Gullapalli, P. M. Ajayan, M. W. Grinstaff and L. M. R. Arava, *ACS Appl. Mater. Interfaces*, 2016, **8**, 15242-15249.
175. E. Markevich, G. Salitra, A. Rosenman, Y. Talyosef, D. Aurbach and A. Garsuch, *RSC Adv.*, 2014, **4**, 48572-48575.
176. K. Ababtain, G. Babu, X. Lin, M.-T. F. Rodrigues, H. Gullapalli, P. M. Ajayan, M. W. Grinstaff and L. M. R. Arava, *Revision submitted*, 2016.
177. Y. Zhu, Y. Xu, Y. Liu, C. Luo and C. Wang, *Nanoscale*, 2013, **5**, 780-787.
178. N. Wongittharom, C.-H. Wang, Y.-C. Wang, C.-H. Yang and J.-K. Chang, *ACS Appl. Mater. Inter.*, 2014, **6**, 17564-17570.
179. C.-Y. Chen, K. Matsumoto, T. Nohira and R. Hagiwara, *J. Electrochem. Soc.*, 2015, **162**, A2093-A2098.
180. T. Sato, G. Masuda and K. Takagi, *Electrochim. Acta*, 2004, **49**, 3603-3611.
181. A. Balducci, R. Dugas, P. L. Taberna, P. Simon, D. Plée, M. Mastragostino and S. Passerini, *J. Power Sources*, 2007, **165**, 922-927.
182. R. Lin, P.-L. Taberna, S. Fantini, V. Presser, C. R. Pérez, F. Malbosc, N. L. Rupasinghe, K. B. K. Teo, Y. Gogotsi and P. Simon, *J. Phys. Chem. Lett.*, 2011, **2**, 2396-2401.
183. C. Largeot, P. L. Taberna, Y. Gogotsi and P. Simon, *Electrochem. Solid State Lett.*, 2011, **14**, A174-A176.
184. C. Masarapu, H. F. Zeng, K. H. Hung and B. Wei, *ACS Nano*, 2009, **3**, 2199-2206.

185. R. S. Borges, A. L. M. Reddy, M.-T. F. Rodrigues, H. Gullapalli, K. Balakrishnan, G. G. Silva and P. M. Ajayan, *Sci. Rep.*, 2013, **3**, 2572.
186. D. E. Fenton, J. M. Parker and P. V. Wright, *Polymer*, 1973, **14**, 589.
187. M. Armand, *Solid State Ionics*, 1983, **9-10**, 745–754.
188. W. H. Meyer, *Adv. Mater.*, 1998, **10**, 439–448.
189. J. W. Fergus, *J. Power Sources*, 2010, **195**, 4554–4569.
190. J. Y. Song, Y. Y. Wang and C. C. Wan, *J. Power Sources*, 1999, **77**, 183–197.
191. P. G. Bruce and C. A. Vincent, *J. Chem. Soc., Faraday Trans*, 1993, **89**, 3187–3203.
192. Q. Hu, S. Osswald, R. Daniel, Y. Zhu, S. Wesel, L. Ortiz and D. R. Sadoway, *J. Power Sources*, 2011, **196**, 5604–5610.
193. D. R. Sadoway, *J. Power Sources*, 2004, **129**, 1–3.
194. R. Bouchet, S. Maria, R. Meziane, A. Aboulaich, L. Lienafa, J.-P. Bonnet, T. N. T. Phan, D. Bertin, D. Gigmes, D. Devaux, R. Denoyel and M. Armand, *Nat. Mater.*, 2013, **12**, 452–457.
195. M. Doyle, T. F. Fuller and J. Newman, *Electrochim. Acta*, 1994, **39**, 2073–2081.
196. D. H. C. Wong, J. L. Thelen, Y. Fu, D. Devaux, A. A. Pandya, V. S. Battaglia, N. P. Balsara and J. M. DeSimone, *Proc. Natl. Acad. Sci.*, 2014, **111**, 3327–3331.
197. M. D. Konieczynska, X. Lin, H. Zhang and M. W. Grinstaff, *ACS Macro Lett.*, 2015, **4**, 533–537.
198. R. Khurana, J. L. Schaefer, L. A. Archer and G. W. Coates, *J. Am. Chem. Soc.*, 2014, **136**, 7395–7402.
199. M. Kono, E. Hayashi and M. Watanabe, *J. Electrochem. Soc.*, 1998, **145**, 1521–1527.
200. F. Alloin, Y. Sanchez and M. Armand, *J. Electrochem. Soc.*, 1994, **141**, 1915–1920.
201. G. M. Stone, S. A. Mullin, A. A. Teran, D. T. Hallinan, A. M. Minor, A. Hexemer and N. P. Balsara, *J. Electrochem. Soc.*, 2012, **159**, A222–A227.
202. Y. Lu, Z. Tu and L. A. Archer, *Nat. Mater.*, 2014, **13**, 961–969.
203. M. Rosso, T. Gobron, C. Brissot, J.-N. Chazalviela and S. Lascaudb, *J. Power. Sources*, 2001, **97-98**, 804–806.
204. S.-K. Kim, H. J. Kim, J.-C. Lee, P. V. Braun and H. S. Park, *ACS Nano*, 2015, **9**, 8569–8577.
205. R. S. Hastak, P. Sivaraman, D. D. Potphode, K. Shashidhara and A. B. Samui, *Electrochim. Acta*, 2012, **59**, 296–303.
206. J. C. Bachman, S. Muy, A. Grimaud, H. H. Chang, N. Pour, S. F. Lux, O. Paschos, F. Maglia, S. Lupart, P. Lamp, L. Giordano and Y. Shao-Horn, *Chem. Rev.*, 2016, **116**, 140–162.
207. P. Knauth, *Solid State Ionics*, 2009, **180**, 911–916.
208. A. D. Robertson, A. R. Westa and A. G. Ritchie, *Solid State Ionics*, 1997, **104**, 1–11.
209. H. Aono, N. Imanaka and G.-y. Adachi, *Acc. Chem. Res.*, 1994, **27**, 265–270.
210. D. Singh, D. Zhu, Y. Zhou and M. Singh, *Design, Development, and Applications of Engineering Ceramics and Composites*, John Wiley & Sons, Inc., Hoboken, NJ, USA, 2010.
211. J. B. Goodenough, H. Y.-P. Hong and J. A. Kafalas, *Mater. Res. Bull.*, 1976, **11**, 203–220.
212. K. S. Nanjundaswamy, A. K. Padhi, J. B. Goodenough, S. Okada, H. Ohtsuka, H. Arai and J. Yamaki, *Solid State Ionics*, 1996, **92**, 1–10.
213. V. Palomares, P. Serras, I. Villaluenga, K. B. Hueso, J. Carretero-Gonzalez and T. Rojo, *Energy Environ. Sci.*, 2012, **5**, 5884–5901.
214. F. Lalère, J. B. Leriche, M. Courty, S. Boulineau, V. Viallet, C. Masquelier and V. Seznec, *J. Power Sources*, 2014, **247**, 975–980.
215. U. v. Alpen, A. Rabenau and G. H. Talat, *Appl. Phys. Lett.*, 1977, **30**, 621–623.

216. R. D. Armstrong, *International Symposium On Solid Ionic and Ionic-Electronic Conductors: Selected Papers from the Conference Held in Rome, September 1976*, Elsevier Science, 2013.
217. R. Mercier, J.-P. Malugani, B. Fahys and G. Robert, *Solid State Ionics*, 1981, **5**, 663-666.
218. H. Wada, M. Menetrier, A. Levasseur and P. Hagenmuller, *Mater. Res. Bull.*, 1983, **18**, 189-193.
219. S. Kondo, K. Takada and Y. Yamamura, *Solid State Ionics*, 1992, **53-56**, 1183-1186.
220. J. H. Kennedy, S. Sahami, S. W. Shea and Z. Zhang, *Solid State Ionics*, 1986, **18-19**, 368-371.
221. A. Mei, Q.-H. Jiang, Y.-H. Lin and C.-W. Nan, *J. Alloys Compd.*, 2009, **486**, 871-875.
222. J. L. Schaefer, Y. Lu, S. S. Moganty, P. Agarwal, N. Jayaprakash and L. A. Archer, *Appl. Nanosci.*, 2011, **2**, 91-109.
223. N. Kamaya, K. Homma, Y. Yamakawa, M. Hirayama, R. Kanno, M. Yonemura, T. Kamiyama, Y. Kato, S. Hama, K. Kawamoto and A. Mitsui, *Nat. Mater.*, 2011, **10**, 682-686.
224. T. Hibino, K. Kobayashi, M. Nagao and S. Kawasaki, *Sci. Rep.*, 2015, **5**, 7903.
225. K. Xu, S. S. Zhang, U. Lee, J. L. Allen and T. R. Jow, *J. Power Sources*, 2005, **146**, 79-85.
226. S. S. Zhang, *Electrochem. Comm.*, 2006, **8**, 1423-1428.
227. S. S. Zhang, *ECS Trans.*, 2007, **3**, 59-68.
228. Z. Chen, J. Liu, A. N. Jansen, G. GirishKumar, B. Casteel and K. Amine, *Electrochem. Solid State Lett.*, 2010, **13**, A39-A42.
229. C. Buhrmester, J. Chen, L. Moshurchak, J. Jiang, R. L. Wang and J. R. Dahn, *J. Electrochem. Soc.*, 2005, **152**, A2390-A2399.
230. R. A. Leising, M. J. Palazzo, E. S. Takeuchi and K. J. Takeuchi, *J. Electrochem. Soc.*, 2001, **148**, A838-A844.
231. X. Zhu, H. Yang and X. Ai, *Electrochim. Acta*, 2003, **48**, 4033-4037.
232. K. M. Abraham, D. M. Pasquariello and E. B. Willstaedt, *J. Electrochem. Soc.*, 1990, **137**, 1856-1857.
233. Z. Chen, Y. Ren, A. N. Jansen, C. K. Lin, W. Weng and K. Amine, *Nat. Commun.*, 2013, **4**, 1513.
234. D. Muñoz-Rojas, J.-B. Leriche, C. Delacourt, P. Poizot, M. R. Palacín and J.-M. Tarascon, *Electrochem. Comm.*, 2007, **9**, 708-712.
235. C. Brissot, M. Rosso, J.-N. Chazalviel, P. Baudry and S. Lascaud, *Electrochim. Acta*, 1998, **43**, 1569-1574.
236. C. Brissot, M. Rosso, J.-N. Chazalviel and S. Lascaud, *J. Power Sources*, 1999, **81-82**, 925-929.
237. C. Zhang, S. Gamble, D. Ainsworth, A. M. Slawin, Y. G. Andreev and P. G. Bruce, *Nat. Mater.*, 2009, **8**, 580-584.
238. Z. Gadjourova, Y. G. Andreev, D. P. Tunstall and P. G. Bruce, *Nature*, 2001, **412**, 520-523.
239. K. J. Baranyai, G. B. Deacon, D. R. MacFarlane, J. M. Pringle and J. L. Scott, *Aust. J. Chem.*, 2004, **57**, 145-147.
240. C. Maton, N. De Vos and C. V. Stevens, *Chem. Soc. Rev.*, 2013, **42**, 5963-5977.
241. R. E. Del Sesto, T. M. McCleskey, C. Macomber, K. C. Ott, A. T. Koppisch, G. A. Baker and A. K. Burrell, *Thermochim. Acta*, 2009, **491**, 118-120.
242. T. J. Wooster, K. M. Johanson, K. J. Fraser, D. R. MacFarlane and J. L. Scott, *Green Chem.*, 2006, **8**, 691-696.
243. M. Pyschik, C. Schultz, S. Passerini, M. Winter and S. Nowak, *Electrochim. Acta*, 2015, **176**, 1143-1152.

244. K. Xu, S. Zhang, J. L. Allen and T. R. Jow, *J. Electrochem. Soc.*, 2002, **149**, A1079-A1082.
245. Z. Chen, P.-C. Hsu, J. Lopez, Y. Li, J. W. F. To, N. Liu, C. Wang, Sean C. Andrews, J. Liu, Y. Cui and Z. Bao, *Nat. Energy*, 2016, **1**, 15009.
246. C. L. Cheng, C. C. Wan, Y. Y. Wang and M. S. Wu, *J. Power Sources*, 2005, **144**, 238-243.
247. L. Xia, S.-L. Li, X.-P. Ai, H.-X. Yang and Y.-L. Cao, *Energy Environ. Sci.*, 2011, **4**, 2845-2848.